STRUCTURAL COUPLING OF HIGH-RISE BUILDINGS LINKED BY SKYBRIDGES

A Thesis

by

ATHEER KHUDHUR JUMAAH

Submitted to the Office of Graduate and Professional Studies of
Texas A&M University
in partial fulfillment of the requirements for the degree of

MASTER OF SCIENCE

Chair of Committee,	John Niedzwecki
Committee Members,	Luciana Barroso
	H. Joseph Newton
Head of Department,	Robin Autenrieth

August 2017

Major Subject: Civil Engineering

ABSTRACT

An example of the creative building concepts is the connection two or more buildings using skybridges, which are also referred to as skyways or skywalks. They can provide direct passage in congested areas, serve to make walking more pleasant for pedestrian passage and protect walkers from the elements like the scorching heat or heavy rain. Further in large cities, a skywalk or skybridge can serve to separate the vehicle traffic from pedestrian traffic.

In this research study, the effect of introducing single skybridge or multiple skybridges on the dynamic response behavior of the linked high-rise buildings is studied. A mathematical matrix formulation using 3-D space frames was implemented for time domain simulations in Matlab and was validated using the finite element software SAP2000. This included a comparison of translational and rotational mode shapes and undamped natural frequency estimates, and time series response predictions. The building systems were excited using very four different strong ground motion time series records. A grouping of nine specific cases was developed to investigate the response of building system that connected two buildings of different height. It was found that multiple skybridge designs influenced the higher modal characteristics and structural response, suggesting some response optimization was possible. In addition, statistical characterization of the excitation and response behavior illustrated that non-Gaussian excitation was filtered by the building system to yielding a reduced non-Gaussian response.

DEDICATION

To my almighty God, Allah

ACKNOWLEDGEMENTS

All of the praise is due to Allah; I ask him for his direction and forgiveness. I would really wish to extend my appreciation to my parents, father, and mother before she passed away, who constantly endeavor to make me a prosperous person, and I seek to please them. I would like to give thanks to my family members, Liqaa, Ahmad, Alaa, Diana, Sarah, and my niece Alaa for their motivation and being supportive. My appreciations to my committee chair Professor John Niedzwecki for his useful directions. I have had an outstanding experience with him during my research course. I would as well say thanks to my committee members Professor Luciana Barroso and Professor H. Joseph Newton for assisting me. My thanks to Layal Almaddah, my officemates, and all friends for being positive in my life. I am really thankful to the Higher Committee for Education Development in Iraq (HCED) for their financial assistance. I thank Texas A&M University for being an extraordinary university for students from various places worldwide. My distinctive thanks to the Zachry Department of Civil Engineering- Faculty, staff, and students-.

CONTRIBUTORS AND FUNDING SOURCES

This work was supervised by a thesis committee consisting of Professor John Niedzwecki [advisor] and Professor Luciana Barroso of Zachry Department of Civil Engineering and Professor H. Joseph Newton of Department of Statistics.

All work for the thesis was completed independently by the student.

Graduate study was supported by a scholarship from the Higher Committee for Educational Development in Iraq (HCED).

TABLE OF CONTENTS

Page

LIST OF FIGURES

Page

Page

Page

Page

LIST OF TABLES

Page

Page

1. INTRODUCTION

1.1. Background and Problem Statement

As Architectural firms develop creative building concepts to meet the demands of their clients, the structural design often becomes quite complicated. An example of the architectural complexity is the connection two or more buildings using skybridges, also referred to as skyways or skywalks. This concept can also be used to provide connections at several elevations on buildings. Generally, a skybridge is intended to serve as a walkway to facilitate pedestrian traffic between buildings and, depending on the skybridge location and elevation, they can provide a spectacular view for pedestrians walking between the connected structures. One example is the distinctive Petronas Twin Towers in Malaysia that are connected by a single skywalk is shown in figure 1. Another example is the Bahrain World Trade Center buildings shown in figure 2. This example is quite interesting as it was designed with multiple skyways that each incorporate a wind turbine. There are many other architectural concepts for the use of skybridges that include gardens and swimming pools.

The use of skybridges to connect buildings can significantly influence the dynamic structural response behavior when these high-rise buildings are subjected to loads involving extreme winds and/or strong ground motions. In comparison, the impact of these loads is expected to be less severe for low-rise buildings. Most of the previous studies have focused the modeling of two identical buildings connected by a single skybridge and subject to various wind loading scenarios. This research study will focus

on the bending and torsional response of high-rise buildings subject to strong ground motions where the buildings need not be identical and multiple skybridge connections are possible.

Lim, Bienkiewicz, & Richards (2011) conducted research in order to study the influence of a single skybridge on the dynamic response behavior of two interconnected identical high-rise buildings. They modeled two high-rise buildings interconnected by a skybridge at the mid-height of each building. In their study, each building was idealized as a MDOF lumped mass model interconnected by a frame element representing the skybridge. They were able to realize that x-in and x-out mode shapes, related to the motion along the axis that is perpendicular to skybridge, are not coupled to other mode shapes. Other modes in the z-direction and torsional modes are coupled. In addition, approximate empirical formulas were introduced to calculate natural frequencies for all mode shapes. The structural system was modeled using a six-degree of freedom representation where the buildings were specified to have identical dynamic properties.

Figure 1. Petronas Twin Tower Skybridge (Printed from Rogers, 2017)

Figure 2. Bahrain World Trade Center (Printed from Lomholt, Lomholt, Solkoff, & Solkoff, 2017)

Effects of structural and aerodynamic couplings on the dynamic response of high-rise twin buildings with a skybridge was also studied by Lim & Bienkiewicz (2009) using a high-frequency force balance (HFFB) technique. In these research studies, they utilized the same structural system model described in the previous research study (Lim, Bienkiewicz, & Richards, 2011) and utilized wind tunnel tests to further study the coupled response behavior. It was realized the inclusion of the structural coupling led to significant reductions, up to 22% in the resultant rooftop accelerations, when compared with the maximum accelerations of the structurally uncoupled buildings.

In another study, (Song & Tse, 2014) increased the complexity of the model that was subjected to wind loads. Each floor in the high-rise building was represented as a MDOF lumped mass system. The published report does not provide enough data on the directionally coupled motion. Nonetheless, they reported that having a link connecting two high-rise buildings might increase the frequencies or reduce them due to the addition of the mass of the skybridge. Also, they suggested (0.8 H) as the most effective height for the skybridge that can reduce the dynamic response as much as possible. Another study (Lee, Kim, & Ko, 2012) considered two different buildings connected by a single skybridge and subjected to wind and earthquake loads. In addition, evaluation of coupling–control effect of a skybridge for adjacent high-rise buildings was considered; they introduced lead rubber bearings (LRB) and linear motion bearings (LMB) to model the connection between the skybridge and the two buildings. They investigated the response of the two structures with and without using lead rubbers and linear motion bearings seeking a means to minimize the dynamic response. They concluded that when

the skybridge is rigidly connected to high-rise buildings, the dynamic response increases because the skybridge increases the irregularity of the building. Another point is that when using LRBs, the dissipation increases up to 30 %, and when using dampers additionally to LRBs, the dissipation increases up to 100%.

In another study, (Zhao, Sun, & Zheng, 2009) discussed the finite-element model modification of a long steel skybridge to related actual dynamic properties that are obtained from the full-scale experiment. Analysis results show that the modal assurance criteria (MAC) values of the correlated structural modal shapes are all close to 1.0, which indicates a strong correlation between calculated and estimated structural modal shapes. The coupled building static response analysis of two high-rise buildings was made, and the modeling of the associated equivalent static wind loads using the HFFB measurement was presented (Chen & Kareem, 2005). Two building systems, coupled by a link and uncoupled, were evaluated through both a simple estimation method and spectral analysis, considering only the axial rigidity of the link (Behnamfar, Dorafshan, Taheri, & Hosseini Hashemi, 2016). Utilizing a semi-active control system utilizing a cable connecting the two structures was investigated as to its ability reduce wind-induced oscillation (Klein & Healey, 1987). A semi-active control system was recommended for a few reasons: an acceptable cost level, retrofit capability, minimal space requirements, and quite effective in removing unwanted kinetic energy. From the structural analysis and design perspective, a research study was conducted to present an optimization of high-rise buildings with hinge-connected skybridges with respect to those are with roller-connected skybridges (McCall & Balling, 2016).

1.2. Research Objective and Plan

An overview of the research plan is presented in Figure 3. The most common methods that are used to develop discretized high-rise buildings are finite element models and shear building models. In this study, the structural designs of existing of skybridges will be investigated in order to determine how best to model them. Of particular interest, will be determining the levels of complexity of the models needed in order to better predict the coupled response behavior of high-rise buildings connected by skybridges. More specifically, this study will scrutinize the force and moment coupling between skybridges and high-rise buildings where roller, hinge, or rigid connections are utilized. The selection of the various end conditions controls the dynamic degrees of freedom and influence the structural models used in the analysis of the high-rise building system. The structural model of the linked high-rise buildings will be subjected to a variety of strong ground motion loading time series records selected from earthquake events such as the 1994 Northridge and the 1940 El-Centro earthquakes in the United States, Umbro-Marchigiano earthquake in Turkey, Mexico City earthquake in Mexico, and NF17 (a part of SAC project) in Japan. The data sets will be carefully chosen from these global events to provide a range of peak ground accelerations and event durations. It is noted that model simulations in structural dynamics can be pursued in the time domain or frequency domain. This study will utilize the most effective way to perform the simulations and present the numerical results.

In this research study, a system of two high-rise buildings will be modeled using increasing levels of complexity. This will include better representations of the buildings

and skywalk geometries and their influence on the dynamic response behavior. Figure 4 presents a basic conservative (undamped) system involving twin high-rise buildings that are linked by a skybridge. In this case, each building is modeled as a single lumped mass located at the geometrical center of each building. These lumped masses are then connected by a frame member representing the skybridge, and based on previous research studies this has been determined to be a reasonable first pass model. This will be done for comparative purposes with previous studies. Next, the level of model complexity will be increased using MDOF models that distribute the mass at each floor of a building, which is important for cases where the buildings are not identical and connected by multiple skybridges. The response behavior of these various system models subjected to selected time domain records of the strong ground motion records will be investigated.

A system of two different high-rise buildings linked by a skybridge is presented in figure 5, and it represents a more general case that will be investigated. The length of the time domain simulation noticeably impacts the structurally coupled response of high-rise buildings linked by a skybridge. Further, the effect of the damping force is expected to also play a significant role the dynamic behavior, which includes flexure and torsional motions. A schematic of the multiple skybridge configurations is illustrated in figure 6. The dynamic response behavior of the building system will be influenced by the mass distribution, the axial and flexural rigidity of the individual buildings, their elevation, the skybridge geometrical configurations and the degree of connectivity they provide between the buildings. The degree to which different configurations will differ will be examined and quantified. A logical question to be considered is what is an optimal number of

skybridges and their elevations that minimize the coupled dynamic response behavior of the system?

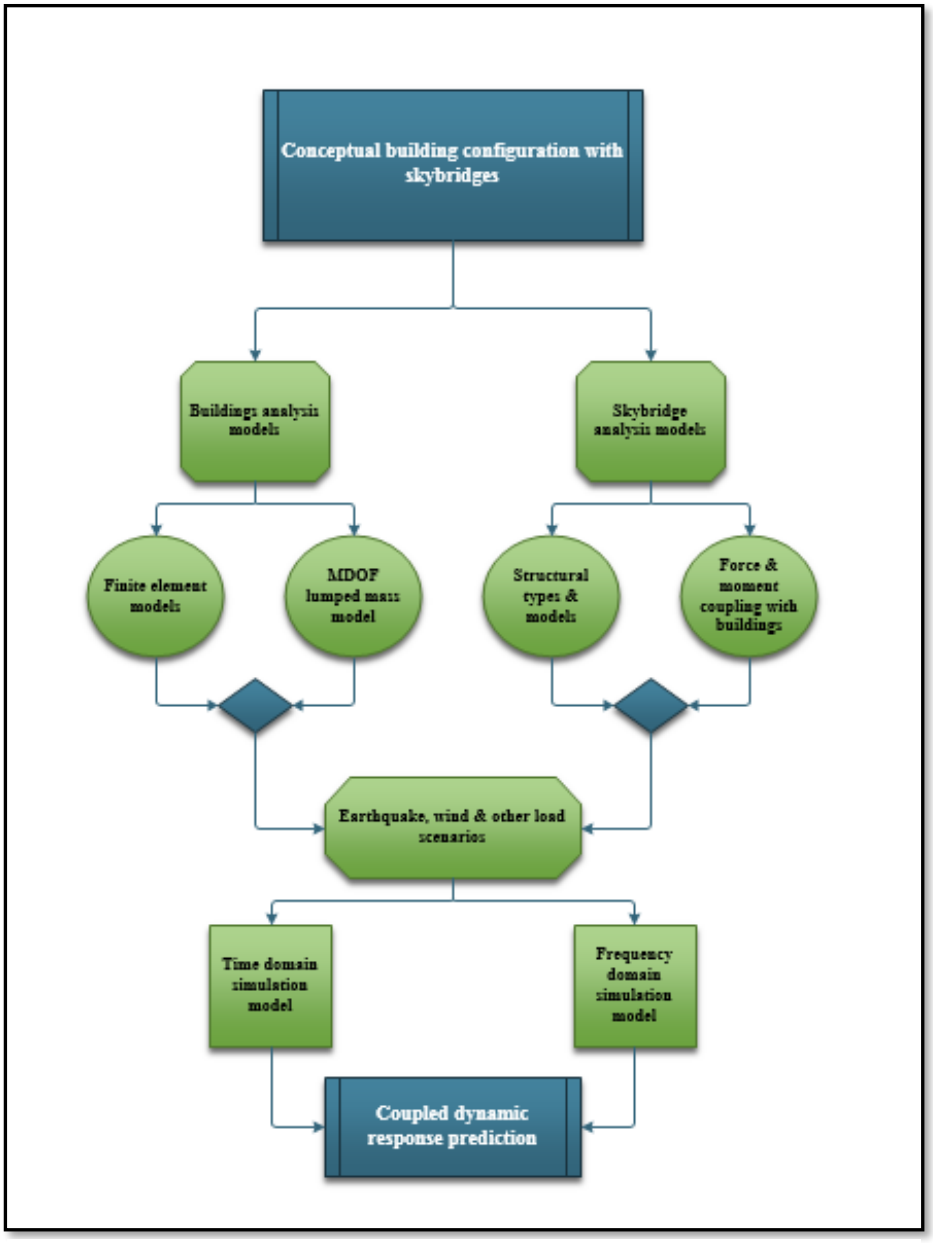

Figure 3. Overview of the research plan

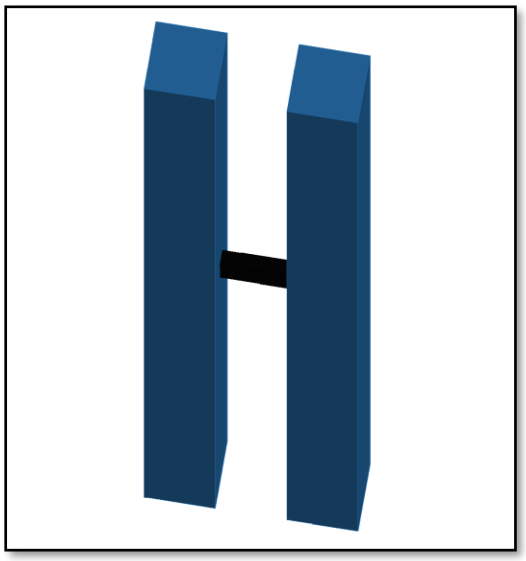

Figure 4. Twin buildings linked by a skybridge

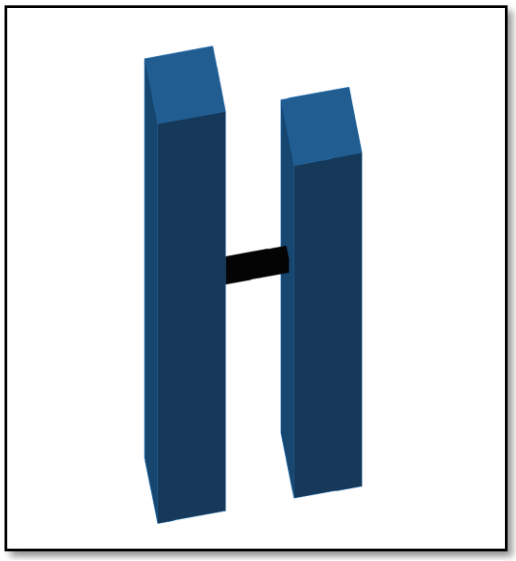

Figure 5. Different buildings linked by a skybridge

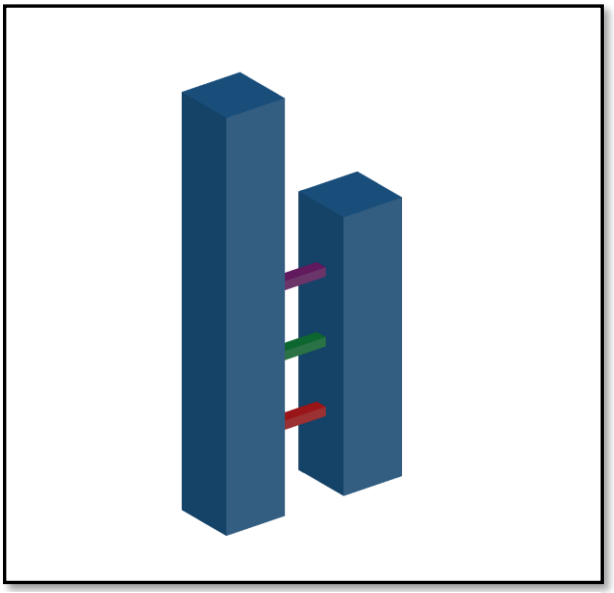

Figure 6. Different buildings linked by three skybridges

2. BUILDING AND SKYBRIDGE MODEL DEVELOPMENT

2.1. Engineering Models with Different Levels of Complexity

To calculate an approximate dynamic response, a building can be represented by an equivalent single lumped mass. Hence, a system of two independent buildings is modeled using two independent lumped masses. The geometry of the two independent buildings with respect to the global axis is indicated in figure 7.

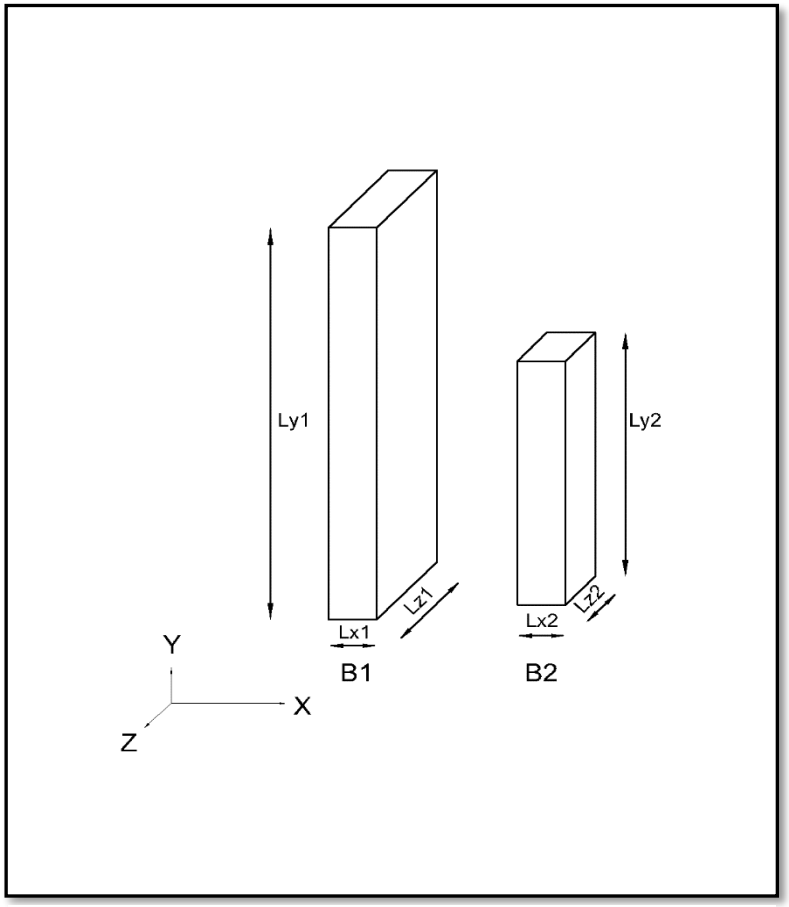

Figure 7. Two independent high-rise buildings

Each single mass has three translational degrees of freedom (u, w, v) and three rotational ones around the three global axes (θ_x, θ_z, θ_y). Figure 8 shows the dynamic degrees of freedom relative to the global axes. However, a more accurate simulation can be performed when using multiple lumped masses to represent each building -a single mass for every floor.

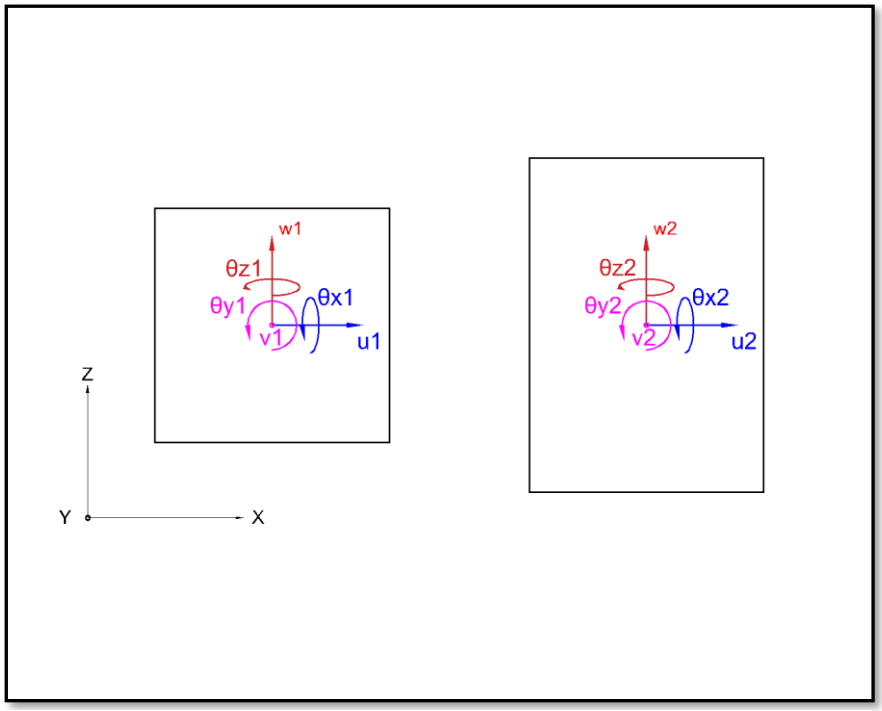

Figure 8. Dynamic degrees of freedom for two independent buildings

Architects are inclined to design the skybridge that links high-rise buildings in a way that achieves both functional and aesthetic goals. Generally, the most common skybridge section shapes are the circular and rectangular ones as shown in figure 9 and 10 respectively. Changing the geometrical characteristics of a skybridge gives different

dynamic coupling effects. It is worth mentioning that this study will deal with values of dynamic properties regardless of what shape of skybridge is used.

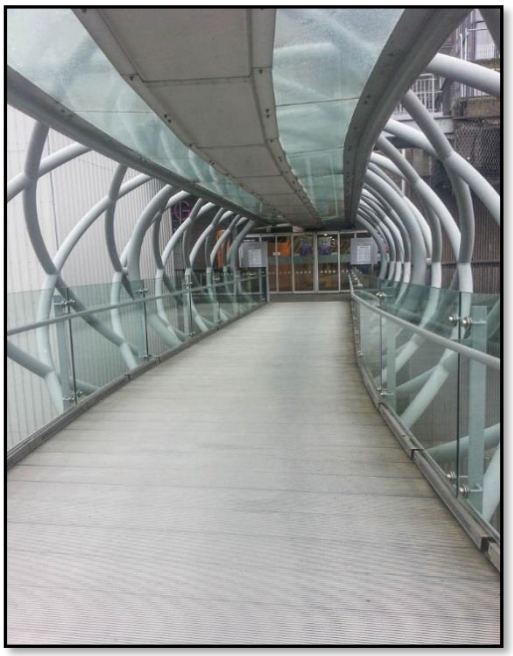

Figure 9. Circular Skybridge (Printed from "The World's Best Photos of skybridge and way - Flickr Hive Mind", 2017)

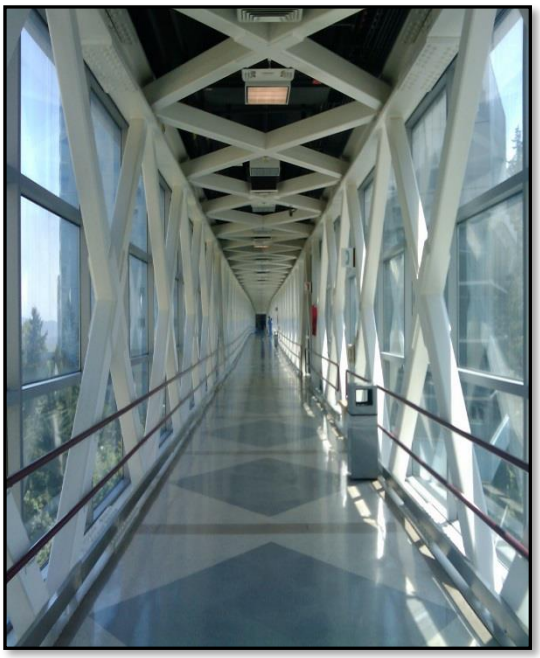

Figure 10. Rectangular Skybridge (Printed from "Skyway or the highway for teaching hospital - Austin Monitor", 2017)

Linking two independent buildings by a skybridge affects the dynamic response of the two-building due to the induced structural coupling between the two buildings. The structural coupling is dependent on the materials used to build it- steel or reinforced concrete, the height, and the supporting condition – a roller, hinge, or fixed support between its ends and the two buildings; the skybridge can be modeled as a truss or frame as shown in figure 11 and 12 respectively.

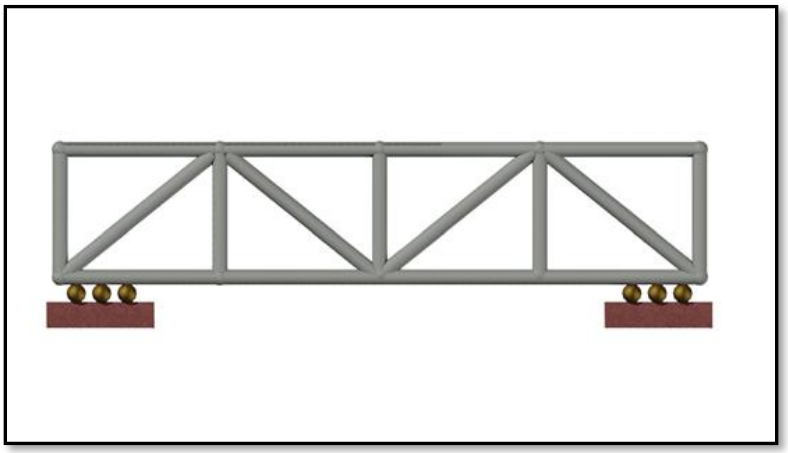

Figure 11. Truss skybridge with roller connections

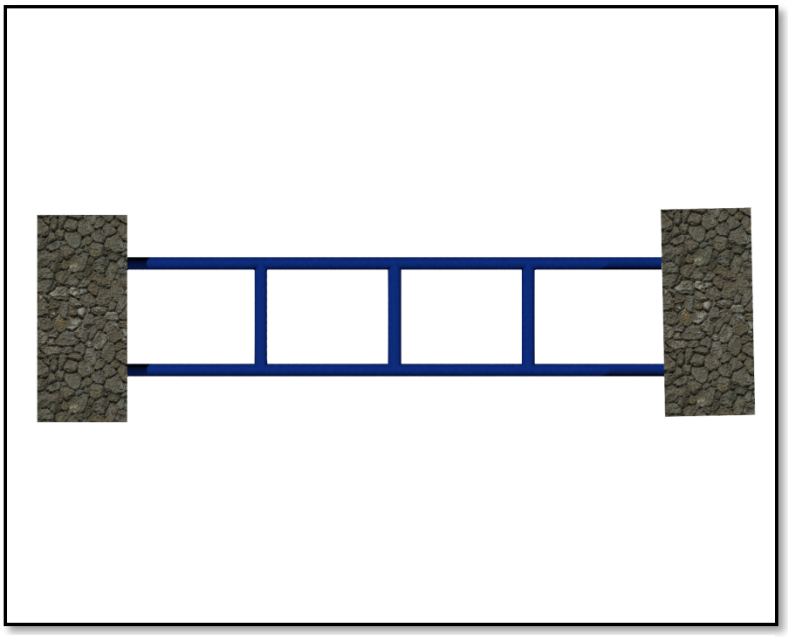

Figure 12. Frame skybridge with fixed connections

In addition, the length of skybridge plays an important role on the coupled dynamic response; some buildings are designed to be close to each other, 30 feet, that leads to short skybridges, while others are designed to have interconnecting by 60 feet length skybridges

or longer. When using multiple masses to model the two buildings, it becomes possible to connect the two buildings by inclined skybridge that connect different floor over the two buildings, which cannot be represented using a single mass.

The coupled dynamic response of linked high-rise buildings can also be calculated by using a single mass or multiple masses to model each building in the system by taking into account the effect of the structural coupling between the dynamic degrees of freedom. Figure 13 and 14 show the geometrical properties and the dynamic degrees of freedom of linked high-rise buildings respectively.

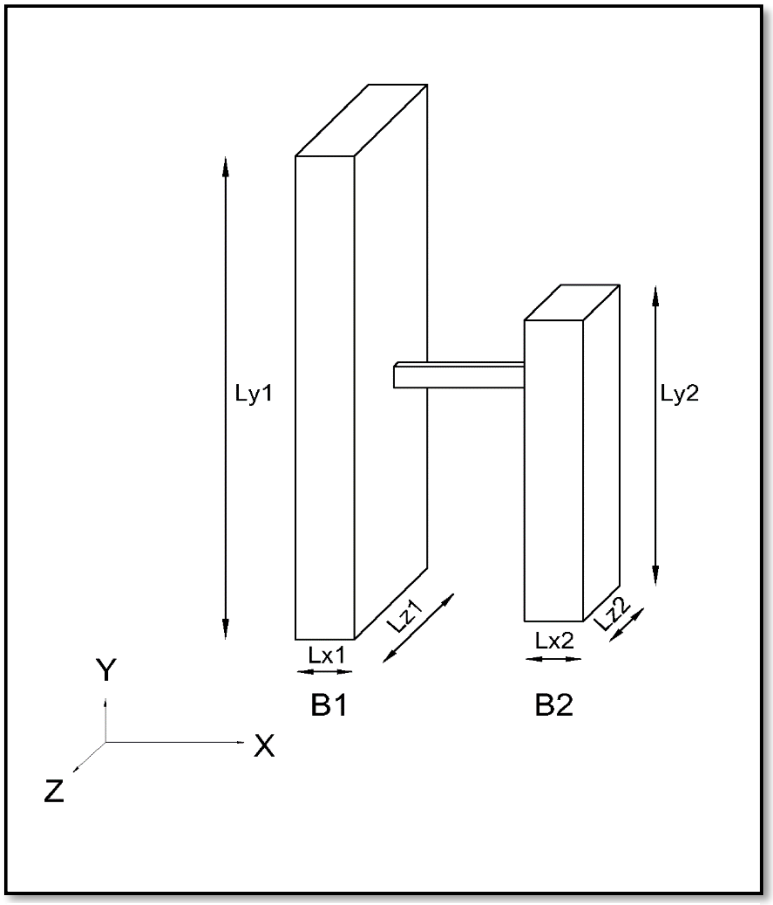

Figure 13. Two linked high-rise buildings

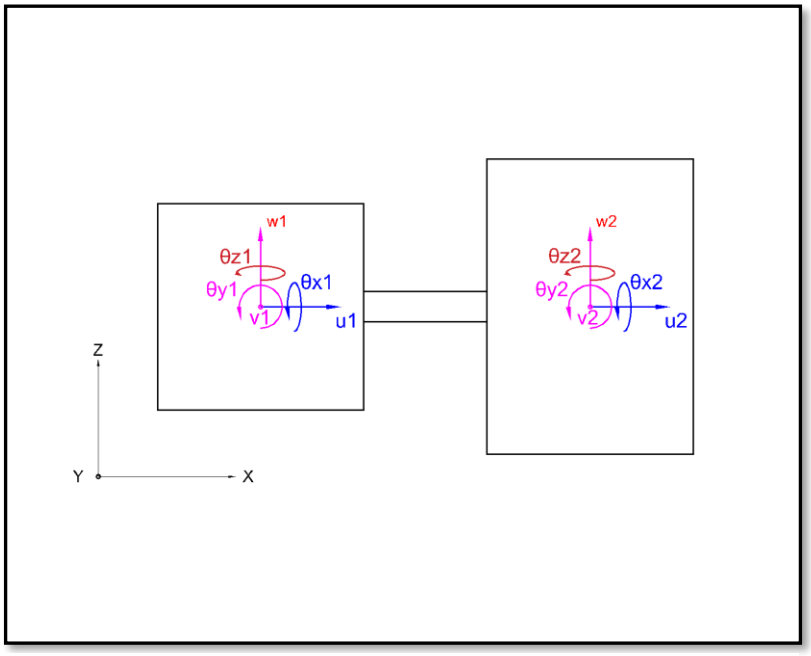

Figure 14. Dynamic degrees of freedom for two linked buildings

Using multiple masses to model each building enables us to accurately simulate systems of two high-rise buildings connected by multiple skybridges as shown in figure 6. Moreover, when using a single mass to model a building in a system of coupled buildings with a height ratio (*Ly1*/*Ly2*) relatively big -not close to one- concentrating the mass at the geometrical center of the buildings and connecting them by a horizontal skybridge is impossible. Whereas, by using multiple masses, different height ratios are considered (1-2).

2.2. General Matrix Formulation

For a 6-DOF model, such as those shown in figure 8 and figure14, the generalized displacement vector is of the form,

$$\{\delta_i\} = \{u_i \;\; w_i \;\; v_i \;\; \theta_{xi} \;\; \theta_{zi} \;\; \theta_{yi}\}^T \tag{1}$$

The generalized velocity and acceleration vectors can be obtained directly by differentiating the generalized displacement vector with respect to time. It follows then that the generalized velocity vector is

$$\{\dot{\delta}_i\} = \{\dot{u}_i \;\; \dot{w}_i \;\; \dot{v}_i \;\; \dot{\theta}_{xi} \;\; \dot{\theta}_{zi} \;\; \dot{\theta}_{yi}\}^T \tag{2}$$

And the generalized acceleration vector is

$$\{\ddot{\delta}_i\} = \{\ddot{u}_i \;\; \ddot{w}_i \;\; \ddot{v}_i \;\; \ddot{\theta}_{xi} \;\; \ddot{\theta}_{zi} \;\; \ddot{\theta}_{yi}\}^T \tag{3}$$

2.2.1. Inertial Force

The inertia force can be expressed as

$$\{F_m\} = [M]\{\ddot{\delta}\} \tag{4}$$

Where $\{F_m\}$ is the inertia force vector, $[M]$ is the mass and mass moment of inertia matrix, and $\{\ddot{\delta}\}$ is the dynamic acceleration vector.

For two lumped masses connected by a frame member as shown in figure 15, the inertia force is

$$\{F_m\} = \{F_1 \;\; F_2\}^T \tag{5}$$

$$\{F_1\} = \{m_1\ddot{u}_1 \;\; m_1\ddot{w}_1 \;\; m_1\ddot{v}_1 \;\; m_1\ddot{\theta}_{x1} \;\; m_1\ddot{\theta}_{z1} \;\; m_1\ddot{\theta}_{y1}\} \tag{6}$$

or

$$\{F_1\} = \{Pm_{x1}\ \ Pm_{z1}\ \ Pm_{y1}\ \ Mm_{x1}\ \ Mm_{z1}\ \ Mm_{y1}\} \tag{7}$$

$$\{F_2\} = \{Pm_{x2}\ \ Pm_{z2}\ \ Pm_{y2}\ \ Mm_{x2}\ \ Mm_{z2}\ \ Mm_{y2}\} \tag{8}$$

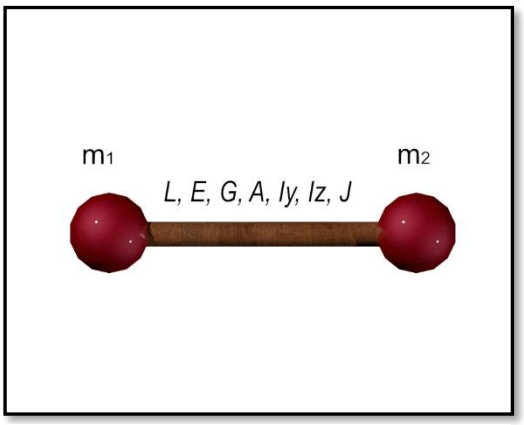

Figure 15. Two linked lumped masses

And the corresponding mass matrix is

$$[M] = \begin{bmatrix} m_1 & & & & & & & & & & & \\ & m_1 & & & & & & & & & & \\ & & m_1 & & & & & & & & & \\ & & & I_{mx1} & & & & & & & & \\ & & & & I_{mz1} & & & & zeros & & & \\ & & & & & I_{my1} & & & & & & \\ & & & & & & m_2 & & & & & \\ & & zeros & & & & & m_2 & & & & \\ & & & & & & & & m_2 & & & \\ & & & & & & & & & I_{mx2} & & \\ & & & & & & & & & & I_{mz2} & \\ & & & & & & & & & & & I_{my2} \end{bmatrix} \tag{9}$$

It is clear that [*M*] is a diagonal matrix, accordingly, it is applicable whether the member connecting between the mass is parallel to the global axes or not. The mass matrix is mapped to the mass matrix of the whole system [M_{sys}].

$$\left[M_{sys}\right]=\begin{bmatrix} [m_{11}] & [0] & \cdots & [0] & \cdots & [0] & \cdots & [0] \\ [0] & [m_{22}] & \cdots & [0] & \cdots & [0] & \cdots & [0] \\ \vdots & \vdots & \ddots & \vdots & \cdots & \vdots & \cdots & \vdots \\ [0] & [0] & \cdots & [m_{ii}] & \cdots & [0] & \cdots & [0] \\ \vdots & \vdots & \vdots & \vdots & \ddots & \vdots & \cdots & \vdots \\ [0] & [0] & \cdots & [0] & \cdots & [m_{jj}] & \cdots & [0] \\ \vdots & \vdots & \vdots & \vdots & \vdots & \vdots & \ddots & \vdots \\ [0] & [0] & \cdots & [0] & \cdots & [0] & \cdots & [m_{nn}] \end{bmatrix} \tag{10}$$

Where *n* is the number of the lumped masses which are used to represent the whole system. Hence, the generalized inertia force can be expressed as,

$$\left\{F_{m-sys}\right\}=\left[M_{sys}\right]\left\{\ddot{\delta}_{sys}\right\} \tag{11}$$

2.2.2. Elastic Force

In general, there are three types of rigidities in any structural element. These are axial (*EA*), flexural (*EI*), and torsional (*GJ*) rigidity. Where (*E*) is the elastic modulus, (*G*) shear modulus, (*A*) is the cross-sectional area, (*I*) is the moment of inertia, and (*J*) is the polar moment of inertia. Each rigidity induces a stiffness that corresponds to a certain axial, shear, moment, or torsional force. Due to the equilibrium in structures, force components are coupled. For example, shear and moments in a structural member are coupled and affected by each other. This requires a stiffness matrix that covers all

structural couplings in a structural member subjected to all perspective external loads as indicated in figure 16. Assumptions were used to simplify the problems as listed below:

1. The material of the members is isotropic and homogenous.
2. The Modulus of Elasticity (*E*) is the same for tension and compression.
3. The transverse sections remain plane after bending.

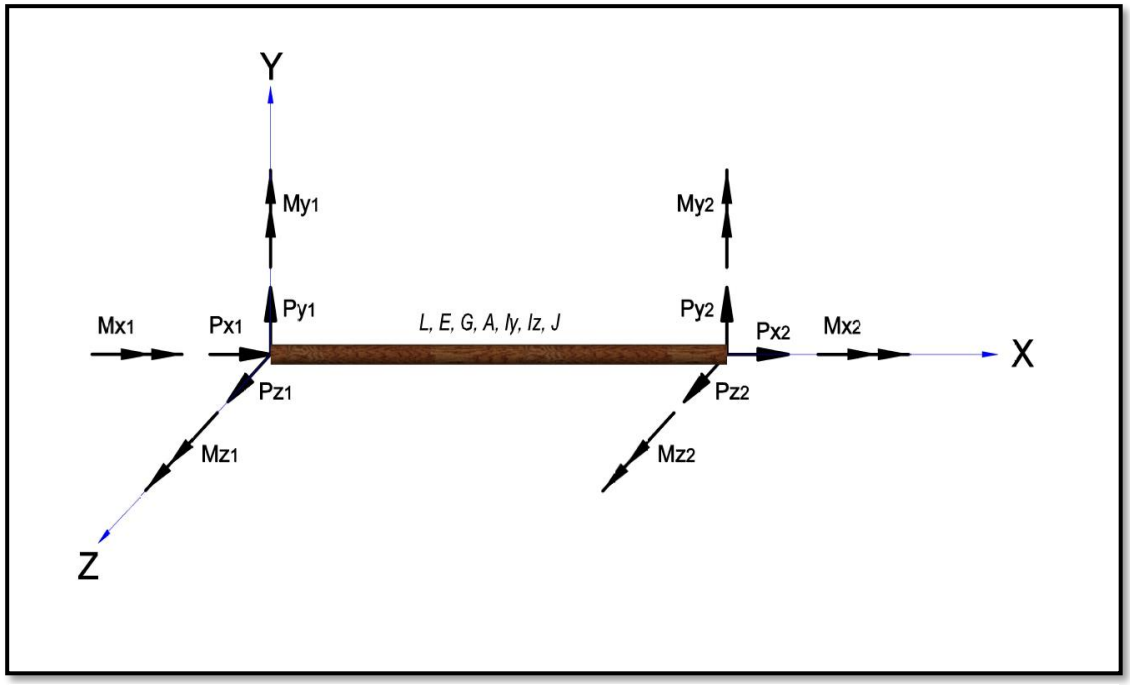

Figure 16. Free body diagram of a frame member in a 3D-space along x-axis

These forces are connected to the corresponding translational and rotational displacements as shown below.

$$\{F_s\} = [K]\{\delta\} \tag{12}$$

Where $\{F_s\}$ is the stiffness force vector, $[K]$ is a stiffness matrix and $\{\delta\}$ is the dynamic displacement vector.

$$\{Fs_{12}\} = \{Ps_{x1}\ \ Ps_{z1}\ \ Ps_{y1}\ \ Ms_{x1}\ \ Ms_{z1}\ \ Ms_{y1}\ \ Ps_{x2}\ \ Ps_{z2}\ \ Ps_{y2}\ \ Ms_{x2}\ \ Ms_{z2}\ \ Ms_{y2}\}^T \tag{13}$$

$$\{\delta_{12}\} = \{\, u_1 \quad w_1 \quad v_1 \quad \theta_{x1} \quad \theta_{z1} \quad \theta_{y1} \quad u_2 \quad w_2 \quad v_2 \quad \theta_{x2} \quad \theta_{z2} \quad \theta_{y2}\}^T \tag{14}$$

$$
\left[K_{local}{}'\right] = \begin{bmatrix}
\frac{EA}{L} & & & & & & & & & & & \\
0 & \frac{12EI_z}{L^3} & & & & & & & & & & \\
0 & 0 & \frac{12EI_y}{L^3} & & & & & & & & & \\
0 & 0 & 0 & \frac{GJ}{L} & & & & & & & & \\
0 & 0 & \frac{-6EI_y}{L^2} & 0 & \frac{4EI_y}{L} & & & & & & & \\
0 & \frac{6EI_z}{L^2} & 0 & 0 & 0 & \frac{4EI_z}{L} & & & & & & \\
\frac{-EA}{L} & 0 & 0 & 0 & 0 & 0 & \frac{EA}{L} & & & & & \\
0 & \frac{-12EI_z}{L^3} & 0 & 0 & 0 & \frac{-6EI_z}{L^2} & 0 & \frac{12EI_z}{L^3} & & & & \\
0 & 0 & \frac{-12EI_y}{L^3} & 0 & \frac{6EI_y}{L^2} & 0 & 0 & 0 & \frac{-12EI_y}{L^3} & & & \\
0 & 0 & 0 & \frac{-GJ}{L} & 0 & 0 & 0 & 0 & 0 & \frac{GJ}{L} & & \\
0 & 0 & \frac{-6EI_y}{L^2} & 0 & \frac{2EI_y}{L} & 0 & 0 & 0 & \frac{6EI_y}{L^2} & 0 & \frac{4EI_y}{L} & \\
0 & \frac{6EI_z}{L^2} & 0 & 0 & 0 & \frac{2EI_z}{L} & 0 & \frac{-6EI_z}{L^2} & 0 & 0 & 0 & \frac{4EI_z}{L}
\end{bmatrix} \qquad (15)
$$

Symmetric

The above stiffness matrix is applicable to a member that is parallel to the x-axis. In order to make the stiffness matrix applicable to any member in the 3D-space, rotations about the three global axes must be considered as will be discussed later. Since this stiffness matrix is used to present a model of two high-rise buildings, not a frame, an additional coupling has to be considered due to the geometrical condition. A skybridge that connects two high-rise buildings is not linking the centers of the buildings. It connects the close sides of the two buildings. Accordingly, the distance from the center of the building to the end of the skybridge forms an arm of the z-translational component, causing a moment in the building about its y-axis as indicated in figure 17. Hence, the dynamic response of the building system necessarily impacted in the translational x-direction and rotational y-direction mainly and the other components indirectly. The inclusion of this effect has not been considered in prior work into coupled buildings modeled using a lumped-mass approach. As such, this modeling coupling effect is termed "Shape Coupling" in this research" and presents an enhancement over prior models for coupled buildings.

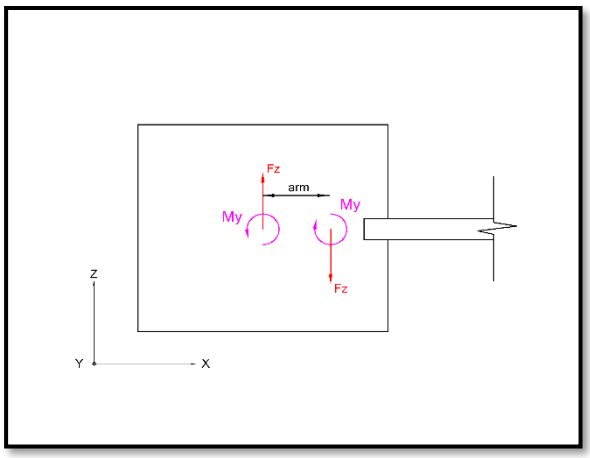

Figure 17. Shape coupling in coupled buildings

2.2.3. Skybridge Considerations

The effect of shape coupling is taken into account by adding the equivalent moment of the difference of the translational z-component displacements at the ends of the skybridge multiplied by the corresponding skybridge stiffness. The induced force causes a torsional force with an arm equals a half of the width of each building. On the other side, the torsional component in each building causes a translational force on the connected end of the skybridge.

$$[K_{sc}] = \begin{bmatrix}
0 & 0 & 0\,0\,0 & 0 & 0 & 0 & 0\,0\,0 & 0 \\
0 & 0 & 0\,0\,0 & \frac{12EI_z}{L^3}\times arm_1 & 0 & 0 & 0\,0\,0 & 0 \\
0 & 0 & 0\,0\,0 & 0 & 0 & 0 & 0\,0\,0 & 0 \\
0 & 0 & 0\,0\,0 & 0 & 0 & 0 & 0\,0\,0 & 0 \\
0 & 0 & 0\,0\,0 & 0 & 0 & 0 & 0\,0\,0 & 0 \\
0 & \frac{-12EI_z}{L^3\times arm_1} & 0\,0\,0 & 0 & 0 & \frac{12EI_z}{L^3\times arm_1} & 0\,0\,0 & 0 \\
0 & 0 & 0\,0\,0 & 0 & 0 & 0 & 0\,0\,0 & 0 \\
0 & 0 & 0\,0\,0 & 0 & 0 & 0 & 0\,0\,0 & \frac{-12EI_z}{L^3}\times arm_2 \\
0 & 0 & 0\,0\,0 & 0 & 0 & 0 & 0\,0\,0 & 0 \\
0 & 0 & 0\,0\,0 & 0 & 0 & 0 & 0\,0\,0 & 0 \\
0 & 0 & 0\,0\,0 & 0 & 0 & 0 & 0\,0\,0 & 0 \\
0 & \frac{-12EI_z}{L^3\times arm_2} & 0\,0\,0 & 0 & 0 & \frac{12EI_z}{L^3\times arm_2} & 0\,0\,0 & 0
\end{bmatrix} \quad (16)$$

arm_1= the distance from the end of the link to the geometrical center of building 1

arm_2= the distance from the end of the link to the geometrical center of building 2

$$[K_{local}] = [K_{local}'] + [K_{sc}] \quad (17)$$

2.2.4. Transformation of Coordinates

The rotation about the x-axis alerts values of the moment of inertia (I_y and I_z are affected), and this rotation is taken into account by considering the values of the moment of inertia with respect to the global axes. The second perspective rotation in the member is about the z-axis that is shown in figure 18. In this case, the member is parallel to the xy-plane forming an angle of rotation (α) with the x-axis. Hence, a transformation matrix is derived below to rotate the degrees of freedoms from the local axes, the local x-axis is parallel to the inclined member, to be parallel to the global axes.

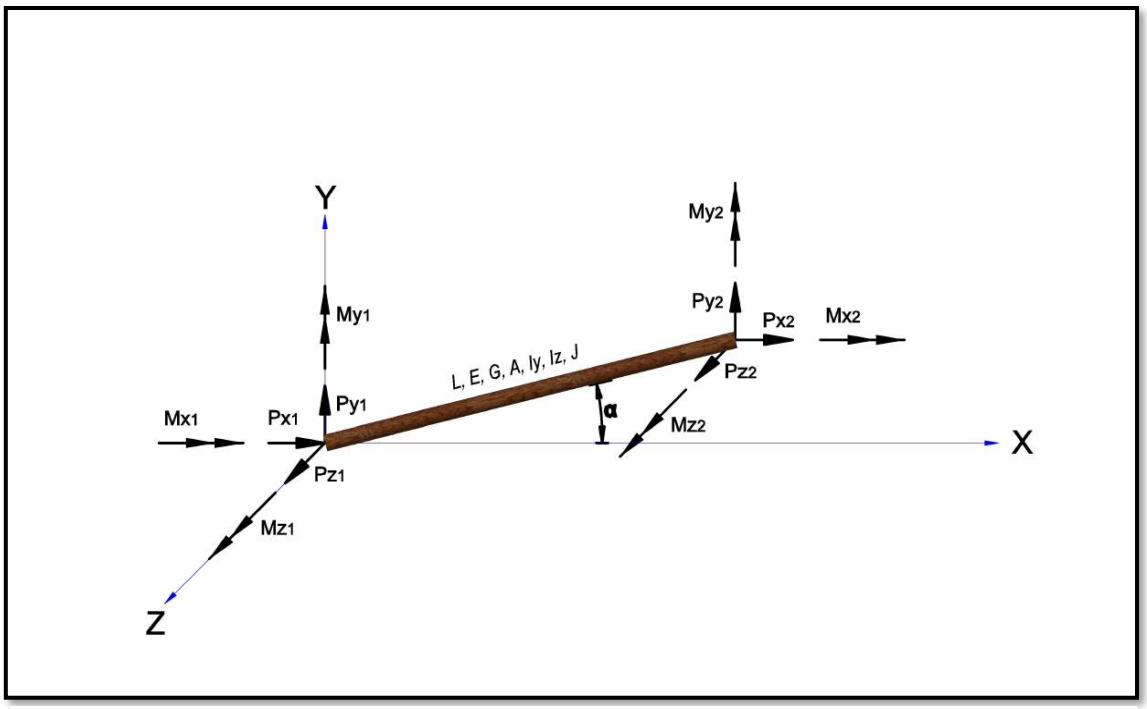

Figure 18. Free body diagram of a frame member in a 3D-space with an angle of rotation (α)

$$\{Fs_{local}\} = [R_z]\{F_s\} \tag{18}$$

$$\{\delta_{local}\} = [R_z]\{\delta\} \tag{19}$$

Then

$$[R_z]^{-1}\{Fs_{local}\} = [K][R_z]^{-1}\{\delta_{local}\} \tag{20}$$

or

$$\{Fs_{local}\} = [R_z][K][R_z]^{-1}\{\delta_{local}\} \tag{21}$$

but

$$\{Fs_{local}\} = [K_{local}]\{\delta_{local}\} \tag{22}$$

then

$$[K_{local}] = [R_z][K][R_z]^{-1} \tag{23}$$

or

$$[K] = [R_z]^{-1}[K_{local}][R_z] \tag{24}$$

hence

$$\{F_s\} = [R_z]^{-1}[K_{local}][R_z]\{\delta\} \tag{25}$$

where

$$[R_z] = \begin{bmatrix} [r_z] & & & \\ & [r_z] & & \\ & & [r_z] & \\ & & & [r_z] \end{bmatrix} \tag{26}$$

and

$$[r_z] = \begin{bmatrix} \cos\alpha & \sin\alpha & 0 \\ -\sin\alpha & \cos\alpha & 0 \\ 0 & 0 & 1 \end{bmatrix} \tag{27}$$

Another perspective rotation is presented by rotating the member about the global y-axis; the member is parallel to xz-plane and having an angle of rotation (β) with the global x-axis as shown in figure 19. The same procedure of (α) rotation is applied to (β); equation 44 is obtained.

$$[K] = [R_y]^{-1}[K_{local}][R_y] \tag{28}$$

or

$$\{F_s\} = [R_y]^{-1}[K_{local}][R_y]\{\delta\} \tag{29}$$

where

$$\left[R_y\right] = \begin{bmatrix} \left[r_y\right] & & & \\ & \left[r_y\right] & & \\ & & \left[r_y\right] & \\ & & & \left[r_y\right] \end{bmatrix} \tag{30}$$

and

$$\left[r_y\right] = \begin{bmatrix} \cos\beta & 0 & \sin\beta \\ 0 & 1 & 0 \\ -\sin\beta & 0 & \cos\beta \end{bmatrix} \tag{31}$$

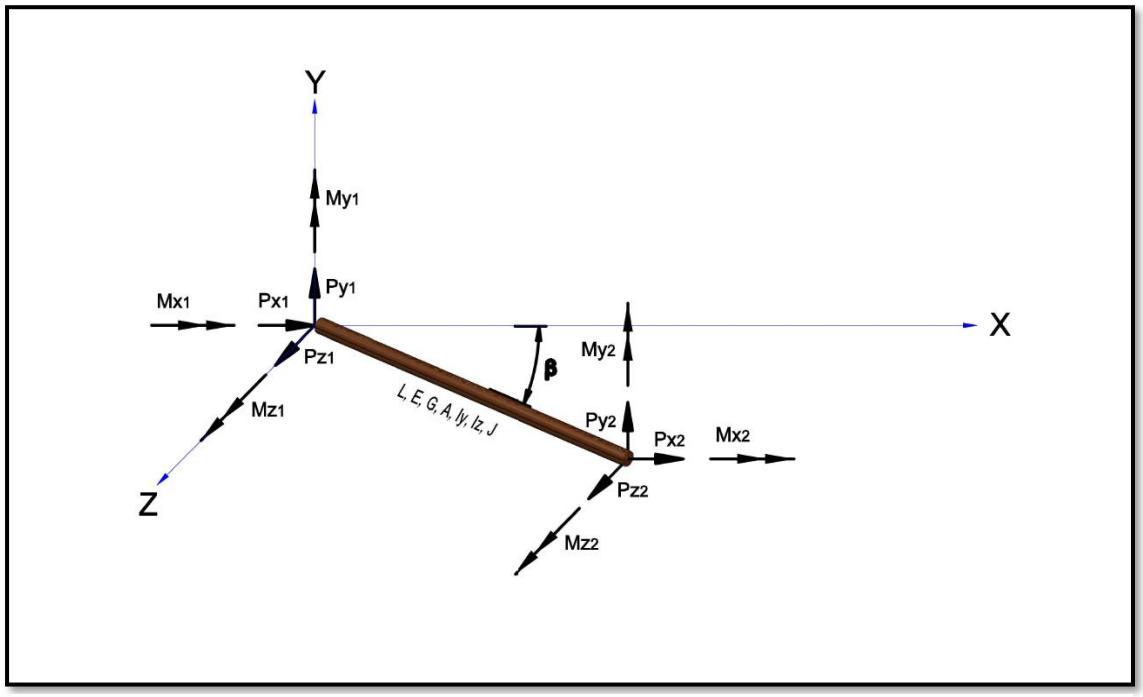

Figure 19. Free body diagram of a frame member in a 3D-space with an angle of rotation (β)

By considering the combined effect of (α) and (β), the stiffness matrix is obtained as illustrated below.

$$\{F_s\} = [R_y]^{-1}[R_z]^{-1}[K_{local}][R_z][R_y]\{\delta\} \tag{32}$$

and

$$[K] = [R_y]^{-1}[R_z]^{-1}[K_{local}][R_z][R_y] \tag{33}$$

or

$$[K] = [R_{zy}]^{-1}[K_{local}][R_{zy}] = [R_{yz}]^{-1}[K_{local}][R_{yz}] \tag{34}$$

where

$$[R_{zy}] = [R_z][R_y] \tag{35}$$

$$[R_{yz}] = [R_y][R_z] \tag{36}$$

$$[R_{zy}] = \begin{bmatrix} [r_{zy}] & & & \\ & [r_{zy}] & & \\ & & [r_{zy}] & \\ & & & [r_{zy}] \end{bmatrix} \tag{37}$$

$$[r_{zy}] = \begin{bmatrix} \cos\alpha\cos\beta & \sin\alpha & \cos\alpha\sin\beta \\ -\sin\alpha\cos\beta & \cos\alpha & -\sin\alpha\sin\beta \\ -\sin\beta & 0 & \cos\beta \end{bmatrix} \tag{38}$$

[K] Is mapped to the stiffness matrix of the whole system (n-MDOF lumped masses). Let [K_{ij}] be the stiffness matrix for a member connecting between i-th and j-th joints in the MDOF system.

$$\left[K_{ij}\right]=\left[R_{zy}\right]^{-1}\left[K_{ij\_local}\right]\left[R_{zy}\right] \tag{39}$$

Then

$$\left[K_{ij}\right]=\left[\begin{array}{ccc:ccc} k_{1,1} & \cdots & k_{1,6} & k_{1,7} & \cdots & k_{1,12} \\ \vdots & \ddots & \vdots & \vdots & \ddots & \vdots \\ k_{6,1} & \cdots & k_{6,6} & k_{6,7} & \cdots & k_{6,12} \\ \hdashline k_{7,1} & \cdots & k_{7,6} & k_{7,7} & \cdots & k_{7,12} \\ \vdots & \ddots & \vdots & \vdots & \ddots & \vdots \\ k_{12,1} & \cdots & k_{12,6} & k_{12,7} & \cdots & k_{12,12} \end{array}\right] \tag{40}$$

Note: the general forms of calculating the elements of the matrix above are listed in the appendix.

$$\left[K_{ij}\right]=\left[\begin{array}{c:c} \left[k_{ij-ii}\right] & \left[k_{ij-ij}\right] \\ \hdashline \left[k_{ij-ji}\right] & \left[k_{ij-jj}\right] \end{array}\right] \tag{41}$$

The way to map $[K_{ij}]$ to the general stiffness matrix of a structural system of *n*-MDOF lumped masses is as shown in the general stiffness matrix of the whole system.

$$\left[K_{sys}\right]=\begin{bmatrix} [\,][\,]\cdots & [\,] & \cdots & [\,] & \cdots & [\,] \\ [\,][\,]\cdots & [\,] & \cdots & [\,] & \cdots & [\,] \\ \vdots\ \vdots\ \ddots & \vdots & \cdots & \vdots & \cdots & \vdots \\ [\,][\,]\cdots & \left[k_{ij-ii}\right] & \cdots & \left[k_{ij-ij}\right] & \cdots & [\,] \\ \vdots\ \vdots\ \vdots & \vdots & \ddots & \vdots & \cdots & \vdots \\ [\,][\,]\cdots & \left[k_{ij-ji}\right] & \cdots & \left[k_{ij-jj}\right] & \cdots & [\,] \\ \vdots\ \vdots\ \vdots & \vdots & \vdots & \vdots & \ddots & \vdots \\ [\,][\,]\cdots & [\,] & \cdots & [\,] & \cdots & [\,] \end{bmatrix} \tag{42}$$

2.2.5. Damping Force

The generalized damping force can be expressed as

$$\{F_s\} = [C]\left\{\dot{\delta}\right\} \tag{43}$$

$$\left\{\dot{\delta}_{sys}\right\} = \left\{\left\{\dot{\delta}_1\right\} \left\{\dot{\delta}_2\right\} \cdots \left\{\dot{\delta}_i\right\} \cdots \left\{\dot{\delta}_j\right\} \cdots \left\{\dot{\delta}_n\right\}\right\}^T \tag{44}$$

Rayleigh Damping was used to calculate the damping force matrix [C_{sys}] of the system, depending on the mass and stiffness matrices of the whole system.

$$\left[C_{sys}\right] = \left\{a_{sys0}\right\}\left[M_{sys}\right] + \left\{a_{sys1}\right\}\left[K_{sys}\right] \tag{45}$$

where

$\{a_{sys0}\}$ is the mass proportional Rayleigh damping coefficient matrix.

$\{a_{sys1}\}$ is the stiffness proportional Rayleigh damping coefficient matrix.

Both $\{a_{sys0}\}$ and $\{a_{sys1}\}$ are calculated depending on the low natural frequencies of each component of response by using Matlab.

3. MATLAB CODE VALIDATION

The Matlab code that was developed was designed to perform the analysis of a large DOF with linkage for multiple skybridges. The focus of the research study is to investigate the dynamic response of high-rise building systems with 1 to 6 skybridges. The Matlab code enables us to analyze systems of two high-rise buildings (twin or different). This Matlab code calculates natural frequencies for various force components, considering the structural coupling and their related modal shapes. A number of verification models were analyzed and the results were compared with those obtained by using SAP2000. Table 1 provides information on the number of lumped masses in each building and the number and locations of skybridges that are used to connect them.

Table 1. Verification models

Model	Number of stories (B1)	Number of stories (B2)	Linked stories	Comments
1	1	1	1	VM1
2	2	2	1&2	
3	2	2	1	
4	2	2	2	VM2
5	2	1	1	
6	3	3	1&2&3	
7	3	3	1	
8	3	3	3	
9	3	1	1	
10	10	10	5&10	
11	10	6	5	VM3

3.1. Verification Model One (VM1)

This model is the first pass model representing two identical buildings, each modeled by a single mass, that are linked by a skybridge shown in figure 20. The height of the vertical members is 120 in, and the values of the equivalent spring flexural rigidity (*EI*) and torsional rigidity (*GJ*) are 133.33×10^6 lb.in^2 and 112.8×10^6 lb.in^2 respectively. The value of mass is 6.47 kip.sec^2/in^4. The horizontal frame member has a length of 120 in with axial and flexural rigidities equal to 4×10^6 lb and 133.33×10^6 lb.in^2 respectively.

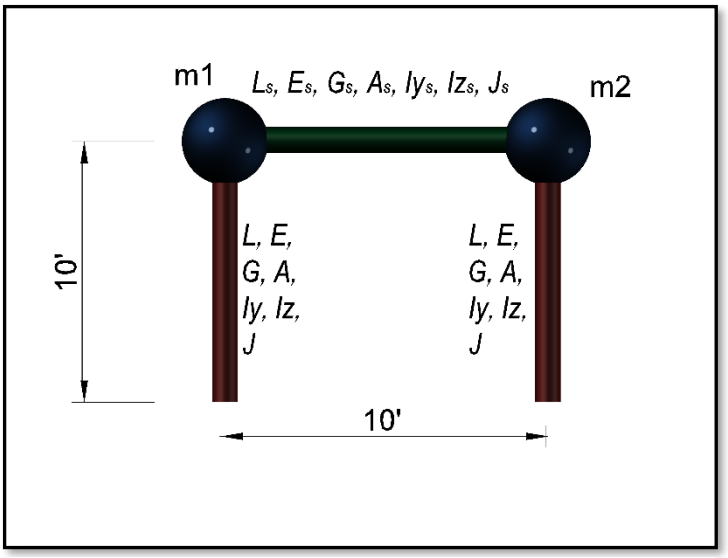

Figure 20. Verification model one (VM1)

The verification model one (VM1) was also modeled by a 2D portal frame with lumped masses connected by frame members using SAP2000. The modal properties and dynamic response that are corresponding to the two horizontal dynamic displacements and torsional displacement were considered. As we can see in table 2, the natural frequencies obtained from the Matlab coding are almost the same as those obtained from SAP2000. The maximum error value is 1%.

Table 2. Natural frequencies for verification model one (VM1)

Verification Model Number One (VM1)			
Mode shape	Natural frequency (Hz)		Error (%)
	SAP2000	Matlab	$\lvert F_S - F_M \rvert / F_S \times 100$
1	1.90	1.90	0.00
2	16.27	16.27	0.00
3	1.90	1.90	0.00
4	2.13	2.11	0.70

Table 3 provides information on the modal shapes for the Matlab and SAP2000 solutions, and it can be seen that they are also very close. These results, as a first verification model, indicate that the effects of structural coupling are correctly considered in the equations of motion regarding the linked high-rise buildings.

Table 3. Mode shapes for verification model one (VM1)

Verification Model Number One (VM1)						
mode shape (1)						
mass	SAP2000			Matlab		
	trans (x)	trans (z)	rot (y)	trans (x)	trans (z)	rot (y)
1		1	0	1	0	0
2		1	0	1	0	0
mode shape (2)						
mass	SAP2000			Matlab		
	trans (x)	trans (z)	rot (y)	trans (x)	trans (z)	rot (y)
1	1	0	0	1	0	0
2	-1	0	0	-1	0	0
mode shape (3)						
mass	SAP2000			Matlab		
	trans (x)	trans (z)	rot (y)	trans (x)	trans (z)	rot (y)
1	0	1	0	0	1	0
2	0	1	0	0	1	0
mode shape (4)						
mass	SAP2000			Matlab		
	trans (x)	trans (z)	rot (y)	trans (x)	trans (z)	rot (y)
1	0	1	-0.0146	0	1	-0.0148
2	0	-1	-0.0146	0	-1	-0.0148

Sine wave dynamic loading was applied to both Matlab and SAP2000 models. Figure 21 and 22 show the dynamic response of both of the two masses in the VM1 in the x-direction. It is the same as the z-direction. Figure 20 was obtained from the Matlab solution, whereas figure 21 was obtained from SAP2000. Accordingly, all previous results for VM1 refer to that the Matlab coding was generated correctly.

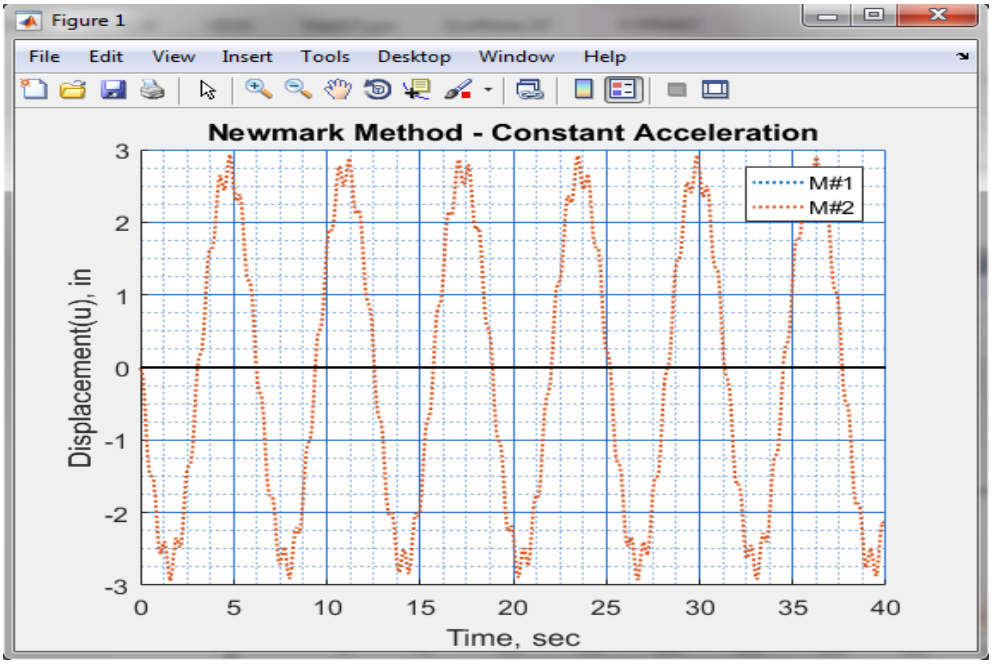

Figure 21. Dynamic response of VM1 by Matlab (u and w are identical)

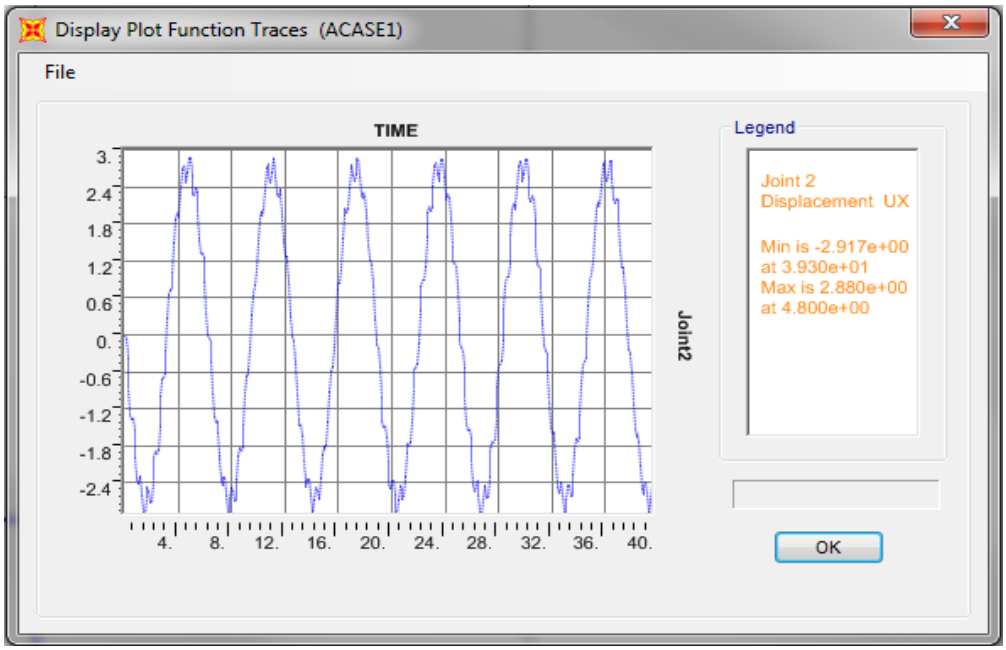

Figure 22. Dynamic response of VM1by SAP2000 (u and w are identical)

3.2. Verification Model Two (VM2)

The second verification model is similar to the first verification model (VM1) in all dynamic and geometrical properties. However, in this case, it has a total of four lumped masses, two per building, as shown in figure 23. VM2 has significantly more changes in the numerical solution steps as a result of the existence of a vertical coupling between lumped masses in addition to the horizontal coupling due to the links. As shown in table 4 and table 5 the modal shapes and the corresponding frequencies obtained from Matlab and SAP2000 match.

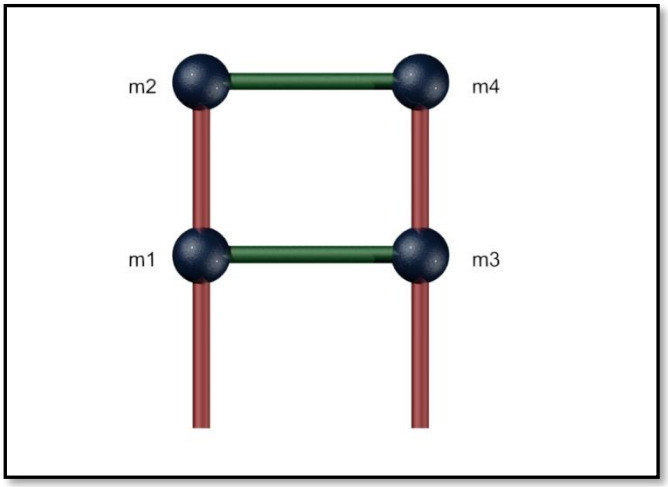

Figure 23. Verification model two (VM2)

Table 4. Mode shapes for verification model two (MV2)

Verification Model Number Two (VM2)						
mode shape (1)						
mass	SAP2000			Matlab		
	trans (x)	trans (z)	rot (y)	trans (x)	trans (z)	rot (y)
1	0.618	0	0	0.618	0	0
2	1	0	0	1	0	0
3	0.618	0	0	0.618	0	0
4	1	0	0	1	0	0
mode shape (2)						
mass	SAP2000			Matlab		
	trans (x)	trans (z)	rot (y)	trans (x)	trans (z)	rot (y)
1	1	0	0	1	0	0
2	-0.618	0	0	-0.618	0	0
3	1	0	0	1	0	0
4	-0.618	0	0	-0.618	0	0
mode shape (3)						
mass	SAP2000			Matlab		
	trans (x)	trans (z)	rot (y)	trans (x)	trans (z)	rot (y)
1	-0.618	0	0	-0.618	0	0
2	-1	0	0	-1	0	0
3	0.618	0	0	0.618	0	0
4	1	0	0	1	0	0
mode shape (4)						
mass	SAP2000			Matlab		
	trans (x)	trans (z)	rot (y)	trans (x)	trans (z)	rot (y)
1	1	0	0	1	0	0
2	-0.618	0	0	-0.618	0	0
3	-1	0	0	-1	0	0
4	0.618	0	0	0.618	0	0
mode shape (5)						
mass	SAP2000			Matlab		
	trans (x)	trans (z)	rot (y)	trans (x)	trans (z)	rot (y)
1	0	0.618	0	0	0.618	0
2	0	1	0	0	1	0
3	0	0.618	0	0	0.618	0
4	0	1	0	0	1	0

Table 4. Continues

mode shape (6)						
mass	SAP2000			Matlab		
	trans (x)	trans (z)	rot (y)	trans (x)	trans (z)	rot (y)
1	0	-0.618	0.0098	0	-0.618	0.0098
2	0	-1	0.0159	0	-1	0.0159
3	0	0.618	0.0098	0	0.618	0.0098
4	0	1	0.0159	0	1	0.0159
mode shape (7)						
mass	SAP2000			Matlab		
	trans (x)	trans (z)	rot (y)	trans (x)	trans (z)	rot (y)
1	0	1	0	0	1	0
2	0	-0.618	0	0	-0.618	0
3	0	1	0	0	1	0
4	0	-0.618	0	0	-0.618	0
mode shape (8)						
mass	SAP2000			Matlab		
	trans (x)	trans (z)	rot (y)	trans (x)	trans (z)	rot (y)
1	0	1	-0.0122	0	1	-0.0124
2	0	-0.618	0.0075	0	-0.618	0.0077
3	0	-1	-0.0122	0	-1	-0.0124
4	0	0.618	0.0075	0	0.618	0.0077

Table 5. Natural frequencies for verification model two (VM2)

Verification Model Number Two (VM2)			
Mode shape	Natural frequency (Hz)		Error (%)
	SAP2000	Matlab	$\lvert F_S - F_M \rvert / F_S \times 100$
1	1.18	1.18	0.00
2	3.08	3.08	0.00
3	16.20	16.20	0.00
4	16.45	16.45	0.00
5	1.18	1.18	0.00
6	1.32	1.31	0.81
7	3.08	3.08	0.00
8	3.38	3.37	0.49

An important question may be raised regarding what is the reason that the natural frequencies relative to third and fourth modal shapes jumping to much bigger values than others. This is because that every two lumped masses over the link have opposite directions, as seen in table 3. Hence, the link is under high tension or compression that increases the stiffness of the structure leading to higher frequencies due to the additional axial stiffness of the link itself.

3.3. Verification Model Three (VM3)

Ultimately, VM3 is considered a sophisticated analysis of a complicated model with sixteen lumped masses, as shown in figure 24. For simplicity, the dynamic properties used were the same as those in VM1 and VM2. However, the number of lumped masses were not the same on the two sides of the link. In addition, not all lumped masses were connected horizontally, instead, some randomness of linking the lumped masses was achieved in order to determine if the Matlab coding gave the same results of SAP2000.

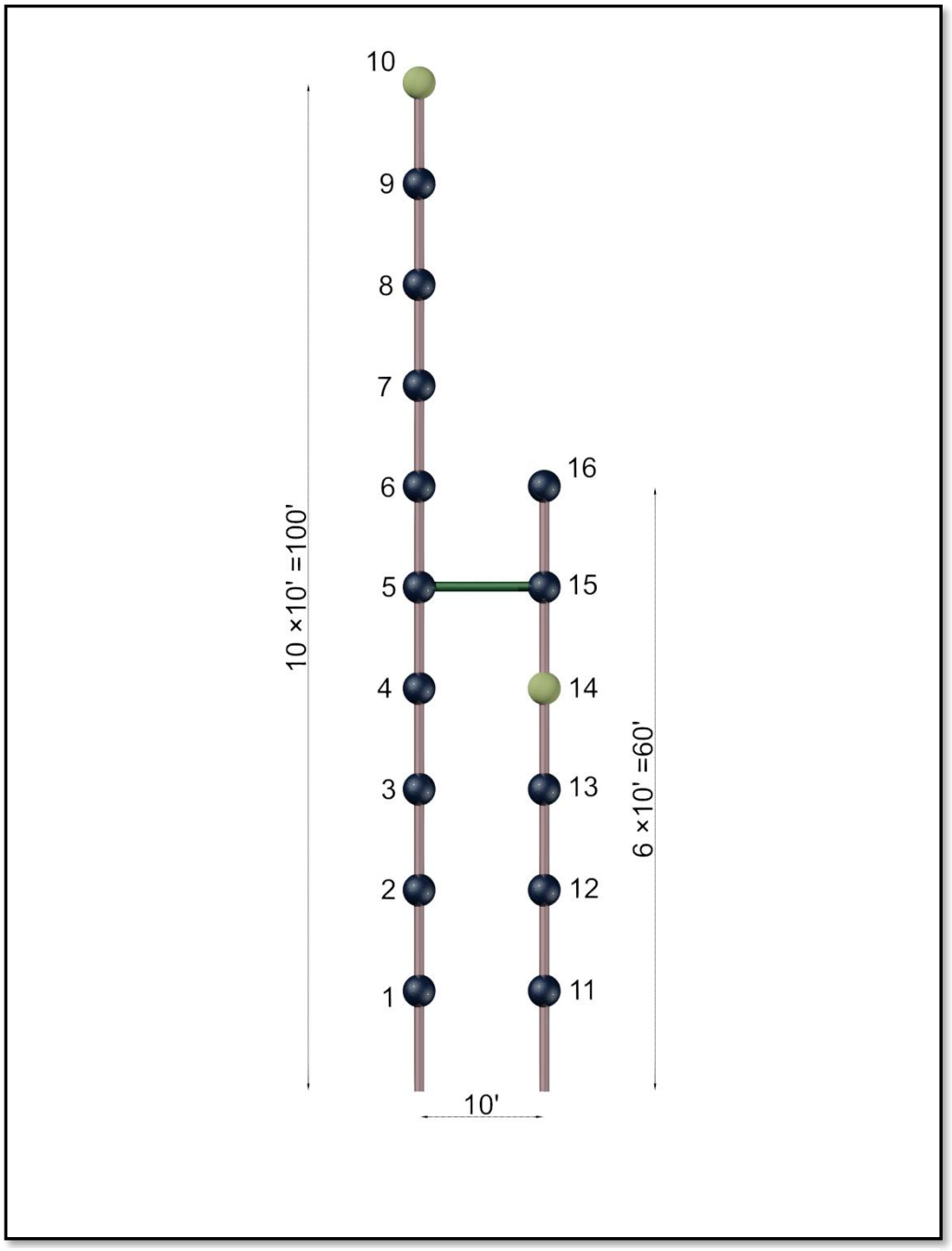

Figure 24. Verification model three (VM3)

Table 6. Natural frequencies for VM3

Verification Model Number Two (VM2)			
Mode shape	Natural frequency (Hz)		Error (%)
	SAP2000	Matlab	$\left\|F_S - F_M\right\| / F_S \times 100$
1	0.33	0.33	0.01
2	0.74	0.74	0.01
3	1.17	1.17	0.00
4	1.37	1.37	0.00
5	1.65	1.65	0.00
6	2.11	2.11	0.00
8	2.43	2.43	0.00
7	2.23	2.23	0.00
9	2.82	2.82	0.00
10	3.08	3.08	0.00
11	3.17	3.17	0.00
12	3.41	3.41	0.00
13	3.62	3.62	0.00
14	3.64	3.64	0.00
15	3.73	3.73	0.00
16	16.38	16.38	0.00
17	0.30	0.30	0.14
18	0.49	0.48	0.62
19	0.85	0.85	0.31
20	1.35	1.35	0.20
21	1.39	1.39	0.21
22	1.91	1.88	1.31
23	2.16	2.17	0.09
24	2.37	2.38	0.04
25	2.79	2.79	0.09
26	2.85	2.85	0.16
27	3.15	3.15	0.02
28	3.38	3.36	0.49
29	3.43	3.42	0.26
30	3.64	3.64	0.01
31	3.70	3.69	0.29
32	3.77	3.75	0.35

As we can see in table 6, the maximum difference in the natural frequencies between the Matlab and SAP2000 solutions is 2%, which is very acceptable. The dynamic response of two lumped masses (m_{10} and m_{14}) in the model was drawn in order to compare them. Three degrees of freedom were examined, which are the translational displacement in the x and z directions and the torsional displacements about the y-axis. Figure 25 through figure 30 show the three components of the dynamic displacements which calculated by Matlab code and SAP2000.

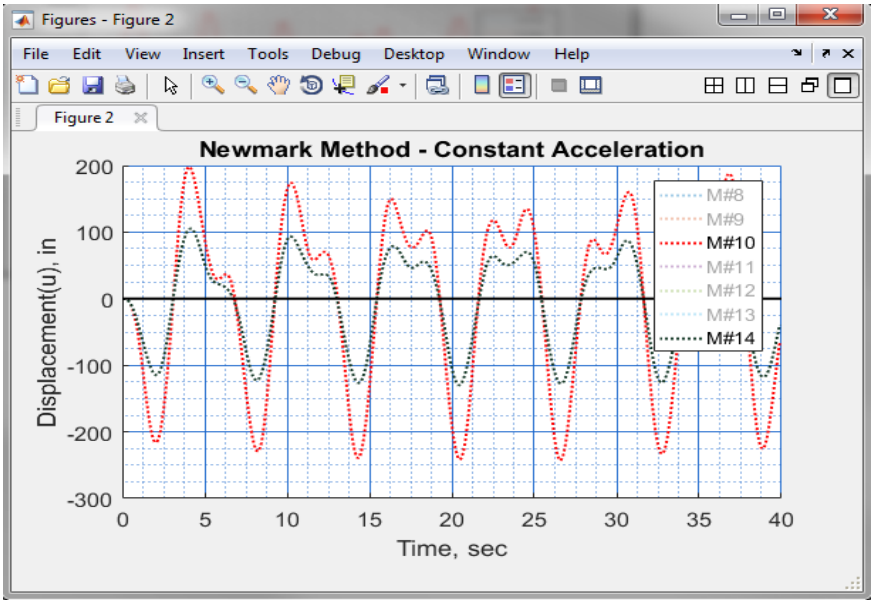

Figure 25. Horizontal displacement (u) at m_{10} and m_{14} of VM3 by Matlab

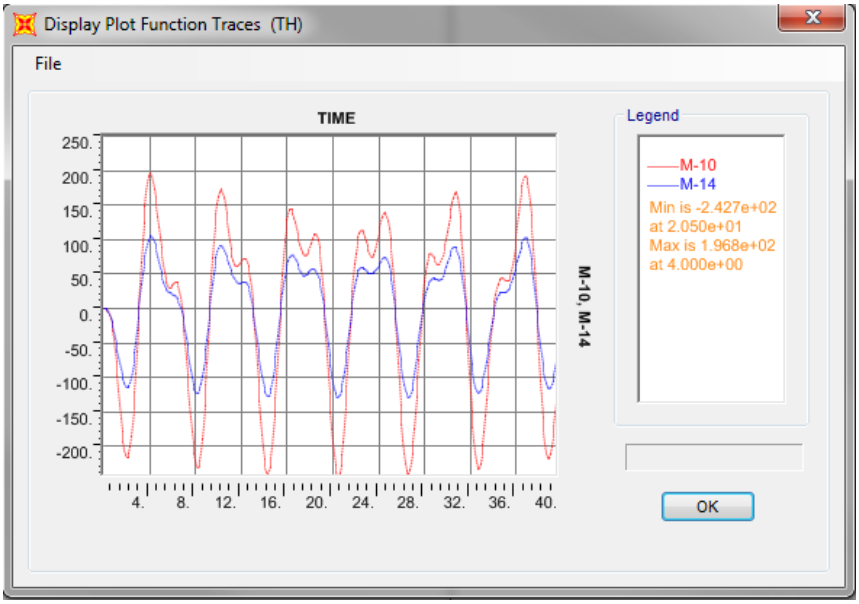

Figure 26. Horizontal displacement (u) at m_{10} and m_{14} of VM3 by SAP2000

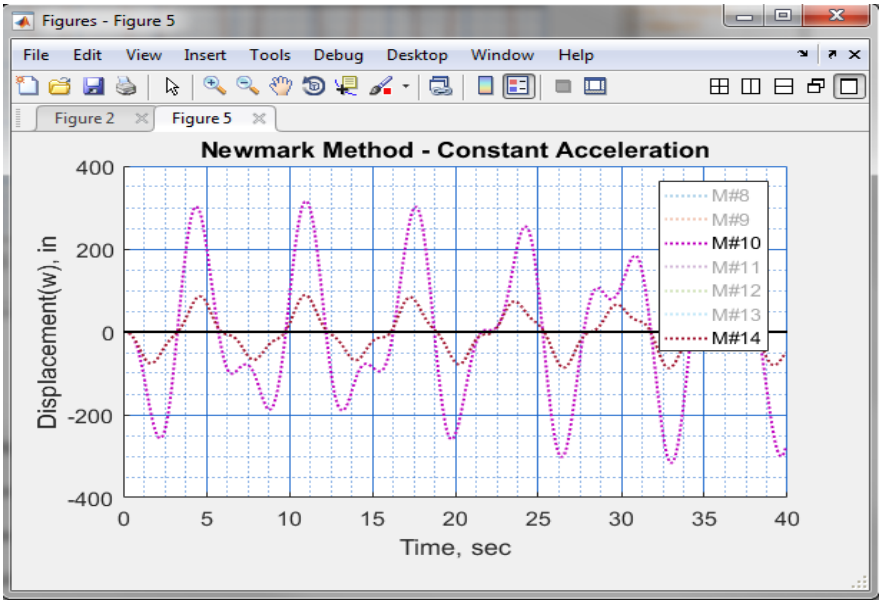

Figure 27. Horizontal displacement (w) at m_{10} and m_{14} of VM3 by Matlab

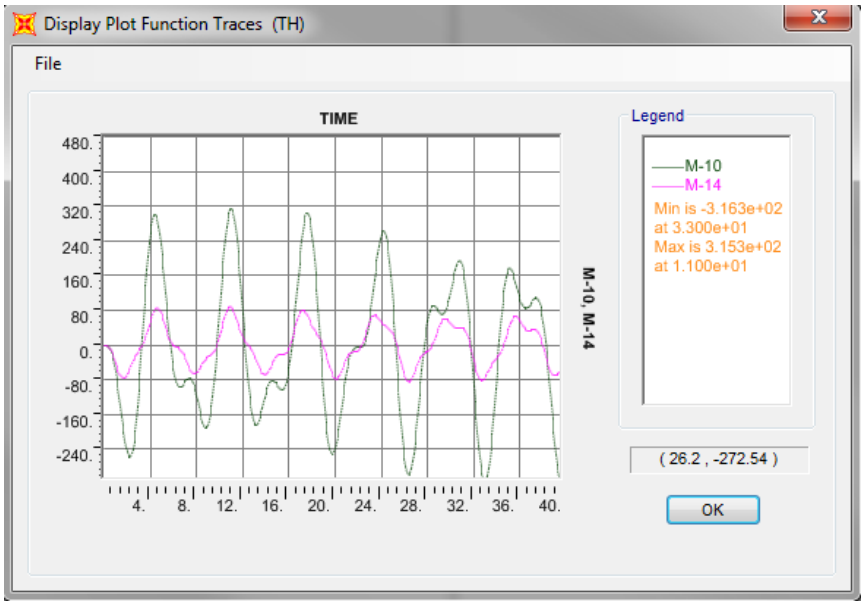

Figure 28. Horizontal displacement (w) at m_{10} and m_{14} of VM3 by SAP2000

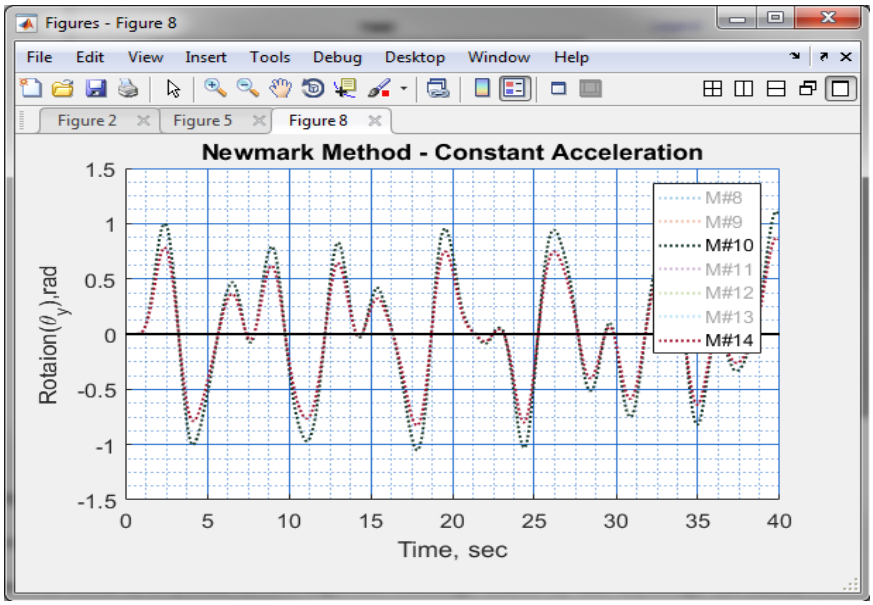

Figure 29. Torsional displacement (y) at m_{10} and m_{14} of VM3 by Matlab

Figure 30. Torsional displacement (y) at m_{10} and m_{14} of VM3 by SAP2000

The first two modal shapes of the dynamic displacement along x-axis and z-axis by Matlab are shown in figure 31 and 32 respectively.

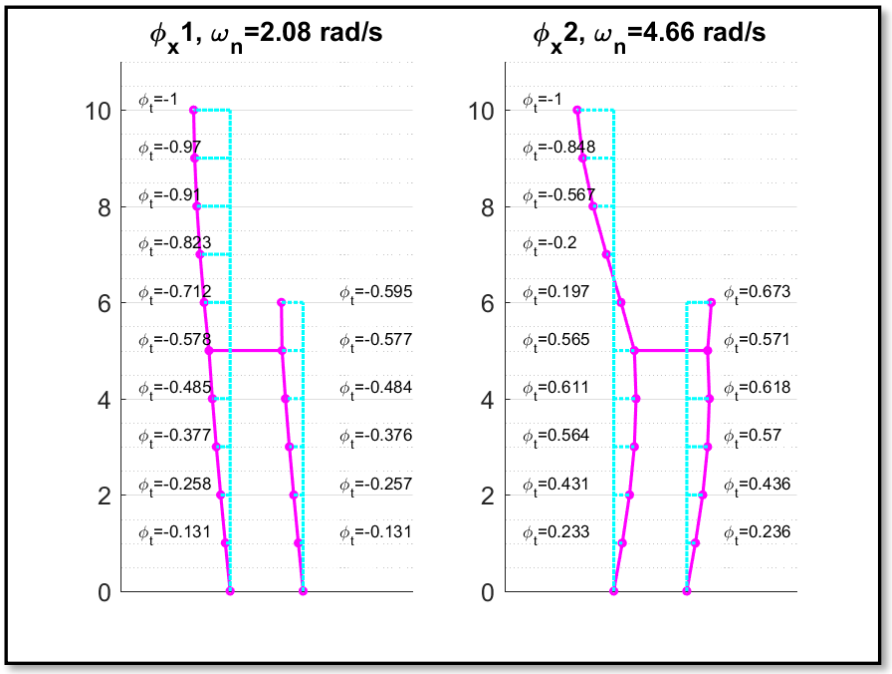

Figure 31. First two modes in x-direction for VM3 by Matlab

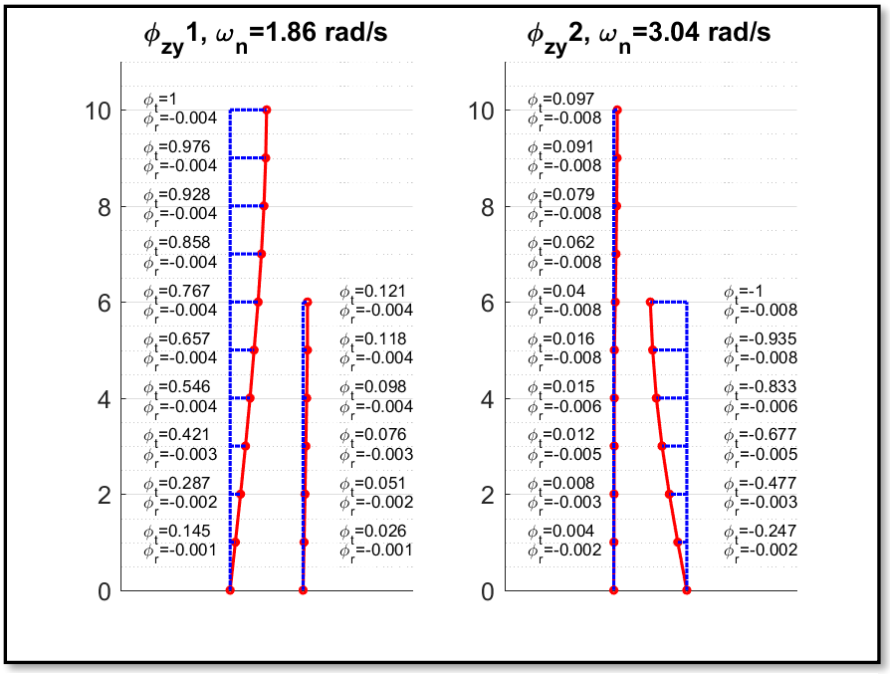

Figure 32. First two modes in coupled y-direction for VM3 by Matlab

All obtained results for VM1, VM2, and VM3 are matched between the semi-analytical solution conducted and the finite-elements solution. Therefore, this confirms that the Matlab coding was correctly developed and can be employed to perform dynamic analyses for coupled high-rise buildings connected by skybridges.

4. ISOLATED AND COUPLED HIGH-RISE BUILDING SIMULATIONS

4.1. Undamped Twin High-rise Building System

This chapter investigates the effect of utilizing the single and multiple masses in the building modeling with respect to the analysis of the high-rise buildings connected by a skybridge. Based on this reason, a system of 'two twins,' is considered, as indicated in figure 4. The acronym, HBS1 is used to express (High-rise Building system 1) for simplicity. For illustrative purposes the height of the building was selected to be 210 feet, corresponding to a 15-story building. The top view of the two buildings is a square-shaped plan form whose structural properties are shown in table 7 below. The total number of the columns in each floor is 25.

Table 7. Structural Properties of B1 and B2 in High-rise building system 1 (HBS1)

Story	1-5	6-10	11-15
Column dimensions (ft)	4 × 4	3× 3	2 × 2
Column height (ft)	14	14	14
Number of columns per story	25	25	25
Beam dimensions (ft)	2 × 1.5	2 × 1.5	2 × 1.5
Slab thickness (in)	8	8	8

The dynamic degrees of freedom considered for the two scenarios included the translation along the x-axis and z-axis directions and the torsional degree of freedom about the y-axis. In addition, the dynamic response of the system was calculated for the case of the independent building response, a skybridge was not present, while the case of the twin buildings is interconnected at the eighteenth and nineteenth floors by a skybridge 50 feet in length. The dynamic properties of the skybridge link are shown in table 8.

Table 8. Structural Properties of the Skybridge in HBS1

Section shape	Length (ft)	A × Ec (kips)	I_z × Ec (kips.in^2)
rectangular	50	53856000	214×10^9

Two modeling scenarios were considered. The first scenario considered the use of the multiple masses, specifically fifteen lumped masses were used to model each building. In the second scenario, the mass of each building was concentrated at the geometrical center of each building as a single mass for each building, resulting in two lumped masses for the entire system. Following that, the structural models of the high-rise buildings were subjected to a strong ground motion relative to the loading time series records selected from an event of the 1940 El-Centro earthquake in the United States, see the appendix for more details.

The obtained dynamic response of the highest point in the HSB1 (m_{15}) by the first modeling scenario shows that the maximum dynamic displacement of about 10" occurred the twenty-sixth second. Whereas the maximum dynamic displacement of the same point in this particular building, which was gotten from the second scenario of the analysis is about 10" at the fourteenth second. For these two scenarios, the dynamic responses along the x-axis and z-axis are identical because of the absence of the structural coupling. Figures 33 and 34 show the dynamic response of the first and second modeling scenarios respectively.

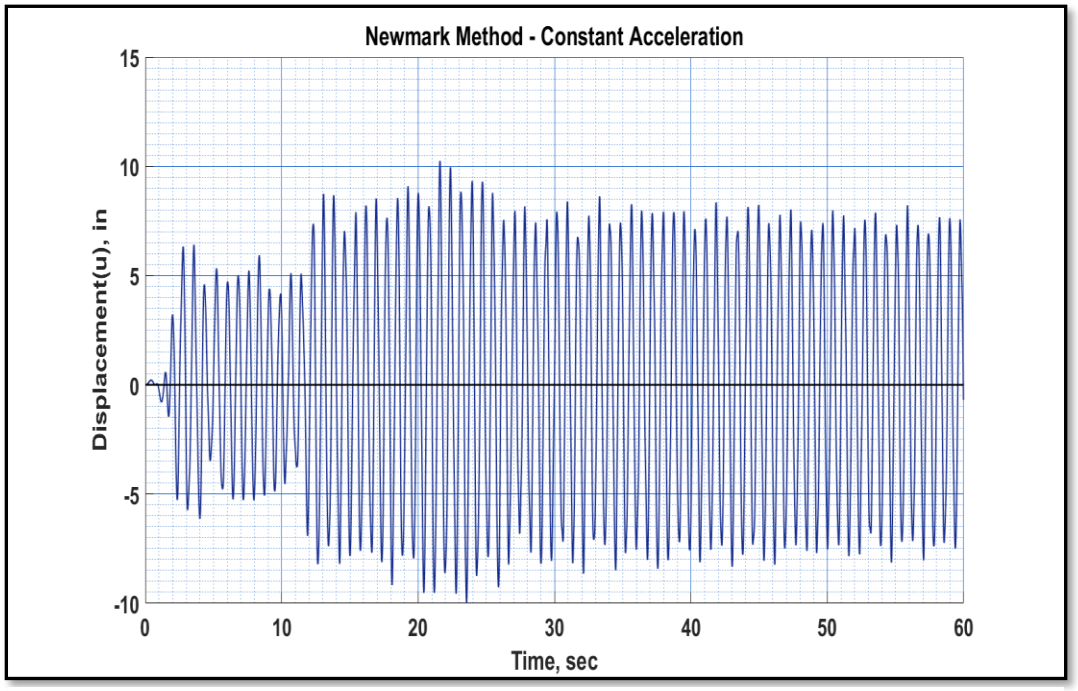

Figure 33. Horizontal displacement (u) at m_{15} (H=210 feet) in HBS1 using Multiple masses

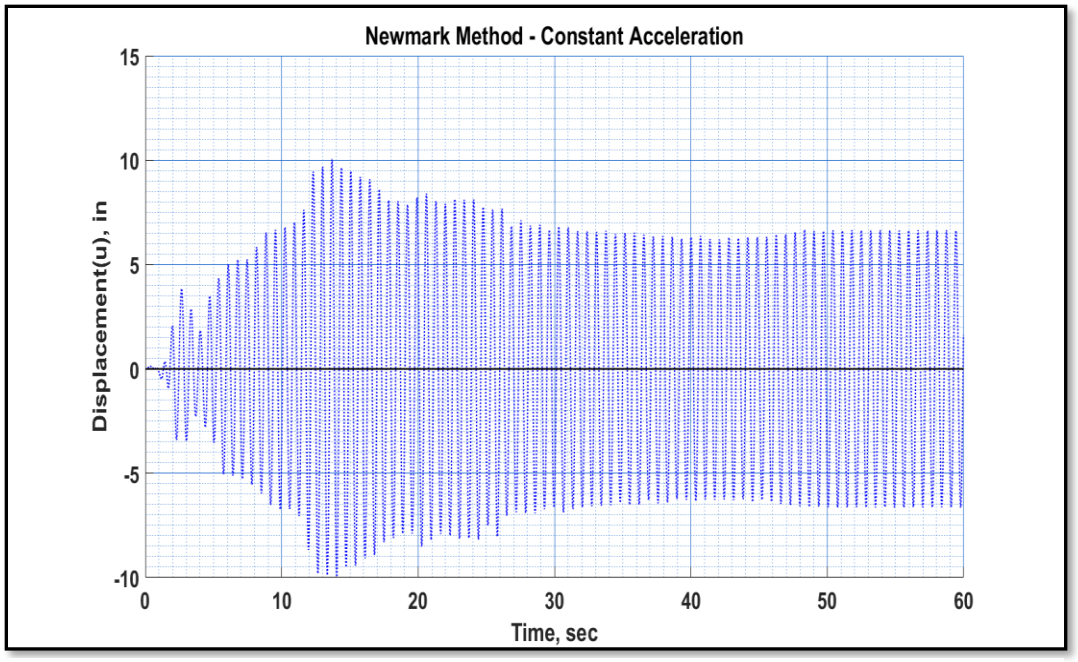

Figure 34. Horizontal displacement (u) at m_{15} (H=210 feet) in HBS1 using a single mass concentrated at 8th floor

Several tests were conducted by changing the height of the equivalent mass so as to ensure the best modeling approximation of the second scenario is achieved to converge to the solution gotten by the first scenario, which is modestly more illustrative of the real dynamic response. The location of the equivalent mass was inserted in the sixth, tenth, and fifteenth floor, considering the change of the equivalent stiffness and damping. The dynamic response under the 1940 El-Centro earthquake was further calculated for each case and the results are shown in figure 35 through figure 38. The general indication is the increase in the natural frequency and the decrease in the dynamic response, when the equivalent lumped mass is kept in the location closest to the first floor and vice versa, and also, when the equivalent lumped mass is kept close to the highest floor in the buildings.

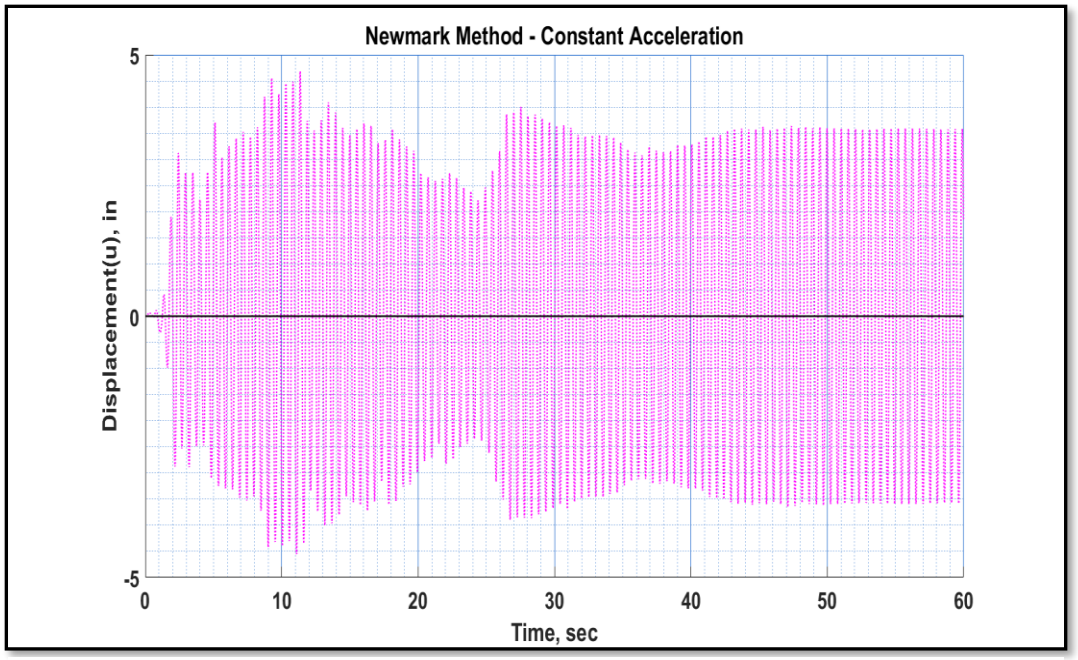

Figure 35. Horizontal displacement (u) at m15 (H=210 feet) in HBS1 using a single mass concentrated at 6th floor

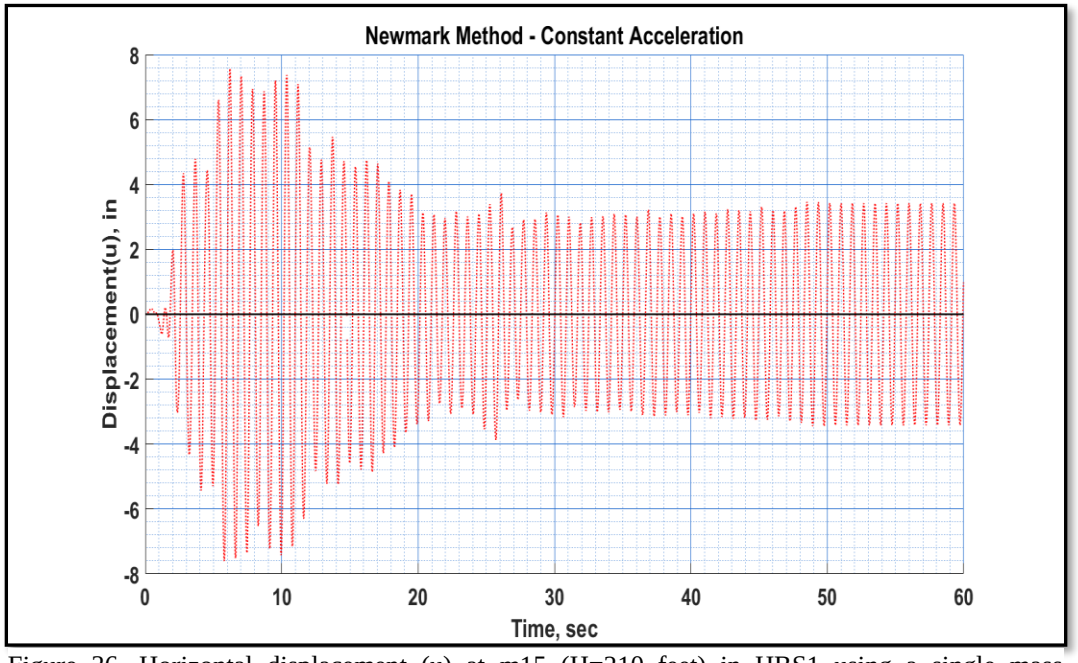

Figure 36. Horizontal displacement (u) at m15 (H=210 feet) in HBS1 using a single mass concentrated at 10th floor

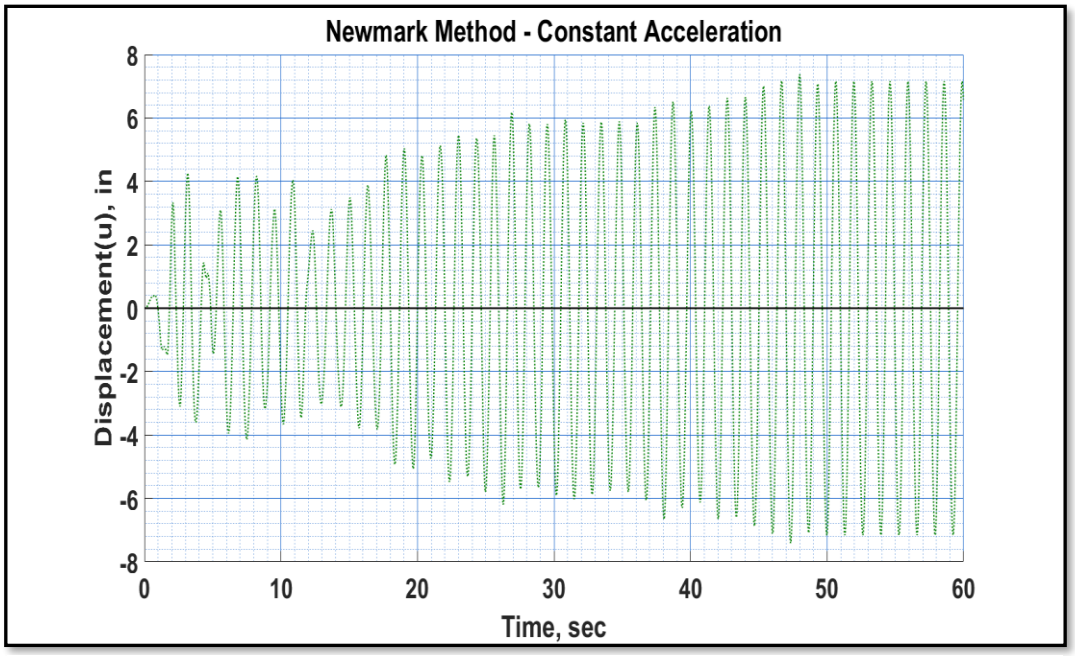

Figure 37. Horizontal displacement (u) at m15 (H=210 feet) in HBS1 using a single mass concentrated at 12th floor

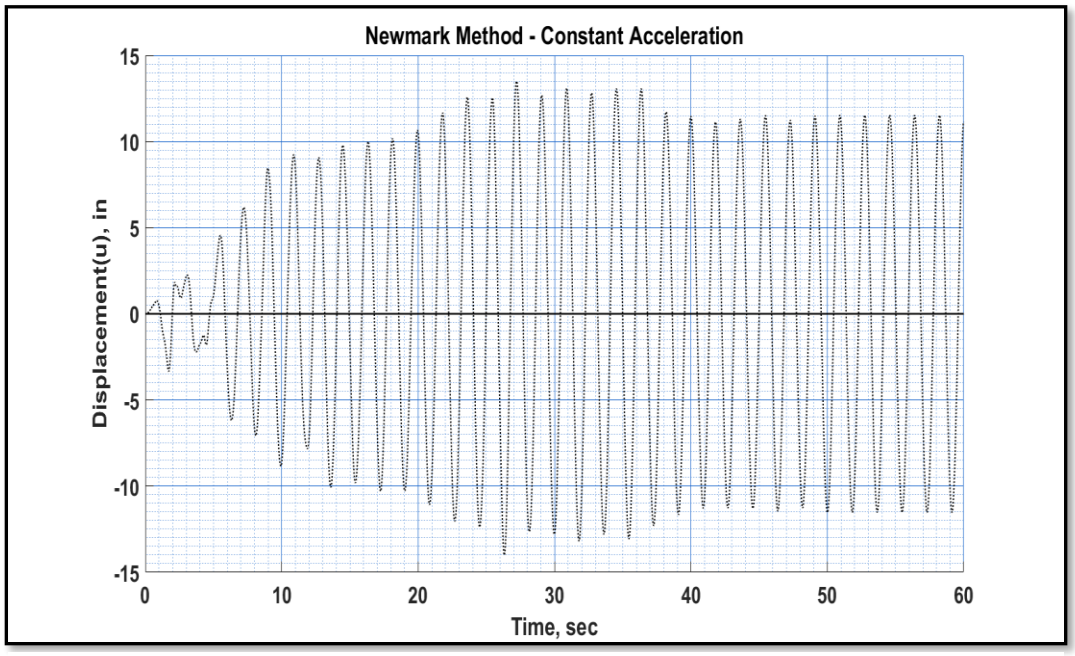

Figure 38. Horizontal displacement (u) at m_{15} (H=210 feet) in HBS1 using a single mass concentrated at 15^{th} floor

As clearly seen, representing the high-rise building with the use of a single lumped mass does not provide the same as the result obtained when the multiple masses were used. In any case, based on the maximum dynamic response values, the best approximation can be achieved by concentrating the mass closer to the mid-height of the high-rise building as indicated in table 9.

Table 9. Maximum horizontal displacement (u) with respect to different equivalent mass locations

Location of equivalent mass	Maximum horizontal response (u), in
6th floor	4.7
8th floor	10
10th	7.75
12th	7.2
15th	14

Moreover, the first scenario gives an indication of no significant effect, beside the slight effect of the additional mass and equivalent stiffness, of the coupled dynamic response due to a skybridge on the twin high-rise buildings; the translational and torsional dynamic displacements are identical in the earlier cases of the isolated and linked buildings. Also, the translational dynamic displacement passing across the x-axis and the z-axis are the same because of the absence of the effect of the structural coupling. Regardless of the difference existing with respect to the calculated dynamic response when making use of a single mass, instead of the multiple masses, the second scenario gives no sign of a change, particularly in the dynamic response. The step that followed was a confirmation of the possibility of the change in the geometric and dynamic properties of

the skybridge makes any possible change or not. The study makes use of different skybridge models as indicated in table 10.

Table 10. Different dynamic characteristics of the skybridge in HBS1

Section shape	Length (ft)	Location	A × Ec (kips)	I_z × Ec (kips.in^2)
rectangular	60	15^{th} -16^{th}	60000000	300 ×10^9
rectangular	50	10^{th} -11^{th}	50000000	250 ×10^9
rectangular	40	6^{th} -7^{th}	45000000	200 ×10^9
rectangular	30	3^{rd} -4^{th}	30000000	150 ×10^9

All of the obtained results give a confirmation that the presence of the skybridge in this system; that is, the twin high buildings, has no significant effect of structural coupling on the dynamic response. Hence, it is possible to conclude that there exists no structural coupling in twin high-rise building, being interconnected by a skybridge subjected to viable ground motions.

4.2. Undamped Different High-rise Building Systems

Different high-rise building systems are considered for the coming sections of this research study. The high-rise building system 2 (HBS2) is another building system considered in this study. It has its first building in 20 stories, having 280 feet in height. However, the second one has 10 stories and is 140 feet in height. The geometrical properties of the first and second high-rise buildings are indicated in table 11 and 12 respectively.

Table 11. Structural properties of B1 in HBS2

Floor	1-5	6-10	11-15	16-20
Column dimensions (ft)	5 × 5	4 × 4	3 × 3	2 × 2
Column height (ft)	14	14	14	14
Number of columns per story	25	25	25	25
Beam dimensions (ft)	2 × 1.5	2 × 1.5	2 × 1.5	2 × 1.5
Slab thickness (in)	8	8	8	8

Table 12. Structural properties of B2 in HBS2

Floor	1-5	6-10
Column dimensions (ft)	3 × 3	2.5 × 2.5
Column height (ft)	14	14
Number of columns per story	25	25
Beam dimensions (ft)	2 × 1.5	2 × 1.5
Slab thickness (in)	8	8

To build a walkway, the slab of the nineteenth and twentieth floors of the two buildings were connected together by a 55” length of skybridge with axial and flexural rigidities of 107.7×10^6 kips and 428×10^9 kips.in^2 respectively. Furthermore, an analysis was conducted, for each independent building subjected to earthquake signals relative to the Umbro-Marchigiano occurrence in Turkey. Then, the dynamic response of the structurally coupled high-rise buildings was calculated. Generally, it is noticed that in the most cases, the translational dynamic displacements along the x-axis and z-axis tend to decrease and the torsional displacement appears, when the skybridge is present, just as the torsional displacement tends not to be present when the high-rise buildings are not interconnected. Figure 39 through figure 42 show the dynamic response for $m_{15,}$ which presents the average of the two buildings heights, in structurally uncoupled and coupled high-rise buildings respectively.

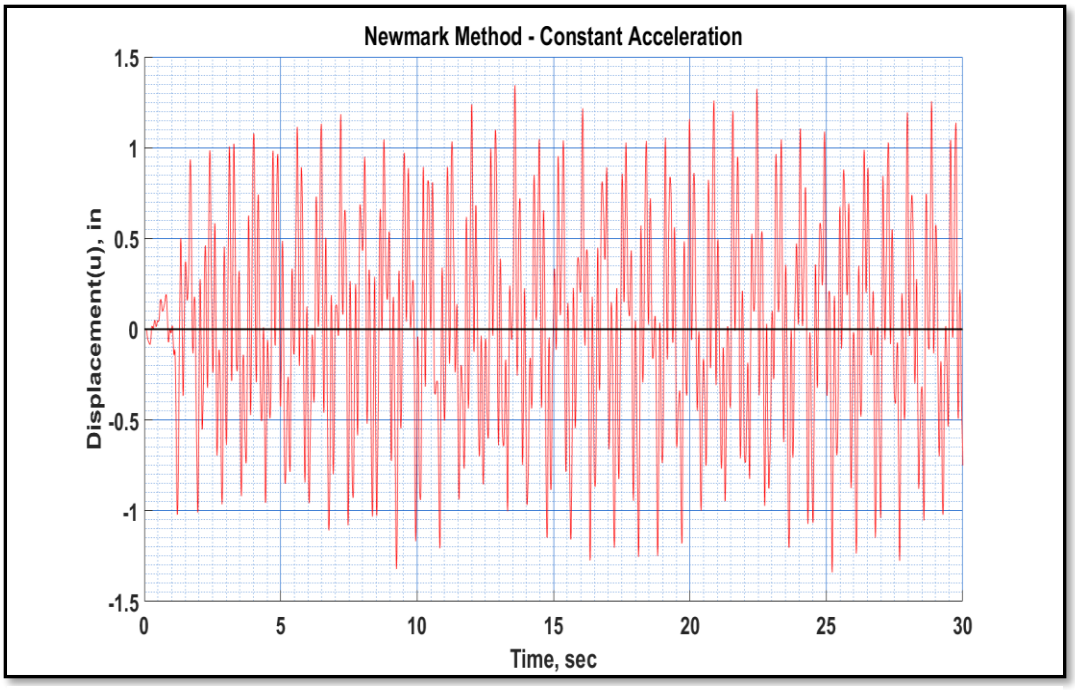

Figure 39. Horizontal displacement (u) of uncoupled HBS2 at m_{15} (H=210 feet)

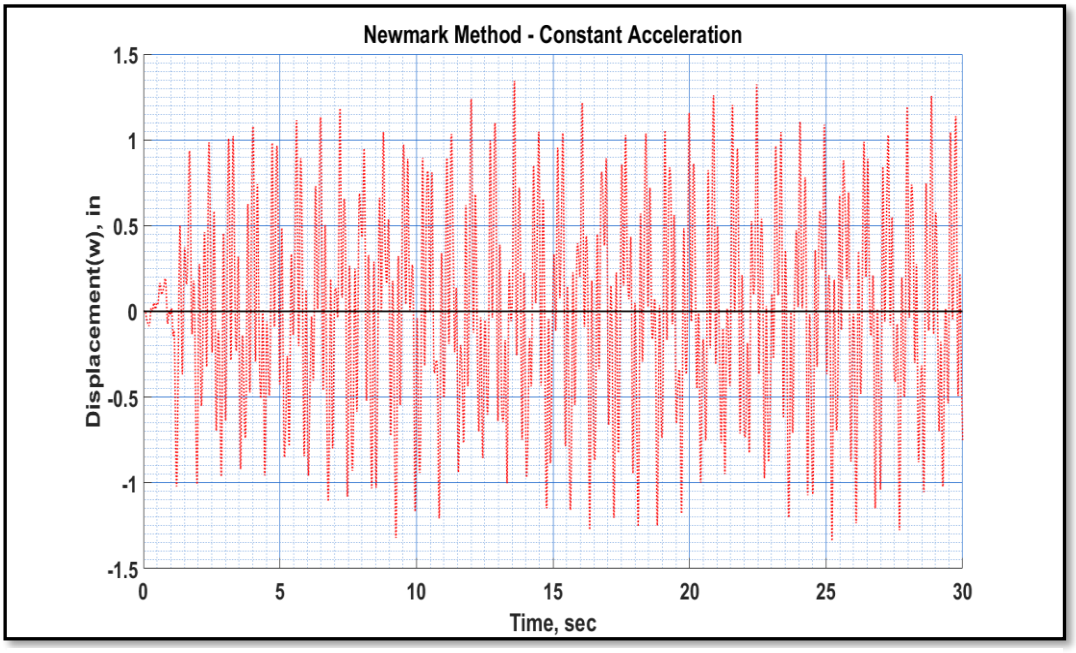

Figure 40. Horizontal displacement (w) of uncoupled HBS2 at m_{15} (H=210 feet)

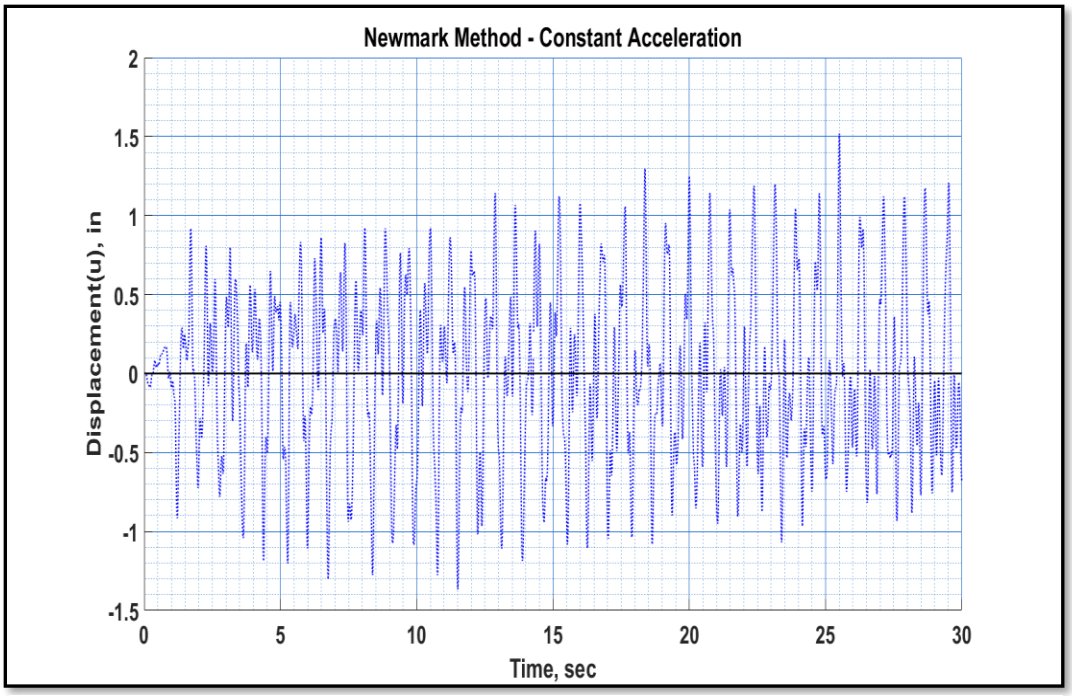

Figure 41. Horizontal displacement (u) of coupled HBS2 at m_{15} (H=210 feet)

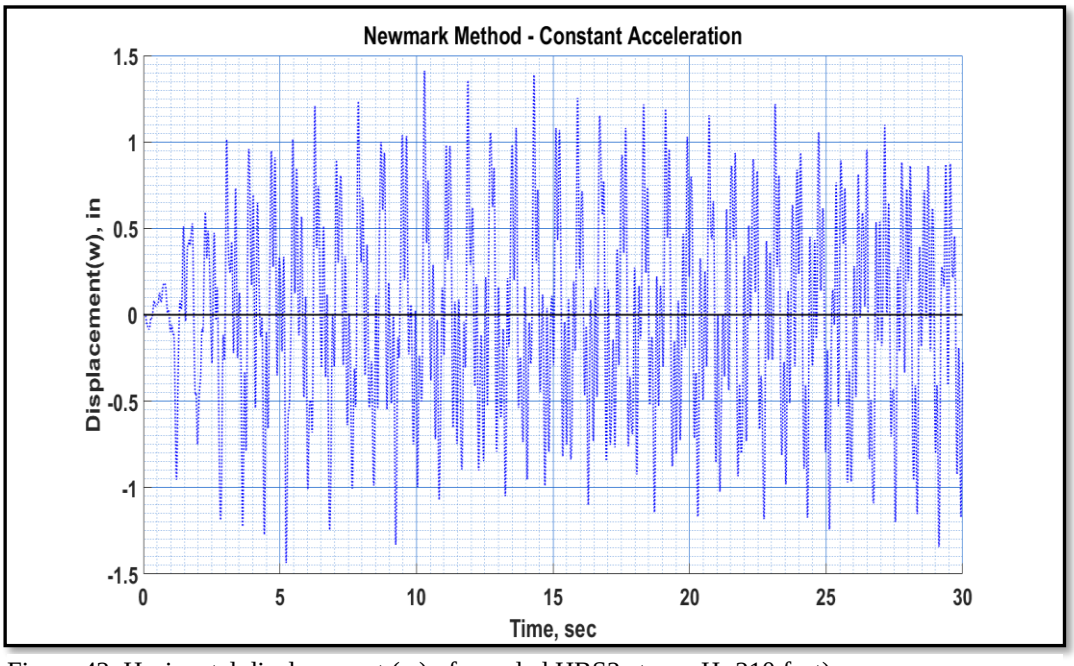

Figure 42. Horizontal displacement (w) of coupled HBS2 at m_{15} (H=210 feet)

4.3. Damped Different High-Rise Building System

HSB2 was utilized to determine the impact of damping force in this section of the thesis. The dynamic displacement was obtained relative to the different value of damping ratio, represented by

$$\xi = 0.02, 0.035, 0.05, 0.065, 0.08, 0.1$$

Furthermore, the proportional viscous damping matrices were constructed with the use of Rayleigh damping, considering the same damping ratios for the first two modes. Figure 43 and figure 44 show the dynamic response of coupled HBS2 with damping ratio equals 0.02 at m_{15}, and figure 45 shows the maximum dynamic displacement passing across the z-axis in the system's top floor, at the twentieth second, on the y-axis, and the damping ratio of the x-axis. The two curves indicate that more energy dissipated in the case of uncoupled buildings under the effect of the damping force.

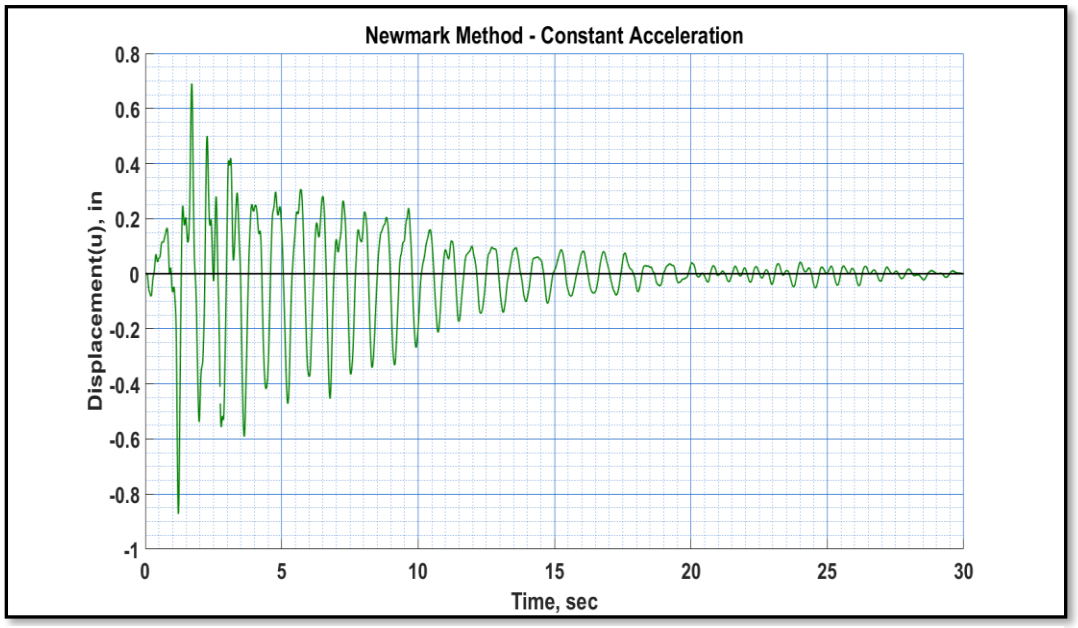

Figure 43. Horizontal displacement (u) of coupled HBS2 at m_{15} (H=210 feet), (ξ=0.02)

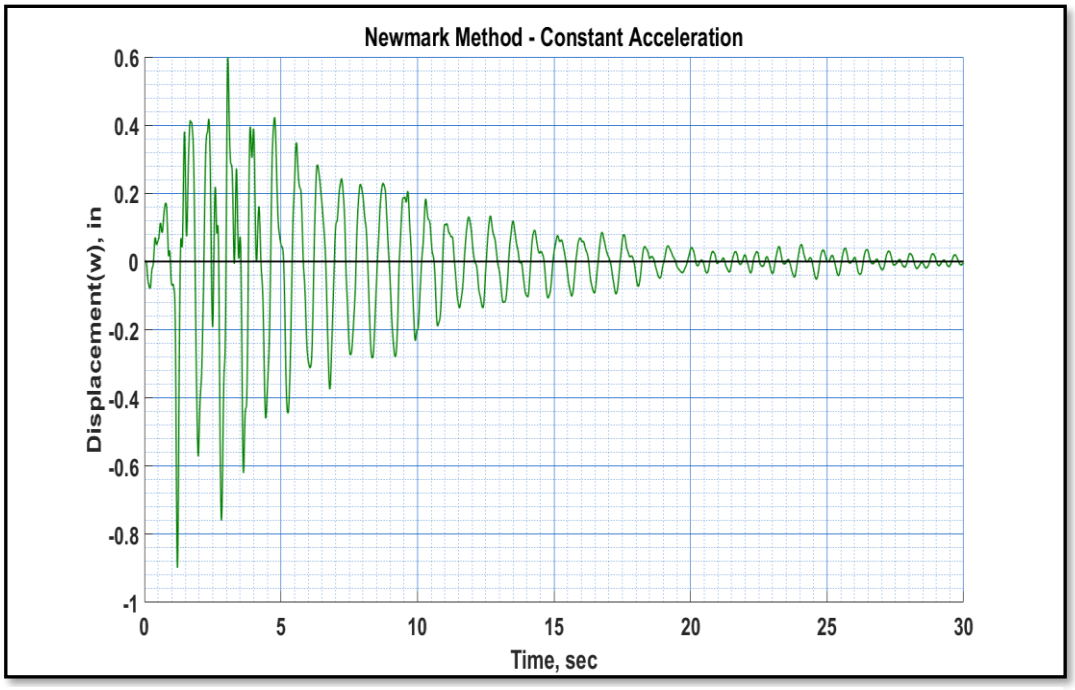

Figure 44. Horizontal displacement (w) of coupled HBS2 at m15 (H=210 feet),(x=0.02)

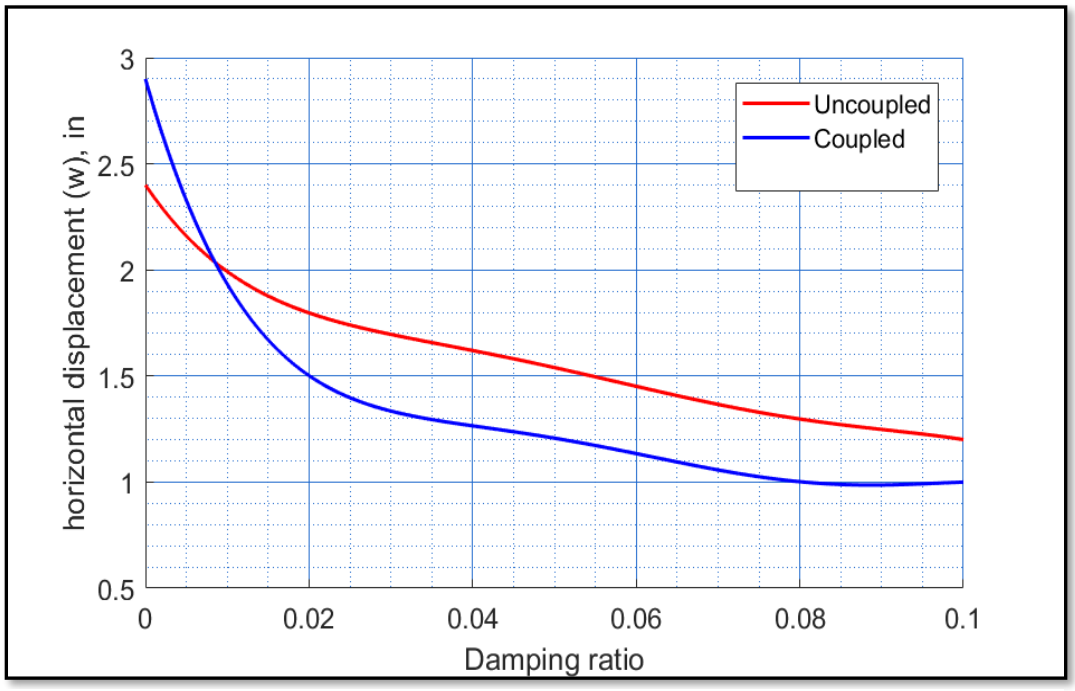

Figure 45. Change of horizontal displacement (w_{max}) at m20 (H=280 feet) with the damping ratio

Finally, the relationship between the required number of cycles for the dynamic horizontal displacement w, along the z-axis, to drop to 10% of the w_{max} as well as the damping ratio is also represented in figure 46. The number of cycles decreases when the damping ratio increases and vice versa.

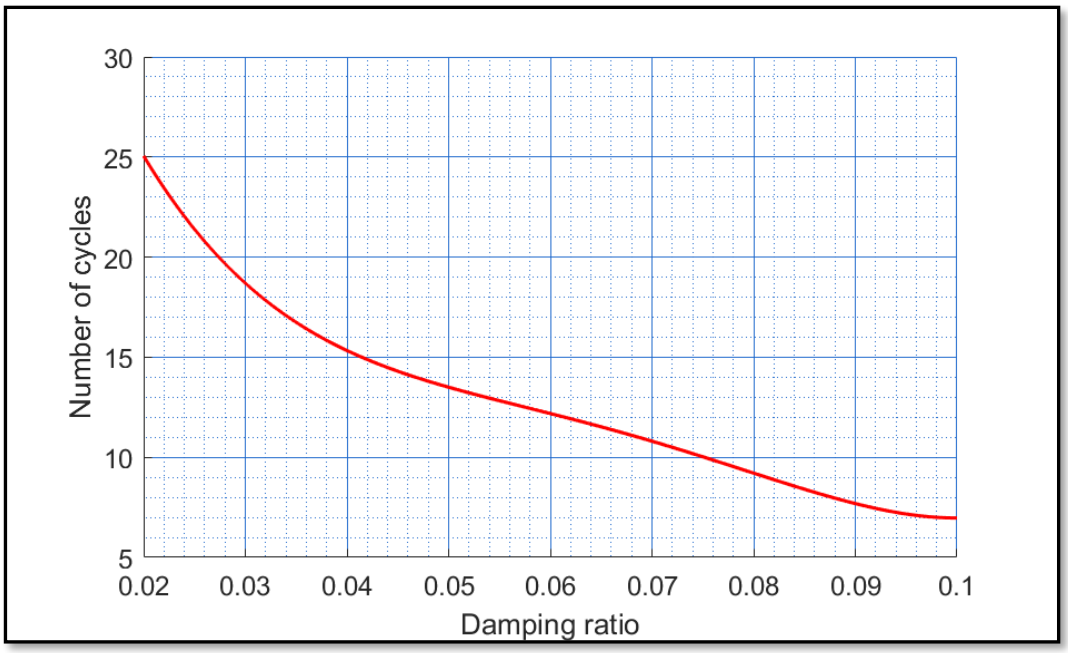

Figure 46. Change of the number of cycles for horizontal displacement (w) at m20 (H=280 feet) to drop to (10%) of the maximum value relative to the damping ratio

5. MULTIPLE SKYBRIDGE SIMULATIONS

This chapter will focus on the investigation of the geometrical and dynamic properties and their effect on the dynamic response of the coupled high-rise building system. In particular, we will examine the variation of the response behavior subject to variations in skybridge stiffness, location, connection end conditions and the number of skybridges used to connect the high-rise buildings. In order to further observe and understand the response behavior, two different high-rise building systems are considered.

5.1. Skybridge Connection End Conditions

Although different connection end conditions may be utilized in the structural design to link a skybridge to the high-rise buildings, the appropriate connection design must be compatible with the type of skybridge structural design. For example, if the structural designer is inclined to eliminate the effect of the structural coupling on the building system dynamic response resulting from the skybridge linkage they would use a roller design for the skybridge end connections. This is the simplest case to model as only the additional relatively small mass of the skybridge need be is taken into account. Linking the ends of the skybridge using hinge-supports induces a coupled dynamic response of the building system. Hinge end connections develop a resistance against the translational degree of freedom along the x-axis, parallel to the skybridge, and this leads to the structural coupling to the corresponding dynamic degree of freedom (u). Any resistance of the translational degree of freedom along the z-axis effects the corresponding

dynamic degree of freedom (w). As can be noted in the formulation of stiffness matrix, presented in chapter two, (u) is not coupled with (w) or (θ_y) whether the skybridge linkage exists or not.

The 1994 Northridge earthquake event was applied to get the dynamic displacements for uncoupled roller design and the coupled hinge-supported skybridge of HBS3 respectively. The geometrical properties of building one denoted by the symbol B1 and building two denoted by the symbol B2 are shown in tables 13 and 14 respectively.

Table 13. Structural properties of B1 in HSB3

Floor	1-10	11-20
Column dimensions (ft)	5 × 5	4 × 4
Column height (ft)	14	14
Number of columns per story	25	25
Beam dimensions (ft)	2 × 1.5	2 × 1.5
Slab thickness (in)	8	8

Table 14. Structural properties of B2 in HSB3

Floor	1-8	9-14
Column dimensions (ft)	4 × 4	3.5 × 3.5
Column height (ft)	14	14
Number of columns per story	25	25
Beam dimensions (ft)	2 × 1.5	2 × 1.5
Slab thickness (in)	8	8

.

The two buildings were connected together by a 70 ft long concrete skybridge with axial and flexural rigidities of 10.77 $\times 10^6$ in^2 and 428 $\times 10^9 in^4$ respectively. A critical damping ratio of $\xi = 0.035$ was used for the first two modes in both of these simulations. Figure 47 and figure 48 show the dynamic response (u) and (w) for seven lumped masses in the HBS3 for uncoupled roller design and the coupled hinge design respectively. It can be seen that the translation displacements in x-directions increased in the coupled high-rise and slightly increased in the z-direction, whereas the horizontal displacements decreased in HBS2 when subjected to the Umbro-Marchigiano earthquake signals in Section 4.2 of this thesis. This illustrates the fact that this is a complicated dynamic design process where many factors affect the behavior of the skybridge.

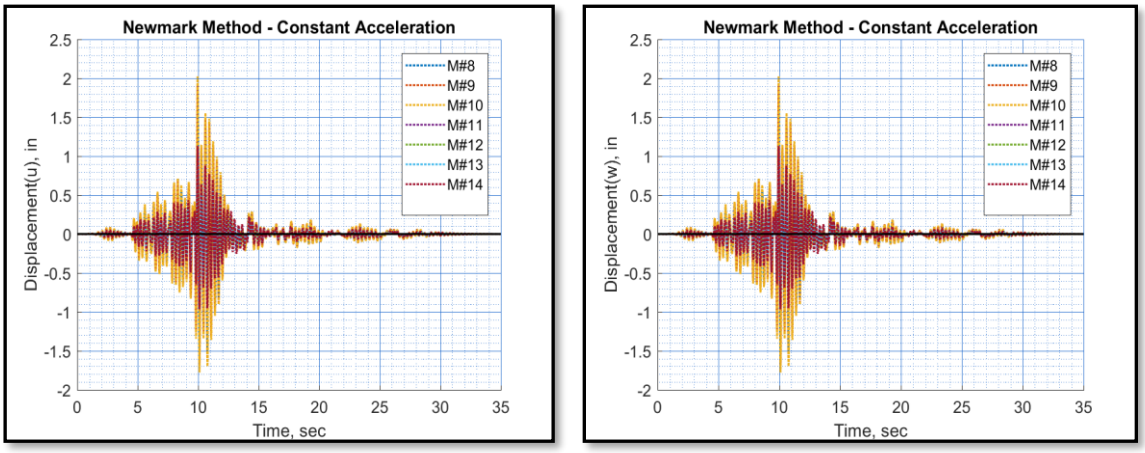

Figure 47. Horizontal displacements in x-direction (u) and z-direction (w) of HBS3 with a roller ends skybridge

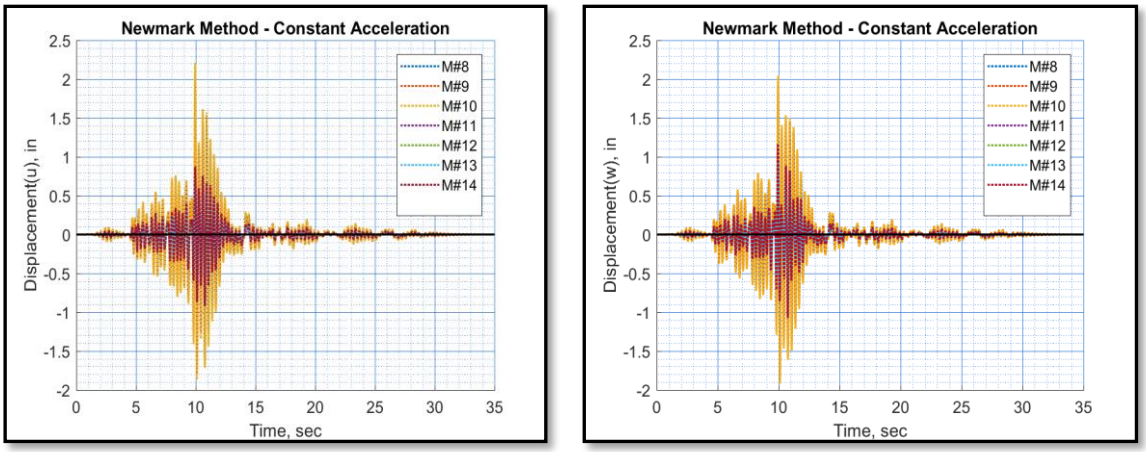

Figure 48. Horizontal displacements in x-direction (u) and z-direction (w) of HBS3 with a hinge ends skybridge

Following that, a resistance against the rotational degree of freedom (θ_y) was introduced to model fixed end conditions of the skybridge. That modification significantly increased the effect of the skybridge by increasing the horizontal dynamic displacement in the z-direction (w). Thus, the hinge support design increased the dynamic displacement (w) slightly and, the introduction of rotational resistance in the fixed support design further increased this effect. Moreover, the rotational constraint introduced a torsional displacement of buildings about their local vertical axes as shown in figure 49.

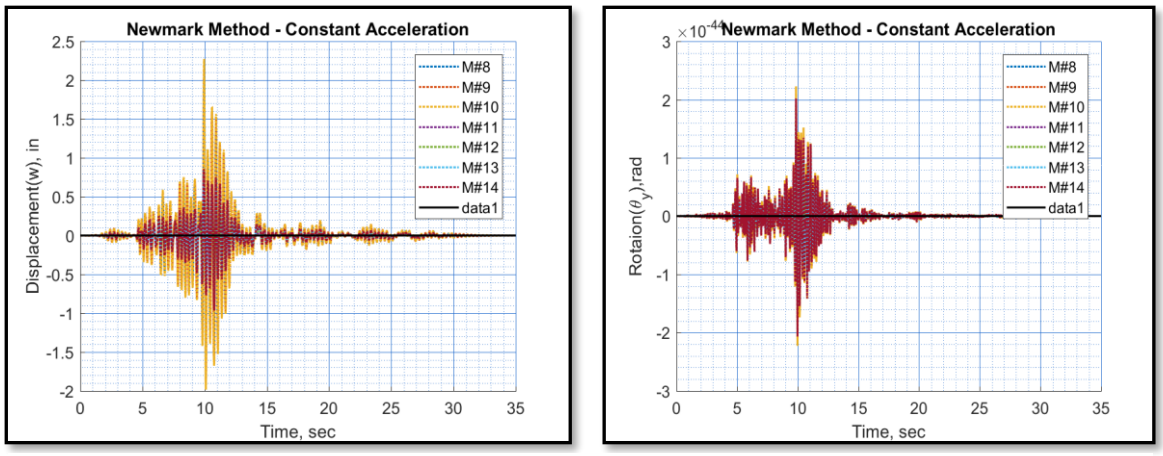

Figure 49. Dynamic displacements (u) and (w) of HSB3 with a fixed ends skybridge

5.2. Skybridge Stiffness

The high-rise building system 4 (HBS4) was linked by a 44 ft long skybridge. The effect of variable skybridge structural stiffness was investigated by changing the equivalent cross-sectional area of the skybridge. This was done in, in order to evaluate the effect of different stiffnesses on the dynamic response, where the axial and flexural stiffens increase by increasing the equivalent cross-sectional area of the skybridge and vice versa. The geometrical properties of the two different buildings are presented in table 15 and table 16.

Table 15. Geometrical properties of B1 in HSB4

Floor	1-10	11-22
Column dimensions (ft)	5 × 5	4 × 4
Column height (ft)	14	14
Number of columns per story	25	25
Beam dimensions (ft)	2 × 1.5	2 × 1.5
Slab thickness (in)	8	8

Table 16. Geometrical properties of B2 in HSB4

Floor	1-8	9-12
Column dimensions (ft)	4 × 4	3.5 × 3.5
Column height (ft)	14	14
Number of columns per story	25	25
Beam dimensions (ft)	2 × 1.5	2 × 1.5

A fixed ended skybridge design was used to connect the tenth floor between the two buildings. The axial and flexural rigidities of the skybridge are 53.85 $\times 10^6$ kips and 214 $\times 10^9$ kips.in^2 respectively. The normalized axial rigidity and flexural rigidity that is based on these a cross-area and the moments of inertia are set to be 1.

A critical damping ratio of $\xi = 0.035$ was used in these simulations. The uncoupled dynamic response of HBS4 is denoted by (u_1) and (w_1). Hence, different values of the translational and rotational stiffness of the skybridge were considered and their corresponding displacements were calculated. It is worth mentioning that the change of the stiffness covers the change of the skybridge shape, the material used to build it, and the length. The artificial NF17 earthquake signals were applied in this part of the study with maximum acceleration 10g and time step 0.01 sec. figure 50 and figure 51 show the impact of different values of normalized rigidities, divided by the axial and flexural rigidity values that were set to be 1, on the dynamic displacements for the twenty-second floor of B1 (mt) and eighteenth floor of B2 (ms).

Note:

mt= the mass of 20th floor in the taller building

ms = the mass of 10th floor in the shorter building

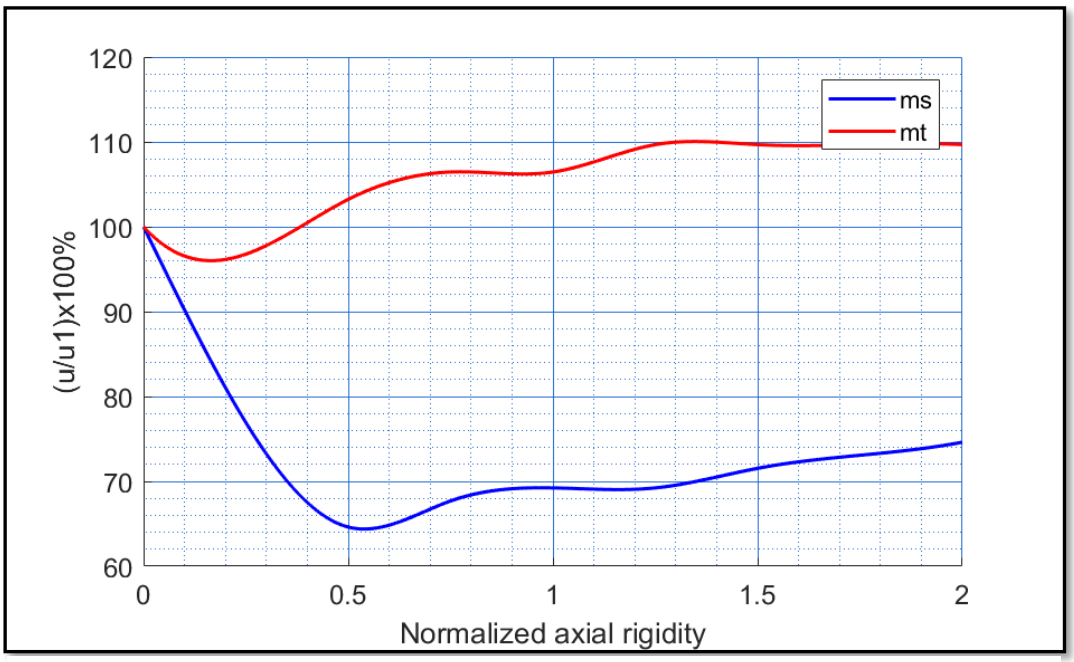

Figure 50. Change of horizontal displacement (u) of mt (H=308 feet) and ms (H=154 feet) at the twenty-second floor with change of the normalized axial rigidity

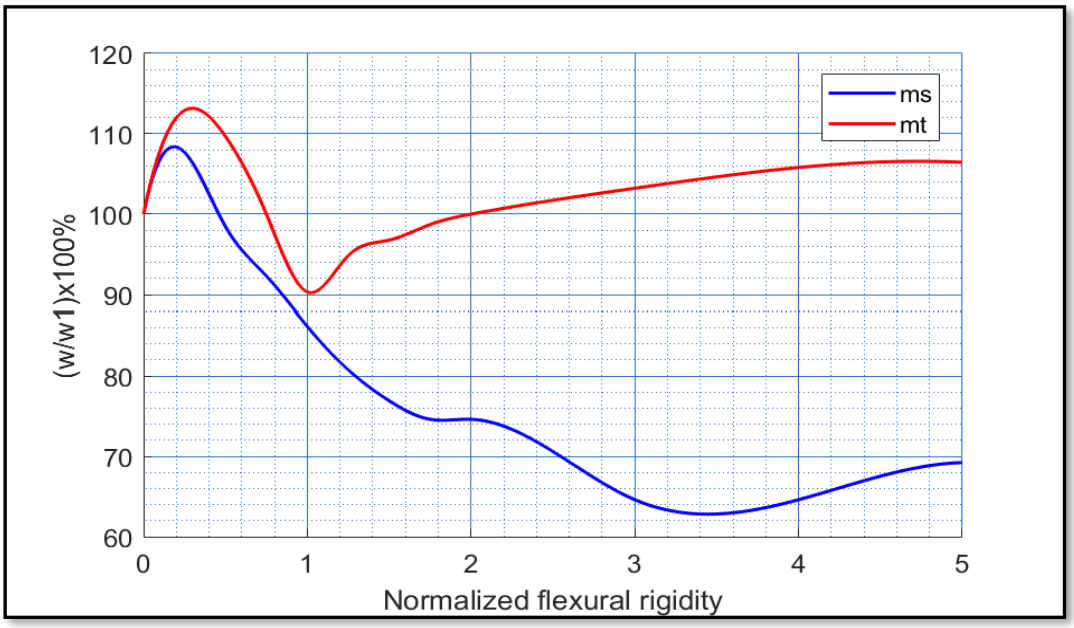

Figure 51. Change of horizontal displacement (w) of mt (H=308 feet) and ms (H=154 feet) with change of the normalized flexural rigidity

As shown in figure 49, the optimum normalized axial stiffness that reduces the overall dynamic displacement along the x-axis (u) for the two buildings is (1/4). Where figure 50 indicates that the normalized flexural stiffness (1) is the optimum value that achieved the minimum value of the overall dynamic displacement along the z-axis (w). The two horizontal displacements (u) and (w) are uncoupled and impacted by different components of frame rigidities; that is why the normalized optimum rigidities are not the same. For this reason, the shape of a skybridge shall be designed to have high flexural rigidity and low axial rigidity values.

5.3. Location of a Skybridge

The high-rise building system 4 (HBS4) was used again with different elevations specified for the skybridges. The dynamic displacement along the x-axis and z-axis were calculated in each case. Figure 52 and figure 53 show the maximum dynamic displacement across the number of floors where the skybridge set. The optimum values of axial and flexural stiffness that are obtained from the previous section were utilized. It is clear that tenth floor 83% of the height of shorter buildings (B2) is the optimum position where the skybridge shall be set.

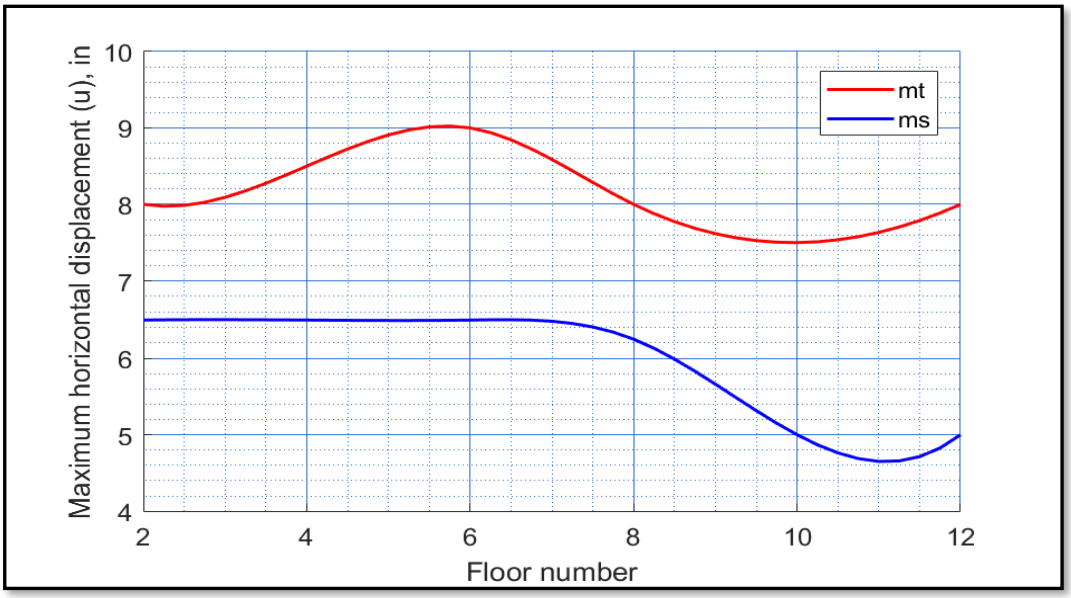

Figure 52. Change of horizontal displacement (u) of mt (H=308 feet) and ms (H=154 feet) with the location of the skybridge

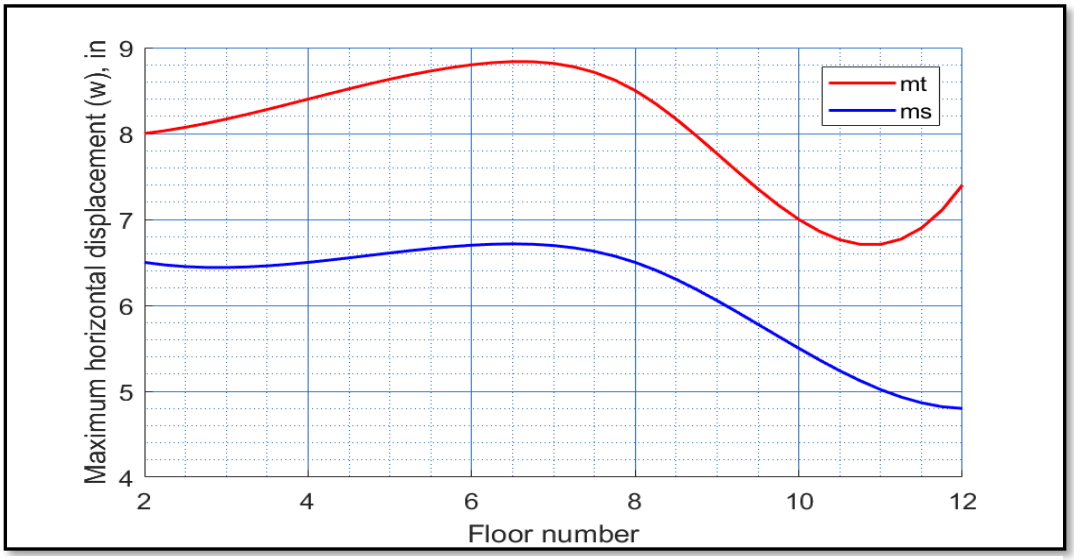

Figure 53. Change of horizontal displacement (w) of mt (H=308 feet) and ms (H=154 feet) with the location of the skybridge

5.4. Number of Skybridges

In this section, the number of skybridges that are specified to connect the two high-rise buildings is varied in order to minimize the dynamic displacement response as much as possible. The damped high-rise building system (HBS4) that was used in Sections 5.2 & 5.3 is used again in these simulations. The same values of the optimum axial and rigid stiffness are used again. The dynamic response was calculated relative to different number of skybridges represented by,

$$N=1, 2, 3, 4, 5, 6$$

The results obtained from the previous part of this section (Section 5.3) were employed to determine the location of these skybridges. Therefore, the first one was set to be on the tenth floor, the first optimum location of a skybridge. When using two skybridges, the second on was put on the twelfth floor, the second optimum location of a skybridge. Table 17 introduced the number of skybridges and their locations.

Table 17. Number of skybridges and their locations

N	Floor
1	10
2	10& 12
3	2& 10& 12
4	2& 8& 10& 12
5	2& 4& 8& 10& 12
6	2& 4& 6& 8&1 0& 12

The variation of the maximum dynamic displacements as a function of the number of skybridges (N) is shown in figure 54 and figure 55. The specification of one skybridge results in the minimum dynamic displacement along the two directions in the higher building (B1), whereas the specification of two skybridges minimizes the dynamic displacement of the shorter building (B2).

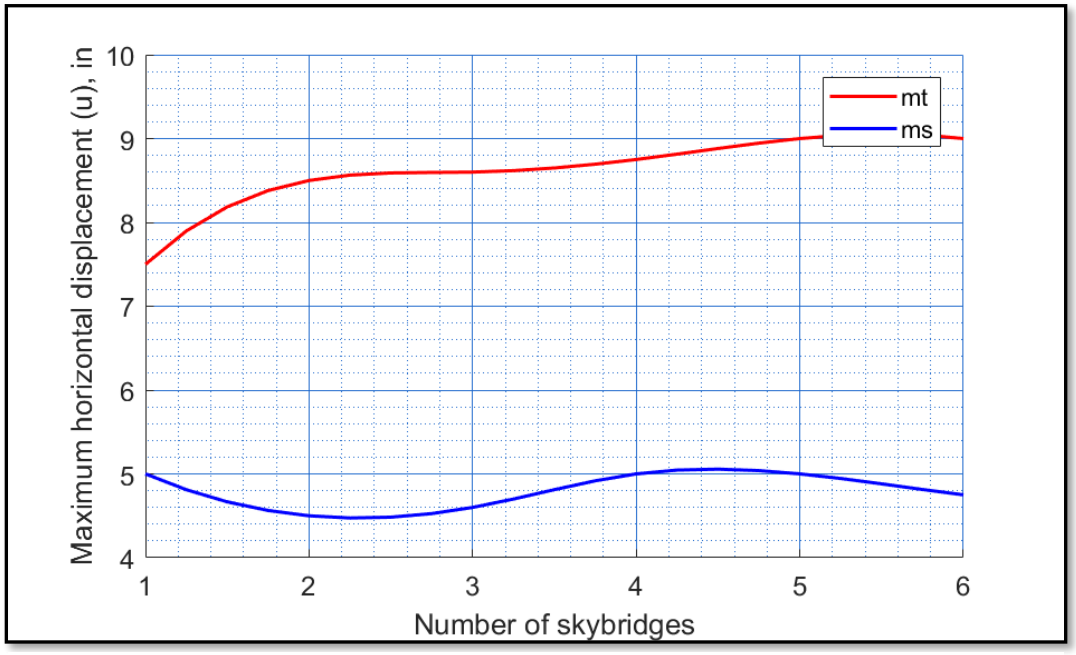

Figure 54. Change of horizontal displacement (u) of mt (H=308 feet) and ms (H=154 feet) with number of skybridges (N)

Figure 56 illustrates the change in the natural frequencies relative to the first four modal shapes of the x-direction motion with respect to the number of skybridges used to connect the buildings. The modal shapes that have a big displacement difference over the two masses that are connected by the skybridges usually witness significant changes in their corresponding natural frequencies.

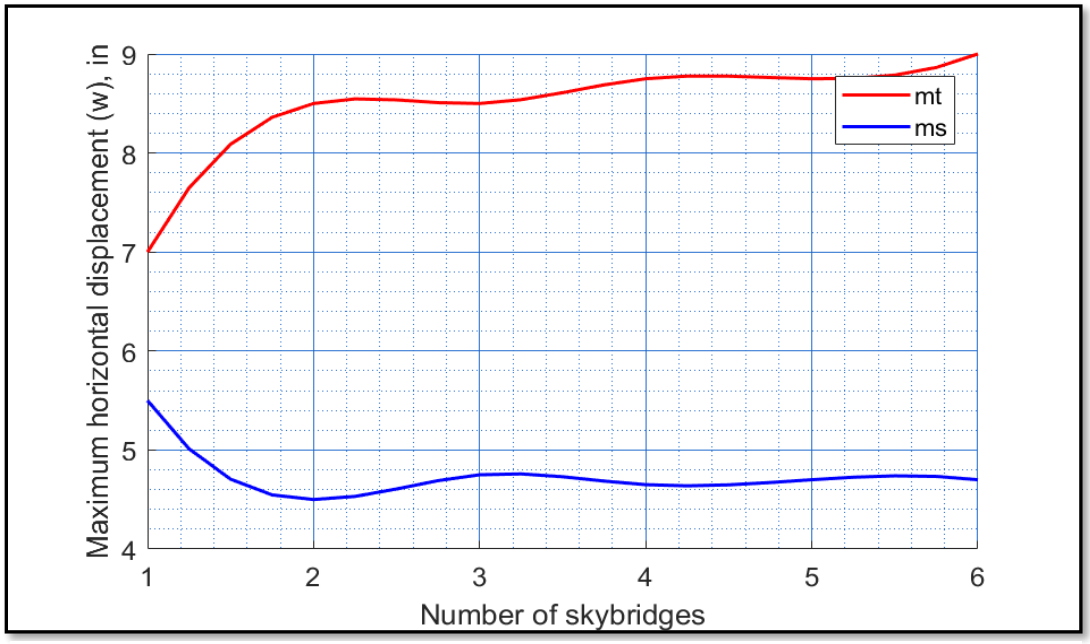

Figure 55. Change of horizontal displacement (w) of mt (H=308 feet) and ms (H=154 feet) with number of skybridges (N)

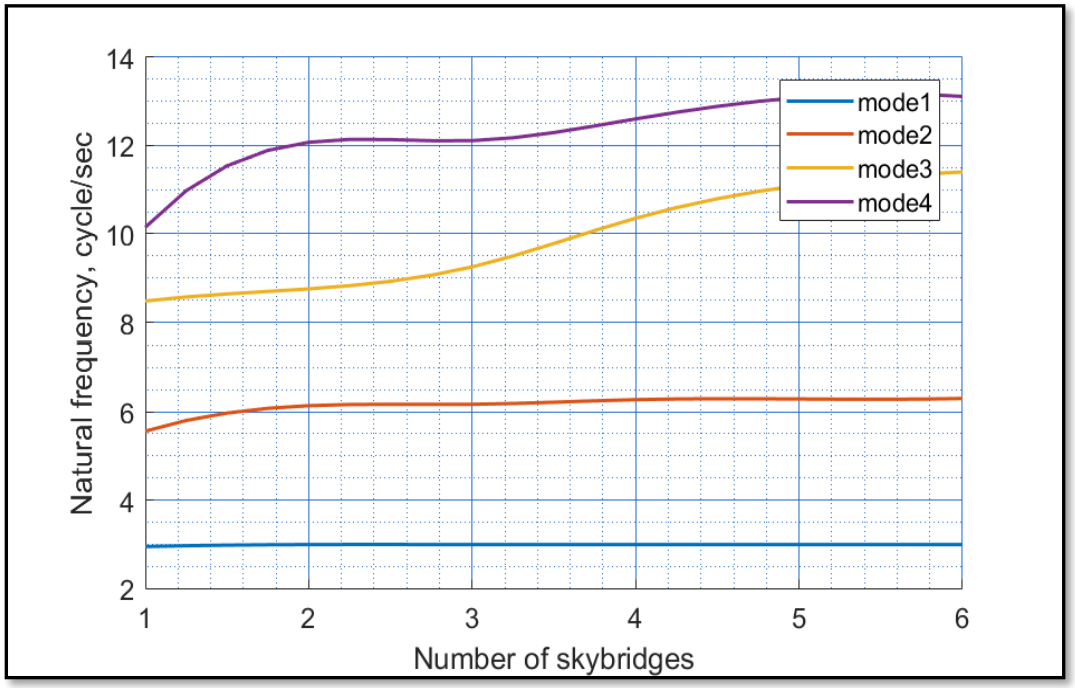

Figure 56. Change of natural frequencies of x-direction with N

5.5. Statistical Characterization of the Excitation and Response

Another perspective from which to investigate the structural coupling of high-rise buildings linked by skybridges involves the statistical characterization of both the strong ground motion excitation and the structural response to that excitation. Herein the mean, standard deviation, skewness, and kurtosis were evaluated for the four strong ground motion time series used in this research study and the resulting building system response. The skewness and kurtosis provide a measure of the deviation of these time series from Gaussian processes. Note that for a Gaussian process the skewness and kurtosis would have values of zero and three respectively. Information on each of the four earthquake

measurements and their statistical characteristics are presented in Table 18. Here one can observe the non-Gaussian nature of each of the earthquake time series.

Table 18. Statistical analysis of earthquake records

Strong ground motion records	Δt (sec)	Duration (sec)	Max a/g	Statistical characteristics			
				mean	std	skewness	kurtosis
1940 El-Centro	0.02	50	0.342	~0	0.0477	0.447	11.01
1994 Northridge	0.02	60	0.273	~0	0.5452	-1.269	68.64
Umbro Marchigiano	0.01	30	0.455	~0	0.5432	0.340	26.55
NF17 - artificial	0.01	5	10.61	~0	1.219	2.176	31.11

The dominant frequencies that are significantly higher than others in each of the time series records were evaluated using a Fast Fourier Transformation (FFT), and the results are listed in Table19.

Table 19. The dominant frequencies of earthquake records

Strong ground motion record	Dominant frequencies (rad/sec)
1940 El-Centro	7.28; 9.17; 13.57
1994 Northridge	2.72; 27.64
Umbro Marchigiano	39.86; 42.71; 45.11
NF17	73.99; 81.52; 90.3; 107.9

The 1940 El-Centro and 1994 Northridge earthquakes were used to excite the two high-rise building system (HBS5) whose geometrical properties are listed for B1 and B2 in table 20 and 21 respectively.

Table 20. Geometrical Properties of B1 in HBS5

Story	1-10	11-15
Column dimensions (ft)	4 × 4	3 × 3
Column height (ft)	14	14
Slab thickness (in)	8	8

Table 21. Geometrical properties of B2 in HBS5

Story	1-8	9-12
Column dimensions (ft)	3 × 3	2 × 2
Column height (ft)	14	14
Slab thickness (in)	8	8

Two cases were investigated where first the buildings were linked by a single skybridge and then by three skybridges. The characteristics of the skybridges are presented in Table 22.

Table 22. Geometrical properties of the skybridge in HBS5

Section shape	Length (ft)	A × Ec (kips)	I_z (in^4)
rectangular	55	26925000	214×10^9

Two different critical damping ratios (ξ = 0.01, 0.1) were applied to the building systems in order to observe their behavior of the system under different loadings, numbers of skybridges, and damping. Table 23 and Table 24 summarize the statistical characterization of the resulting response behavior.

Next, we consider the use of histograms to visualize the response behavior of the highest point on the shorter building and this is presented in Figures 57 through 60. The decrement in the standard deviation values and the increment in the absolute values of the

kurtosis when the damping ratio goes from 0.01 to 0.1 can be interpreted as the overall dynamic response over the whole period of the earthquake is reduced. On the other hand, when using three skybridges to connect the two buildings instead of one, the value of standard deviation decreases and the absolute values of skewness and kurtosis increase, and this gives an indication of the same positive impact of using multiple skybridges. However, in the case of high manufactured damping (0.1), the effect of the existence of three skybridges (verse one skybridges) is not significant due to fast dissipation in the energy of the building system.

Table 23. Statistical characterization of HBS5 response subjected to the 1940 El-Centro record

The 1940 El-Centro									
Number of skybridges	Damping ratio	Direction	Mean (in)	SD (in)		Skewness		Kurtosis	
				min	max	min	max	min	max
1	0.01	x_t	~0	0.15	2.05	-0.01	0.02	3.56	3.83
		z_t	~0	0.00	1.74	-0.03	0.14	1.87	3.73
		y_r	~0	0.00	0.00	-	-	-	-
	0.1	x_t	~0	0.04	0.59	-0.30	0.06	8.75	9.04
		z_t	~0	0.00	0.81	-0.08	0.39	6.35	8.87
		y_r	~0	0.00	0.00	-	-	-	-
3	0.01	x_t	~0	0.14	1.85	-0.10	0.03	4.49	4.67
		z_t	~0	0.00	1.74	-0.03	0.14	1.87	3.74
		y_r	~0	0.00	0.00	-	-	-	-
	0.1	x_t	~0	0.05	0.56	-0.34	0.06	8.80	9.04
		z_t	~0	0.00	0.81	-0.08	0.39	6.37	8.86
		y_r	~0	0.00	0.00	-	-	-	-

Table 24. Statistical characterization of HBS5 response subjected to the 1994 Northridge record

The 1994 Northridge									
Number of skybridges	Damping ratio	Direction	Mean(in)	SD(in)		Skewness		Kurtosis	
				min	max	min	max	min	max
1	0.01	x_t	~0	0.06	0.79	-0.11	0.12	3.05	7.70
		z_t	~0	0.00	2.85	-0.07	0.28	2.96	7.51
		y_r	~0	0.00	0.00	-	-	-	-
	0.1	x_t	~0	0.03	0.34	-0.15	1.12	8.65	11.96
		z_t	~0	0.00	0.63	0.06	0.96	7.92	12.48
		y_r	~0	0.00	0.00	-	-	-	-
3	0.01	x_t	~0	0.06	0.78	-0.08	0.19	2.79	3.97
		z_t	~0	0.00	2.83	-0.06	0.28	2.97	7.50
		y_r	~0	0.00	0.00	-	-	-	-
	0.1	x_t	~0	0.03	0.32	-0.09	1.19	8.46	11.26
		z_t	~0	0.00	0.62	0.06	0.97	7.94	12.47
		y_r	~0	0.00	0.00	-	-	-	-

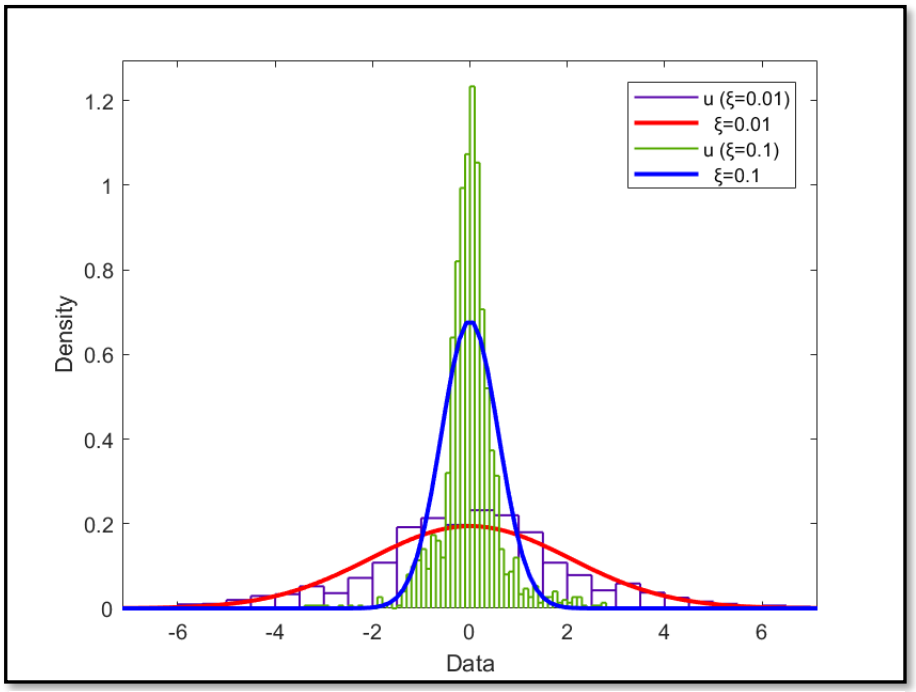

Figure 57. Normal distribution of (u) with a skybridge (El-Centro)

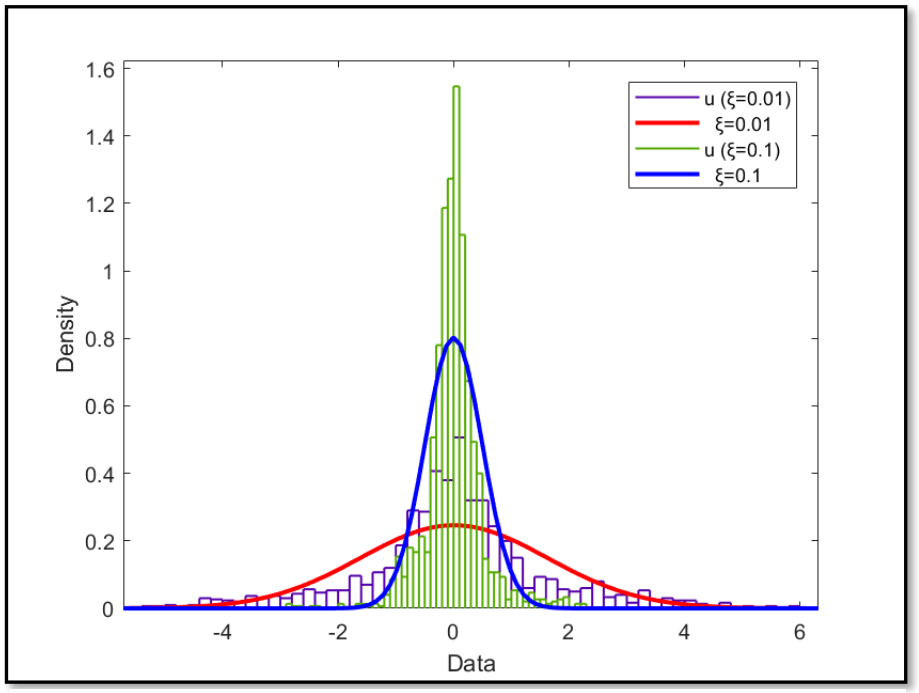

Figure 58. Normal distribution of (u) with three skybridges (El-Centro)

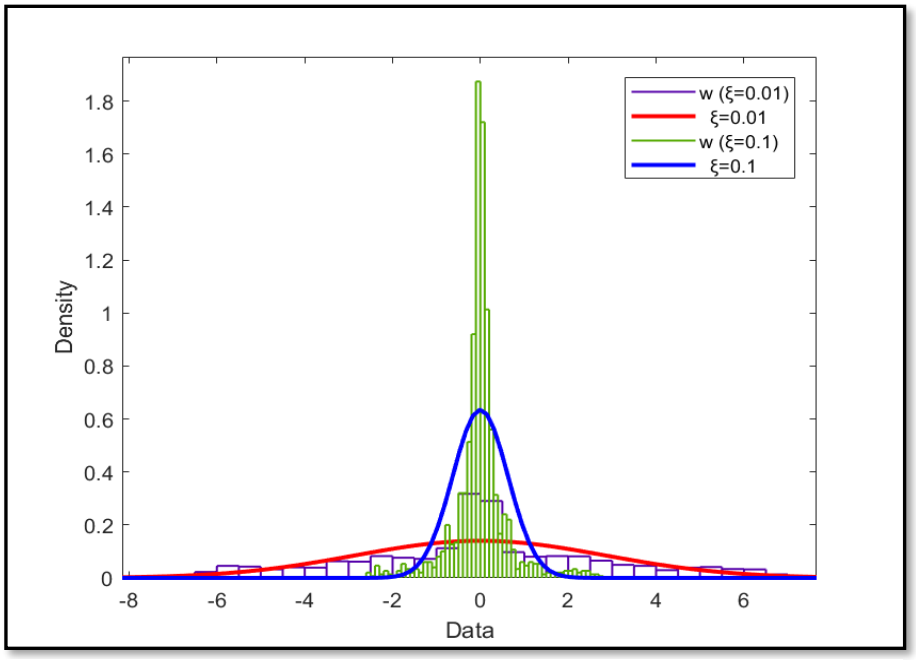

Figure 59. Normal distribution of (w) with a skybridge (Northridge)

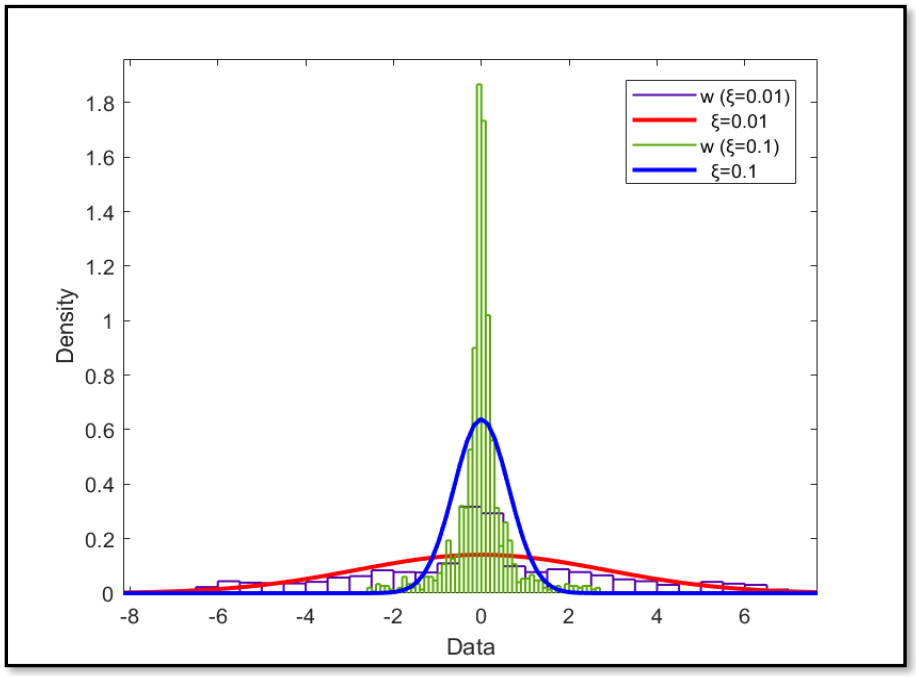

Figure 60. Normal distribution of (w) with three skybridges (Northridge)

6. SUMMARY AND CONCLUSIONS

This study presented a structural model that focused on the dynamic response of adjacent buildings connected at one or more elevations by skybridges. The frame based multi-degree-of-freedom model utilized allowed for the inclusion of both translational and rotational degrees of freedom. The focus of the illustrative examples was the modeling of high-rise buildings of different story height that were linked by one or more skybridges. The building systems were subjected to earthquake loads.

A review previous relevant research studies allowed the identification of knowledge gaps that guided this research investigation. It was found that three earlier studies directly addressed the structural coupling of twin buildings coupled by a single skybridge. Lim, Bienkiewicz, & Richards (2011), examined the response of a coupled twin high-rise building system subjected to wind loading. Their model assumed a single lumped mass for each building that was allowed to have multiple degrees of freedom (MDOF). The three-degree of freedom models allowed for translation in the inline and transverse directions, as well as rotation around the vertical axis. Lee, Kim, & Ko (2012) utilized a finite element model and were able to consider lead rubber bearings and linear motion bearings to model the connection between the skybridge and the two high-rise buildings subjected to wind and earthquake loads. Their study focused on the simulation of translational degrees of freedom. Later in the study by Song and Tse (2014), they considered the effect of wind loads where they modeled each building using a series of lumped masses, one at each floor elevation.

Consequently, a more general formulation that could address translational and rotational degrees of freedom for buildings of different plan form and elevation, and single or multiple skywalks was developed in this research study. The resulting formulation was implemented in Matlab and validated using SAP2000. Due to the complexity of the structural system, a Newmark-Beta time integration model was used to solve for the dynamic response behavior. Eleven building systems with different geometries and dynamic properties using were investigated and it was found that the predicted results using the 3-D frame formulation resulted in an error on the order of less than 2%.

The nine building systems that were the focus of this research investigation was the nine cases identified in Table 25, which is repeated here for clarity. A total of 51 numerical simulations were systematically analyzed and documented in this thesis. The system parameters varied in these simulations included: building height, number of skybridges, their elevation and connectivity boundary conditions, lumped sum mass characteristics, story stiffness, and system damping. The role of critical damping ratios in modifying the structural response behavior was investigated. For very lightly damped systems a range of 1-3% was assumed and a value of 10% that might result from manufactured damping was briefly investigated. A statistical analysis characterizing the nature of four different earthquakes and the corresponding structural system response behavior was performed.

Table 25. Case studies that were considered in this research study

Case Number	Case Description	Number of Runs	Variation
1	Single lumped mass model for twin buildings	5	Concentrating the lumped mass in different locations
2	Multiple lumped mass model for twin buildings	5	Height and properties of the skybridge
3	Multiple lumped mass model for different buildings	2	Coupled (with a skybridge) and uncoupled.
4	Multiple lumped mass model for non-conservative different buildings	7	Damping ratio (0 to 10%)
5	Multiple lumped mass model for different buildings	3	Supporting condition of the skybridge ends: Roller, hinge, and fixed
6	Multiple lumped mass model for non-conservative different buildings	9	Stiffness of the skybridge
7	Multiple lumped mass model for non-conservative different buildings	6	Height of the skybridge
8	Multiple lumped mass model for non-conservative different buildings	6	Number of skybridges (1 to 6)
9	Multiple lumped mass model for non-conservative different buildings	8	Statistical characterization

The central conclusions of this research study based on the numerical simulations of adjacent buildings with an unequal number of stories connected by one or more skybridges are as follows:

1. The introduction of skybridges to connect adjacent buildings can significantly impact the mode shapes and natural frequency estimates and dynamic response behavior.
2. The introduction of multiple skybridge connections impacts the higher modes and has a significant impact on the structural system response behavior.
3. The structural system displacement response is modified by the introduction of skybridges designed with hinged end supports and is also influenced by the structural characteristics of the skybridge design.
4. The structural system displacement and rotational response behavior is modified by skybridges designed with fixed ended connections and is also influenced by the structural characteristics of the skybridge design.
5. It was observed that there are optimum translational stiffness and flexural stiffness characteristics for skybridge design that would minimize the building system dynamic response behavior. Further, it was observed that deviations of skybridge stiffness required to minimize the dynamic response of the shorter building system is more than that required for a taller building system.
6. For the building systems investigated, it was observed that a single skybridge located at an elevation of about 80% of the shorter building height would minimize the dynamic displacement behavior.

7. The introduction of a single skybridge reduces the dynamic response of the taller building, whereas the introduction of two skybridges was observed to minimize the dynamic response for the shorter building.
8. Based on the numerical simulations it was determined that the best approximation for the inclusion of a skybridge can be achieved by concentrating its mass contributions closer to the center of the geometry of each high-rise building.
9. Statistical characterization of the excitation and response behavior illustrated that non-Gaussian excitation was filtered by the building system to yielding a reduced non-Gaussian response.

It is clear that further investigation into this challenging structural design problem is needed to better understand some of the results found in this research study. The analysis and Matlab code developed, as part of this research study is quite general and can address skybridge vertical connection between different floors and situations where there is horizontal miss-alignment of buildings. The idea of optimizing/minimizing the building system dynamic response is also quite intriguing especially for high-rise buildings that are located in dense population area where space for building footprints is often quite limited.

REFERENCES

Behnamfar, F., Dorafshan, S., Taheri, A., & Hosseini Hashemi, B. (2016). A method for rapid estimation of dynamic coupling and spectral responses of connected adjacent structures. *The Structural Design of Tall and Special Buildings*, *25*(13), 605-625.

Chen, X., & Kareem, A. (2005). Dynamic Wind Effects on Buildings with 3D Coupled Modes: Application of High Frequency Force Balance Measurements. *Journal of Engineering Mechanics*, *131*(11), 1115-1125.

Chopra, A. K. (2001). *Dynamics of structures: theory and applications to earthquake engineering. 2nd ed. Anil K. Chopra*: Upper Saddle River, NJ: Prentice-Hall, [2001] 2nd ed.

Clough, R. W., & Penzien, J. (2010). *Dynamics of structures. 2nd ed., Rev. Ray W. Clough, Joseph Penzien*: Berkeley, Calif. : Computers and Structures, [2010] 2nd ed., Rev.

Klein, R. E., & Healey, M. D. (1987). Semi-Active Control of Wind Induced Oscillations in Structures. In H. H. E. Leipholz (Ed.), *Structural Control: Proceedings of the Second International Symposium on Structural Control, University of Waterloo, Ontario, Canada, July 15–17, 1985* (pp. 354-369). Dordrecht: Springer Netherlands.

Le, T.-H., & Caracoglia, L. (2015). Wavelet-Galerkin analysis to study the coupled dynamic response of a tall building against transient wind loads. *Engineering Structures, 100*, 763-778.

Lee, D.-G., Kim, H.-S., & Ko, H. (2012). Evaluation of coupling–control effect of a sky-bridge for adjacent tall buildings. *The Structural Design of Tall and Special Buildings, 21*(5), 311-328.

Lim, J., & Bienkiewicz, B. (2009). Effects of Structural and Aerodynamic Couplings on the Dynamic Response of Tall Twin Buildings with a Skybridge *Structures Congress 2009* (pp. 1-9).

Lim, J., Bienkiewicz, B., & Richards, E. (2011). Modeling of structural coupling for assessment of modal properties of twin tall buildings with a skybridge. *Journal of Wind Engineering and Industrial Aerodynamics, 99*(5), 615-623.

Lim, J., & University, C. S. (2008). *Structural Coupling and Wind-induced Response of Twin Tall Buildings with a Skybridge*: Colorado State University.

Lomholt, I., Lomholt, I., Solkoff, J., & Solkoff, J. (2017). *Bahrain World Trade Center: Manama, BWTC - e-architect*. *e-architect*. Retrieved 28 April 2017, from https://www.e-architect.co.uk/bahrain/bahrain-world-trade-centre

McCall, A. J., & Balling, R. J. (2016). Structural analysis and optimization of tall buildings connected with skybridges and atria. *Structural and Multidisciplinary Optimization*, 1-18.

Paz, M., & Leigh, W. E. (2004). *Structural dynamics: theory and computation. 5th ed. Mario Paz, William Leigh*: Boston: Kluwer Academic Publishers, [2004] 5th ed.

Rogers, S. (2017). *Sky Bridges: 14 Aerial Structures that Span Skyscrapers*. *WebUrbanist*. Retrieved 28 April 2017, from http://weburbanist.com/2013/09/16/sky-bridges-14-aerial-structures-that-span-skyscrapers/2/

Skyway or the highway for teaching hospital - Austin Monitor. (2017). Austin Monitor. Retrieved28 April 2017, from https://www.austinmonitor.com/stories/2014/09/skyway-highway-teaching-hospital/

Song, J., & Tse, K. T. (2014). Dynamic characteristics of wind-excited linked twin buildings based on a 3-dimensional analytical model. *Engineering Structures*, *79*, 169-181.

The World's Best Photos of skybridge and way - Flickr Hive Mind. (2017). Hiveminer.com. Retrieved 28 April 2017, from https://hiveminer.com/Tags/skybridge,way

Zhao, X., Sun, H. H., & Zheng, Y. M. (2009). Identification and updating for the three-dimensional finite element model of a long span steel skybridge. *The Structural Design of Tall and Special Buildings*, *18*(6), 625-646.

APPENDIX A

STRUCTURAL STIFFNESS MATRIX DEVELOPMENT

The following analysis provides the details used in the development of the stiffness equations used in equation (40) elements presented in chapter 2 of this thesis:

$$f_1 = \sin(\alpha)\sin(\beta)$$

$$f_2 = \sin(\alpha)\cos(\beta)$$

$$f_3 = \cos(\alpha)\sin(\beta)$$

$$f_4 = \cos(\alpha)\cos(\beta)$$

$$k_{1,1} = \left(EAL^2(1-(\sin\alpha)^2-(\sin\beta)^2+f_1^2)+12EI_y(\sin\beta)^2+12EI_z((\sin\alpha)^2-f_1^2\right)\Big/L^3$$

$$k_{1,2} = k_{2,1} = -\left(f_4\sin\alpha(-EAL^2+12EI_z)\right)\Big/L^3$$

$$k_{1,3} = k_{3,1} = -\left(f_3(-EAL^2(\cos\alpha)^2+12EI_y+12EI_z((\cos\alpha)^2-1)\right)\Big/L^3$$

$$k_{1,4} = k_{4,1} = -\left(6f_2\sin(\beta)(EI_y-EI_z)\right)\Big/L^2$$

$$k_{1,5} = k_{5,1} = 6f_3EI_y\Big/L^2$$

$$k_{1,6} = k_{6,1} = -6\left(EI_y f_1\sin(\beta)+EI_z\sin(\beta)(1-f_1)\right)\Big/L^2$$

$$k_{1,7} = k_{7,1} = -k_{1,1}$$

$$k_{1,8} = k_{8,1} = -k_{1,2}$$

$$k_{1,9} = k_{9,1} = -k_{1,3}$$

$$k_{1,10} = k_{10,1} = k_{1,4}$$

$$k_{1,11} = k_{11,1} = k_{1,5}$$

$$k_{1,12} = k_{12,1} = k_{1,6}$$

$$k_{2,2} = \left(12EI_z - 12EI_y(\sin\alpha)^2 + EAL^2(\sin\alpha)^2\right)\Big/L^3$$

$$k_{2,3} = k_{3,2} = -\left(f_1\cos(\alpha)(-EAL^2 + 12EI_z)\right)\Big/L^3$$

$$k_{2,4} = k_{4,2} = -6EI_z f_3\big/L^2$$

$$k_{2,5} = k_{5,2} = 0$$

$$k_{2,6} = k_{6,2} = 6EI_z f_2\big/L^2$$

$$k_{2,7} = k_{7,2} = -k_{2,1}$$

$$k_{2,8} = k_{8,2} = -k_{2,2}$$

$$k_{2,9} = k_{9,2} = -k_{2,3}$$

$$k_{2,10} = k_{10,2} = k_{2,4}$$

$$k_{2,11} = k_{11,2} = k_{2,5}$$

$$k_{2,12} = k_{12,2} = k_{2,6}$$

$$k_{33} = \left(EAL^2((\sin\beta)^2 - f_1^2)) + 12EI_y(1-(\sin\beta)^2) + 12EI_z f_1^2\right)\Big/L^3$$

$$k_{3,4} = k_{4,3} = 6\sin(\alpha)\left(EI_y(1-(\sin\beta)^2) + EI_z(\sin\beta)^2\right)\Big/L^2$$

$$k_{3,5} = k_{5,3} = -6EI_y f_4\big/L^2$$

$$k_{3,6} = k_{6,3} = 6\,f_2\sin(\beta)(EI_y - EI_z)\big/L^2$$

$$k_{3,7} = k_{7,3} = -k_{3,1}$$

$$k_{3,8} = k_{8,3} = -k_{3,2}$$

$$k_{3,9} = k_{9,3} = -k_{3,3}$$

$$k_{3,10} = k_{10,3} = k_{3,4}$$

$$k_{3,11} = k_{11,3} = k_{3,5}$$

$$k_{3,12} = k_{21,3} = k_{3,6}$$

$$k_{4,4} = \left(4EI_y((\sin\alpha)^2 - f_1^{\,2}) + 4EI_z(\sin\beta)^2 + GJ(1 + f_1^{\,2} - (\sin\alpha)^2 - (\sin\beta)^2)\right)\Big/L$$

$$k_{4,5} = k_{5,4} = -\left(f_4 \sin(\alpha)(4EI_y - GJ)\right)\Big/L$$

$$k_{4,6} = k_{6,4} = \sin(2\beta)\left(2EI_y(1-\cos(2\alpha)) - 4EI_z + \frac{GJ}{2}(1+\cos(2\alpha))\right)\Big/2L$$

$$k_{4,7} = k_{7,4} = -k_{4,1}$$

$$k_{4,8} = k_{8,4} = -k_{4,2}$$

$$k_{4,9} = k_{9,4} = -k_{4,3}$$

$$k_{4,10} = k_{10,4} = \left(2EI_y((\sin\alpha)^2 - f_1^{\,2}) + 2EI_z(\sin\beta)^2 + GJ(-1 - f_1^{\,2} + (\sin\alpha)^2 + (\sin\beta)^2)\right)\Big/L$$

$$k_{4,11} = k_{11,4} = -\left(f_4 \sin(\alpha)(2EI_y + GJ)\right)\Big/L$$

$$k_{4,12} = k_{12,4} = -\sin(2\beta)\left(EI_y(\cos(2\alpha) - 1) + 2EI_z + \frac{GJ}{2}(1+\cos(2\alpha))\right)\Big/2L$$

$$k_{5,5} = \left(4EI_y(1-(\sin\alpha)^2) + GJ(\sin\alpha)^2\right)\Big/L$$

$$k_{5,6} = k_{6,5} = -f_3 \sin(\alpha)\left((4EI_y - GJ)\right)\Big/L$$

$$k_{5,7} = k_{7,5} = -k_{5,1}$$

$$k_{5,8} = k_{8,5} = 0$$

$$k_{5,9} = k_{9,5} = -k_{5,3}$$

$$k_{5,10} = k_{10,5} = -\left(f_4 \sin(\alpha)(2EI_y + GJ) \right) \Big/ L$$

$$k_{5,11} = k_{11,5} = -\left(2EI_y((\sin\alpha)^2 - 1) + GJ(\sin\alpha)^2 \right) \Big/ L$$

$$k_{5,12} = k_{12,5} = -f_3 \sin(\alpha) \left((2EI_y + GJ) \right) \Big/ L$$

$$k_{6,6} = \left(4f_1^2 EI_y + 4EI_z(1 - (\sin\beta)^2) + GJ(-f_1^2 + (\sin\beta)^2) \right) \Big/ L$$

$$k_{6,7} = k_{7,6} = -k_{6,1}$$

$$k_{6,8} = k_{8,6} = -k_{6,2}$$

$$k_{6,9} = k_{9,6} = -k_{6,3}$$

$$k_{6,10} = k_{10,6} = -\sin(2\beta) \left(2EI_y(-1 + \cos(2\alpha)) + 2EI_z + \frac{GJ}{2}(1 + \cos(2\alpha)) \right) \Big/ 2L$$

$$k_{6,11} = k_{11,6} = -f_3 \sin(\alpha) \left((2EI_y + GJ) \right) \Big/ L$$

$$k_{6,12} = k_{12,6} = \left(2f_1^2 EI_y + 2EI_z(1 - (\sin\beta)^2) + GJ(f_1^2 - (\sin\beta)^2) \right) \Big/ L$$

$$k_{7,7} = -k_{7,1}$$

$$k_{7,8} = k_{8,7} = -k_{7,2}$$

$$k_{7,9} = k_{9,7} = -k_{7,3}$$

$$k_{7,10} = k_{10,7} = k_{7,4}$$

$$k_{7,11} = k_{11,7} = k_{7,5}$$

$$k_{7,12} = k_{12,7} = k_{7,6}$$

$$k_{8,8} = -k_{8,2}$$

$$k_{8,9} = k_{9,8} = -k_{8,3}$$

$$k_{8,10} = k_{10,8} = k_{8,4}$$

$$k_{8,11} = k_{11,8} = 0$$

$$k_{8,12} = k_{12,8} = k_{8,6}$$

$$k_{9,9} = -k_{9,3}$$

$$k_{9,10} = k_{10,9} = k_{9,4}$$

$$k_{9,11} = k_{11,9} = k_{9,5}$$

$$k_{9,12} = k_{21,9} = k_{9,6}$$

$$k_{10,10} = k_{4,4}$$

$$k_{10,11} = k_{11,10} = -f_4 \sin(\alpha)\left((4EI_y - GJ)\right)\Big/L$$

$$k_{10,12} = k_{12,10} = \sin(2\beta)\left(2EI_y(1-\cos(2\alpha)) - 4EI_z + \frac{GJ}{2}(1+\cos(2\alpha))\right)\Big/2L$$

$$k_{11,11} = \left(4EI_y(1-(\sin\alpha)^2) + GJ(\sin\alpha)^2\right)\Big/L$$

$$k_{12,11} = k_{11,12} = -f_3 \sin(\alpha)\left((4EI_y - GJ)\right)\Big/L$$

$$k_{12,12} = \left(4f_1^2 EI_y + 4EI_z(1-(\sin\beta)^2) + GJ(-f_1^2 + (\sin\beta)^2)\right)\Big/L$$

APPENDIX B

EARTHQUAKE RECORDS

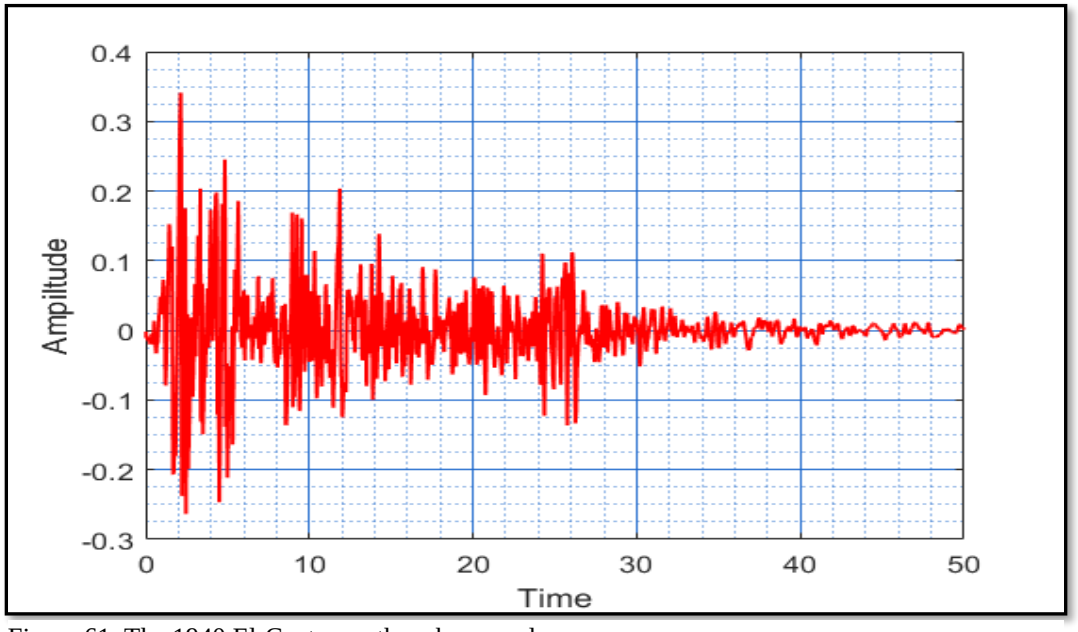

Figure 61. The 1940 El-Centro earthquake record

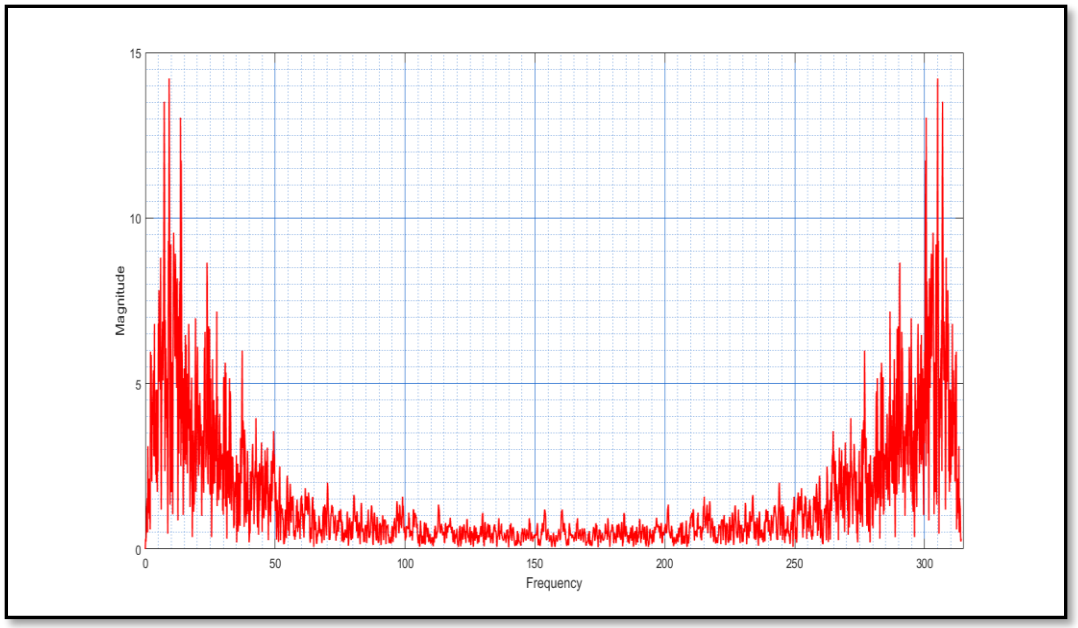

Figure 62. The 1940 El-Centro power spectral density

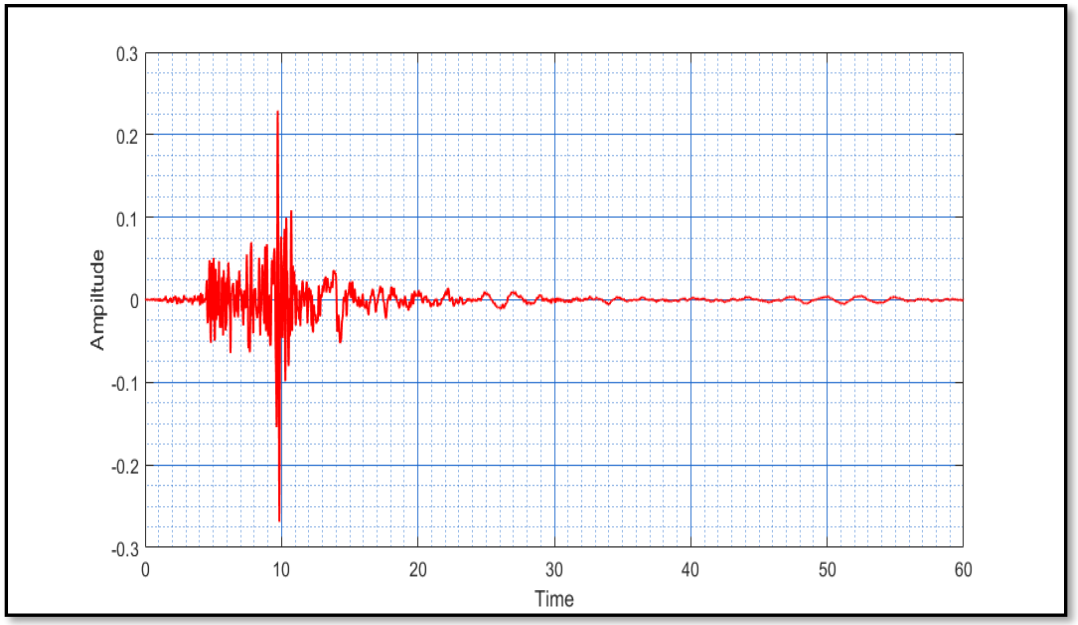

Figure 63. The 1994 Northridge earthquake record

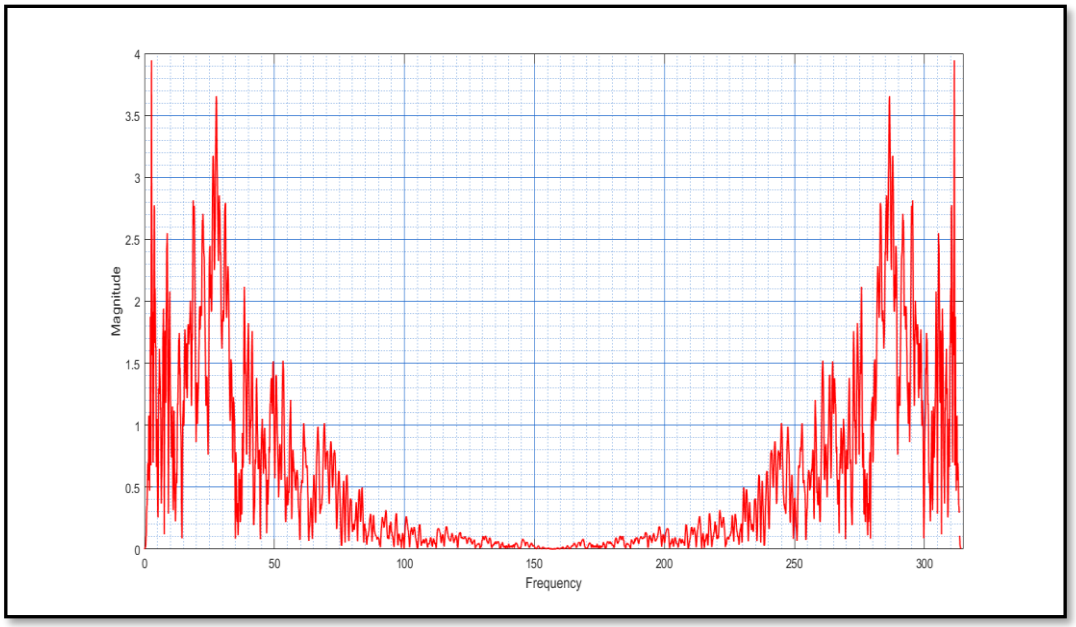

Figure 64. The 1994 Northridge power spectral density

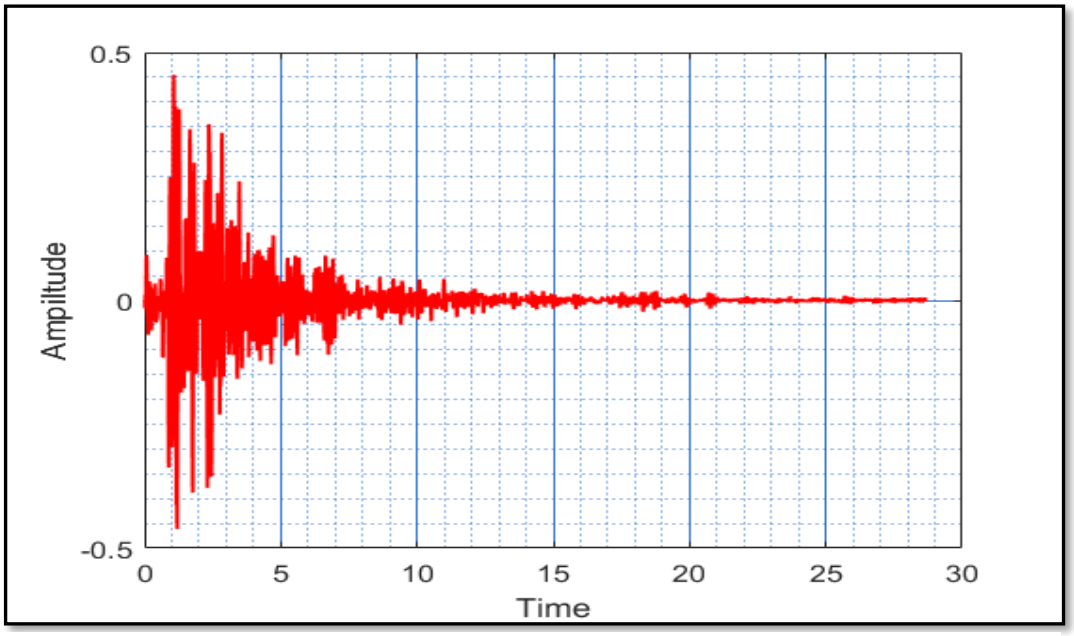

Figure 65. The Umbro-Marchigiano earthquake record

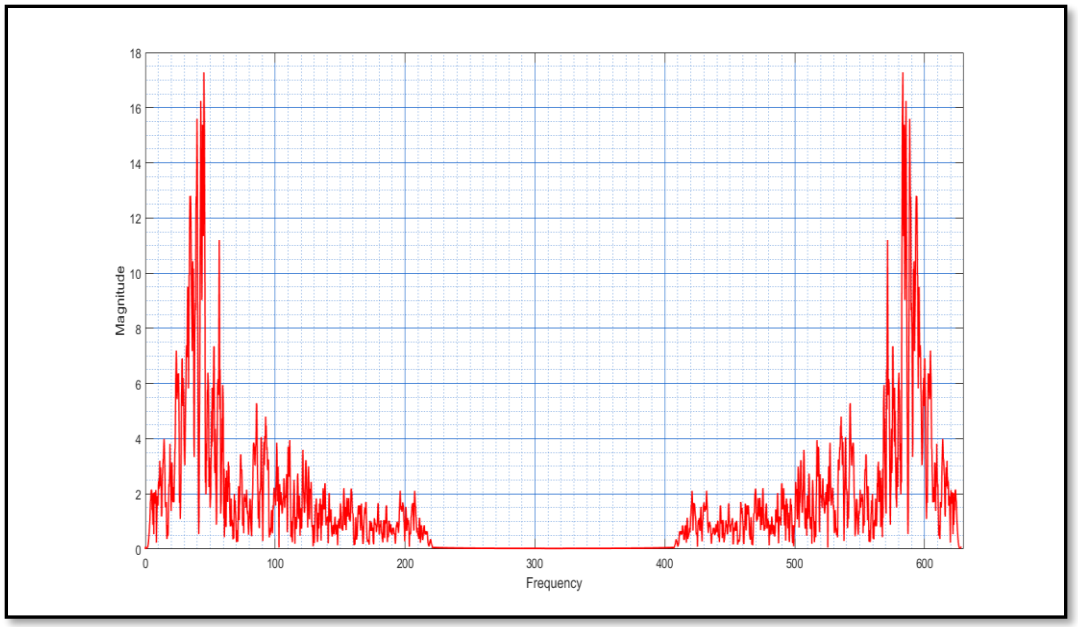

Figure 66. The Umbro-Marchigiano power spectral density

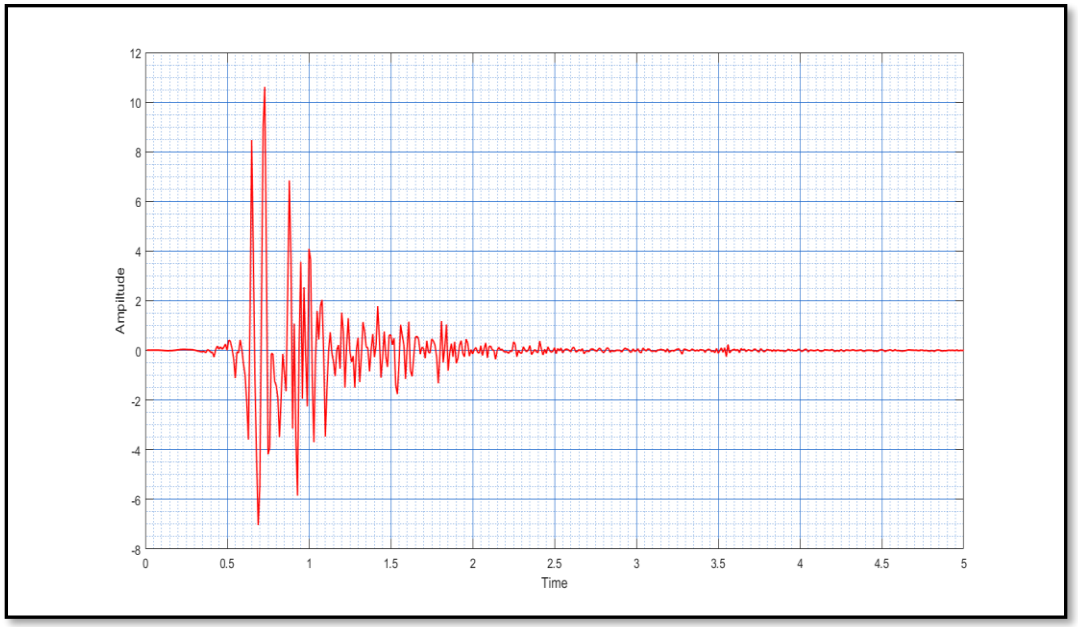

Figure 67. The artificial NF-17 earthquake record

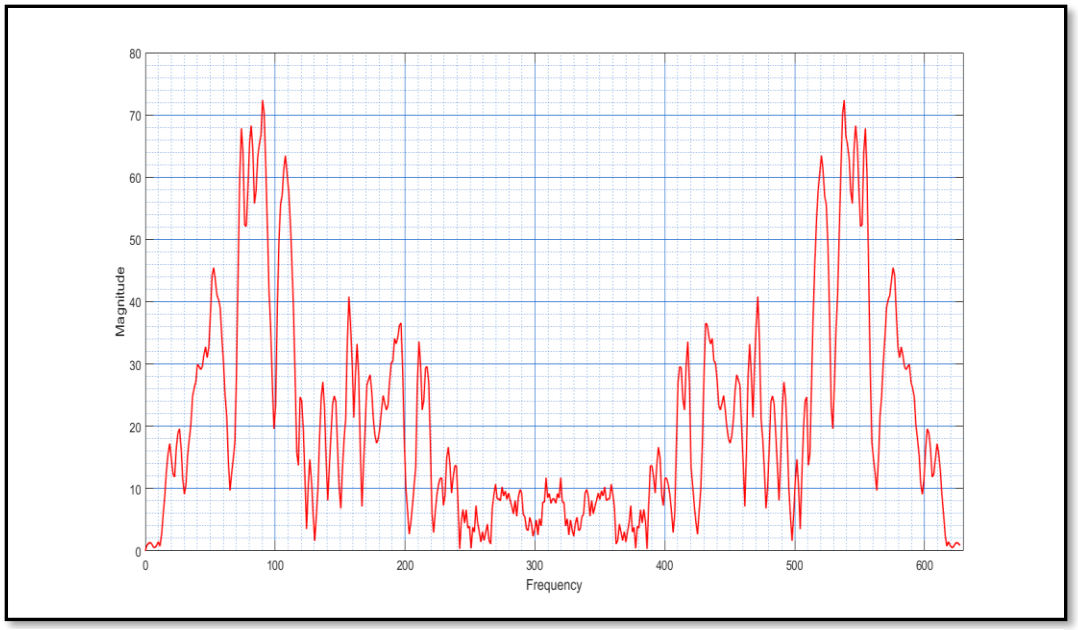

Figure 68. The artificial NF-17 power spectral density